Dissertation

Ökologische und ökonomische Betrachtungen im Straßenbau und -betrieb

ausgeführt zum Zwecke der Erlangung des akademischen Grades eines
Doktors der technischen Wissenschaften
eingereicht an der TU Wien, Fakultät für Bau- und Umweltingenieurwesen

Doctoral Thesis

Ecological and Economic Aspects of Road Construction and Operation

submitted in satisfaction of the requirements for the degree of
Doctor of Science in Civil Engineering of the TU Wien,
Faculty of Civil and Environmental Engineering

by

Dipl.-Ing. Michael R. Gruber
Student ID: 00728128

Supervisor

Univ. Prof. Dipl.-Ing. Dr. techn. Bernhard Hofko
Institute of Transportation, Technische Universität Wien
Karlsplatz 13/230-3, 1040, Vienna, Austria

Examiner

Prof. Dipl.-Ing. Dr. Christiane Raab
EMPA—Eidgenössische Materialprüfanstalt
Überlandstrasse 129, CH-8600 Dübendorf, Switzerland

Examiner

Univ. Prof. Dipl.-Ing. Dr. techn. Dr. h.c. Helmut Rechberger
Institute of Water Quality and Resource Management, Technische Universität Wien
Karlsplatz 13/226-2, 1040, Vienna, Austria

Vienna, May 2023

i Preamble and acknowledgments

With ageing transport infrastructures in developed countries, road operation, maintenance, and rehabilitation are of increasing importance as a prerequisite for functioning societies and markets. Starting my education in a time with focus on minimizing costs of transport infrastructure operators, the focus has shifted substantially towards a more holistic and sustainable point of view. In this regard the starting point of my scientific approach was to provide both a scientific and practice-oriented contribution towards safe and sustainable road construction, operation, maintenance, and rehabilitation. The scientific contributions that form the basis of this dissertation are therefore broadly based yet provide essential insights for a more sustainable future in terms of both road maintenance and operations, with a particular focus on winter maintenance.

Regardless of previously acquired knowledge the real challenge is always provided by specific scientific questions with an actual practical background, as the answers will be tested soon thereafter. Constantly being faced with such challenges during my time at the Institute of Transportation at TU Wien, I was able to acquire the necessary prerequisites and qualifications to provide specific answers. The knowledge and instruments I developed during my time at the institute are largely owed to the contributions of Prof. Bernhard Hofko and Prof. Ronald Blab and the cooperation with Priv.-Doz. Markus Hoffmann during our research cooperations. However, the scientific projects would not have been possible without the contribution of the federal state's governments, BMK, ASFINAG, OEBB and the Austrian research promotion agency FFG. Nonetheless, the majority of the scientific projects contributing to this dissertation, especially in the field of sustainable road construction and maintenance, would not have been possible without the generous contributions of Strabag, Porr, Pittel+Brausewetter, Gestrata, VIBOE and OEBA.

Personally, I would also like to thank my supervisor, Univ. Prof. Dipl.-Ing. Dr. techn. Bernhard Hofko for his unwavering support and guidance during the last four years. Despite setting up a successful Christian Doppler Laboratory among other achievements he was available helping me to overcome all challenges on my way. In addition, he provided me with the opportunity to extend my horizon by paving my way towards a scholarship at the Massachusetts Institute of Technology in Cambridge (USA). As a conclusion my heartfelt gratitude goes to him for supporting me during my entire scientific career both on an academic and personal level. Furthermore, I would like to thank Priv.-Doz. Dipl.-Ing. Dr. techn. Markus Hoffmann (TU Wien and Hoffmann Consult e.U.) for his contributions to my development. His academic advice was available upon request and his experience in the field of winter maintenance has been a tremendous help. Without his support I would not have come this far.

As scientific progress and personal development require a horizon beyond disciplines, a substantial part of the scientific progress presented in this thesis would not have been possible without the ongoing cooperation with the Institute of Materials Chemistry of TU Wien. Both the scientific contributions and guidance foremost by Univ. Prof. Dipl.-Chem. Dr.rer.nat. Hinrich Grothe and his staff Dipl.-Ing. Dr.rer.nat. Teresa Seifried and Dipl.-Ing. David Stinglmayr have provided invaluable expertise in design and execution of the corrosion and deicing performance tests. As David was tasked with the time-consuming corrosion tests also acting as an ambassador in an interdisciplinary team his contributions cannot be overstated. In my institute special thanks go to Dipl.-Ing. Franziska Gober and Dipl.-Ing. Sophia Astner for their support in gathering data for the energy and materials flow in the asphalt mix and concrete production. During my time at the laboratory of Prof. Hofko I particularly appreciated the help of the lab technician David Valentin, as a reliable partner in all matters of experimental support and organization. Last but not least, I would like to thank my fiancée Milena, who put up with me despite challenging hours of writing the papers and the dissertation. I owe you much and I do want to believe that the truth is out there.

ii Abstract

Road construction contributes to a significant part of greenhouse gas (GHG) emissions in the construction sector. Therefore, a major approach for ecological and economic improvements lies in durable construction, low emission maintenance and operation as well as in efficient recycling. Building on years of experience in the research department with the ageing of asphalt and bitumen, the first publication of the thesis provides the most recent research results on GHG emissions of road materials. In the paper, the critical production factors are analyzed in detail. In addition, an extensive literature survey provides additional validation of the findings towards evidence based environmental product declarations in accordance with EN 15804. Highlighting a key result, the research has shown that asphalt mix production exhibits a strong dependence on the production conditions, demonstrating the advantage of substituting virgin material with recycled material. In a further step the dissertation provides a comparison of concrete and asphalt roads over the life cycle on a functional level using road sections with different volumes of traffic. As the results have consistently shown the GHG footprint of the asphalt mix and concrete construction becomes relatively insignificant compared to the road traffic emissions during service life.

In the field of road operation, the task of winter maintenance accounts for roughly 20% to 25% of expenditures in alpine countries. It is therefore a good starting point for extensive ecological and economic improvements. Based on substantial knowledge from previous research projects in the field, the dissertation focuses on the development of a suitable set of decision criteria for selecting deicing agents and additives. As a result, the second publication focuses on the development of innovative test methods for temperature- and time-dependent determination of deicing performance. Both, the literature survey, theoretical consideration and material testing in our lab have confirmed the deicing performance and cost efficiency of sodium chloride compared to almost any known deicing chemical. However, as sodium chloride triggers substantial corrosion rates leading to a significant loss in service life and asset value of transport infrastructure, reducing these corrosive effects is key.

As a consequence, the third publication of the thesis compares existing test methods for corrosion assessment according to international standards. As part of a larger FFG project, an efficient corrosion test method is developed providing a high repeatability and sample rates at reasonable costs. The results obtained from these tests provide optical and analytical evidence of the corrosion effect of all known principal deicing agents as well as various corrosion inhibitors on unalloyed steel, galvanized steel, and copper. The results of these tests have been already applied in the field on critical transport infrastructures being able to sufficiently extend the service life with acceptable environmental effects.

The fourth publication is another example of the applicability of the theoretical considerations and the practical experiments both in the laboratory and the field. As the logistics and storability of deicing agents in winter maintenance is key, the fourth paper examines the storability (expressed by pourability) of sodium chloride. From practical experience caking can be a major factor affecting storability and availability. Therefore, the pourability has been tested in regard of anticaking agents and influence of moisture. A further relevant issue in winter maintenance is the amount of residual snow after clearing. Therefore, the dissertation provides a practice-oriented test method for the comparison of different snowplow systems together with an assessment of the efficiency of commonly used equipment. As the quality and durability of snowplow blades comes with a price, special emphasis has been given on practical durability tests for service life estimation. Using a specially developed field test method, the wear under winter conditions is tested and the resistance and efficiency of different snowplow blades is assessed.

In summary, the dissertation covers a wide range of topics providing evidence on ecological and economic improvement potential based on extensive theoretical considerations and tests both in the laboratory and the field.

iii Kurzfassung

Der Straßenbau trägt zu einem erheblichen Teil zu den Treibhausgasemissionen (THG-Emissionen) im Bausektor bei. Ein wesentlicher Ansatz für ökologische und ökonomische Verbesserungen liegt daher in einer langlebigen Bauweise, einem emissionsarmen Unterhalt und Betrieb sowie einem effizienten Recycling. Aufbauend auf jahrelangen Erfahrungen des Forschungsbereichs mit der Alterung von Asphalt und Bitumen liefert die erste Publikation in dieser Dissertation die neuesten Forschungsergebnisse zu den THG-Emissionen von Straßenbaustoffen. In der Arbeit werden die kritischen Produktionsfaktoren im Detail analysiert. Darüber hinaus liefert eine umfangreiche Literaturübersicht eine zusätzliche Validierung der Ergebnisse im Hinblick auf evidenzbasierte Umweltproduktdeklarationen gemäß EN 15804. Ein zentrales Ergebnis der Untersuchung ist, dass die Asphaltherstellung stark von den Produktionsbedingungen abhängt, was den Vorteil der Substitution von Neumaterial durch Recyclingmaterial hervorhebt. In einem weiteren Schritt wurde ein Vergleich von Beton- und Asphaltstraßen über den Lebenszyklus auf funktionaler Ebene anhand von Straßenabschnitten mit unterschiedlichem Verkehrsaufkommen durchgeführt. Die Ergebnisse zeigen durchweg, dass der geringere THG-Fußabdruck der Asphalt- und Betonkonstruktion im Vergleich zu den Emissionen des Straßenverkehrs während der Nutzungsdauer relativ unbedeutend ist.

Im Bereich des Straßenbetriebs macht der Winterdienst in den Alpenländern etwa 20 bis 25% der Ausgaben aus und ist daher ein guter Ansatzpunkt für umfassende ökologische und ökonomische Verbesserungen. Basierend auf umfangreichem Wissen und vorangegangenen Forschungsprojekten in diesem Bereich konzentriert sich die Arbeit auf die Entwicklung von Entscheidungskriterien für die Auswahl von Taumitteln und Additiven. Die zweite Publikation der Dissertation befasst sich daher mit der Entwicklung innovativer Prüfverfahren zur temperatur- und zeitabhängigen Bestimmung der Tauleistung. Sowohl die Literaturrecherche als auch theoretische Überlegungen und Materialprüfungen in unserem Labor haben die Tauleistung und Kosteneffizienz von NaCl im Vergleich zu fast allen bekannten Taumitteln bestätigt. Da NaCl als gängigstes Taumittel jedoch erhebliche Korrosion verursacht, die zu einem substanziellen Verlust an Lebensdauer und Wert der Verkehrsinfrastrukturen führt, ist die Verringerung dieser Auswirkungen von entscheidender Bedeutung.

Die dritte Veröffentlichung der Dissertation vergleicht daher bestehende Prüfmethoden zur Korrosionsbewertung nach internationalen Standards. Im Rahmen eines größeren FFG-Projekts werden effiziente Korrosionsprüfverfahren entwickelt, die eine hohe Wiederholbarkeit und Probenzahl bei vertretbaren Kosten ermöglichen. Die mit diesen Tests erzielten Ergebnisse liefern den optischen und analytischen Nachweis der Korrosionswirkung aller bekannten Haupttaumittel sowie verschiedener Korrosionsinhibitoren auf unlegiertem Stahl, verzinktem Stahl und Kupfer. Die Ergebnisse dieser Tests wurden bereits in der Praxis an kritischen Verkehrsinfrastrukturen angewendet und konnten die Lebensdauer bei akzeptablen Umwelteinflüssen ausreichend verlängern.

Die vierte Publikation ist ein weiteres Beispiel für die Anwendbarkeit der theoretischen Überlegungen und der praktischen Versuche sowohl im Labor als auch im Feld. Da die Logistik und Lagerfähigkeit von Taumitteln im Winterdienst von zentraler Bedeutung ist und deren Festbacken ein wichtiger Faktor zur Beeinträchtigung der Lagerfähigkeit und Verfügbarkeit sein kann, wurde die Lagerfähigkeit (ausgedrückt durch die Rieselfähigkeit) von NaCl im Hinblick auf Antibackmittel und Feuchtigkeitseinfluss getestet. Ein weiterer wichtiger Aspekt des Winterdienstes ist die Menge des Restschnees nach der Räumung. Die Arbeit zeigt daher ein praxisorientiertes Prüfverfahren zum Vergleich verschiedener Schneepflugsysteme. Dabei wurde ein besonderer Schwerpunkt auf praxisnahe Haltbarkeitstests zur Lebensdauerabschätzung gelegt und mit einer speziell entwickelten Feldtest-methode der Verschleiß und die Widerstandsfähigkeit verschiedener Schneeräumleisten bewertet.

Zusammenfassend deckt die Dissertation ein breites Themenspektrum ab und liefert auf der Grundlage theoretischer Überlegungen sowie Tests im Labor und im Feld Hinweise auf ökologische und ökonomische Verbesserungspotenziale.

iv Contents

1 Introduction

1.1 Motivation and problem statement

The Research Center for Road Engineering of the Institute of Transportation at TU Wien deals with theoretical and practical issues in the field of construction, operation and testing technology in road engineering. In the course of this activity, cross-sectional questions such as the consideration of the life cycle of road construction materials as well as in-depth questions on individual tasks from road construction and operation, such as winter maintenance, are included and connected with the framework of the circular economy as shown in Figure 1.

This dissertation is intended to make a scientific and practice-oriented contribution in this field by answering selected questions in both in breadth and in depth. This will be exemplified by the treatment of cross-sectional subjects such as the greenhouse gas (GHG) emissions of asphalt and concrete pavements during their life cycle, as well as by in-depth research on winter maintenance with a focus on deicing agent suitability, corrosion and optimization potential. In all cases, the maxim is to achieve theoretically and experimentally sound results, to advance the findings to the stage of scientific publication and finally to practical applicability.

Figure 1: Framework of this dissertation

Road construction is a significant contributor to GHG emissions in the construction sector, therefore an essential approach for ecological and economic improvements can be found in more durable constructions as well as in the recycling of construction materials. These aspects are elements of the circular economy and, considering the current geopolitical situation, additionally help to reduce the need for new (petroleum-based) raw materials and thus the dependency on global actors. Since building structures are mostly "custom-made" and have long lifetimes, the construction industry falls short in transitioning from linear economy ("make, use, dispose" [1]) to circular economy. The latter is usually applied to short-lived products [2] with static production processes (mass production) and immediate success (recycling rates) in a short time.

Consideration of depleting resources, increased landfilled volumes and environmental impact, a shift to the circular economy with the main objective to "maximizing value at each point of a product's life cycle" [1], seem inevitable and its implementation is addressed by more and more initiatives and studies [3, 4]. Circular economy is also part of the "Sustainable Development Goals of the United Nations" [5] and is included in the EU Action Plan for "a cleaner and more competitive Europe" [6].

The transition from a linear economy to a circular economy is thereby established with Article 11(2)b of the "Waste Framework Directive 2008/98/EC" [7]. This directive sets the following targets for the reuse of construction waste: "by 2020, the preparing for re-use, recycling and other material recovery, including backfilling operations using waste to substitute other materials, of non-hazardous construction and demolition waste excluding naturally occurring material defined in category 17 05 04 in the list of waste shall be increased to a minimum of 70% by weight" [7]. Category 17 05 04 includes soil and stones other than those mentioned in category 17 05 03 (which includes soil and stones containing dangerous substances) [8]. As stated, this excludes (naturally occurring) mineral aggregates from the recycling directive [7]. In Austria, the EU regulation is implemented by the recycling building materials regulation (RBV) [9], which provides precise information on the usability of construction waste and the reasons for its exclusion due to contamination.

In road construction, the reuse of construction materials particularly means the reprocessing of asphalt pavements as reclaimed asphalt pavement (RAP) and concrete pavements as recycled concrete aggregate (RCA). Because asphalt and concrete are used only on the top layers of a road, only the following layers are relevant for recycling:

- Surface layer: asphalt pavement surface layer, top-level concrete layer;
- Binder layer: asphalt pavement binder layer;
- Base layer: asphalt pavement base layer, bottom-level concrete layer.

Because the cement in the concrete layer is cured completely, it cannot be reused in its original state as a binding material. Therefore, concrete pavements can only be reused as RCA. By contrast, RAP has the advantage that the asphalt binder it contains can be reused as a binding material. However, certain aspects of binder ageing have to be considered in case of higher recycling rates or multiple recycling cycles.

Building on the long-term experience of the Institute with the ageing of asphalt mix and asphalt binder, **Paper I** addresses the assessment of these (recycled) materials in terms of GHG emissions, providing value to the research field by systematically answering the ecological and economic question of how much emissions can be reduced at which stage of the production in a sustainable and cost-effective manner.

A basic method for such an environmental assessment is provided by type III ecolabels in accordance with ISO 14025 [10]. These labels regulate how environmental declarations (such as an environmental product declaration (EPD) in accordance with EN 15804 [11]) are made and specify the generation of life cycle assessment (LCA) according to ISO 14040 [12]. This, in turn, provides the framework for a holistic view of resource use (i.e., material input and output flows) of products and processes related to the entire life cycle (i.e., life cycle inventory (LCI)) and enables, with the help of their allocation to impact categories, the estimation of environmental impacts (i.e., life cycle impact assessment (LCIA)).

To create an LCI, material flow analysis is necessary that enables a systematic and clear representation of the material input and output flows in relation to the system boundaries, which can be achieved with specialized software. Following the Austrian standard ÖNORM S2096 [13], the software developed at the Institute for Water Quality, Resource and Waste Management, TU Wien, i.e., STAN, [14] can be used.

Accordingly, the results of the LCA can be structured according to EN 15804 [11] to ensure the comparability of construction products (more precisely, products with the same function) in general, as shown in Figure 2, where the life cycle is subdivided into stages and modules. For a valid EPD, a set of product category rules (PCRs) needs to be specified to ensure the comparability of products. These PCRs set the system boundaries, impact categories (e.g., GHG emissions or climate change), functional units (e.g., tons or cubic meters), and stages and modules (e.g., from cradle to gate: Modules A1-A3) that

must be included. Because PCRs do not exist for all considered production materials at this time (e.g., asphalt mix), the results presented in this dissertation cannot be directly linked to an EPD.

A1 – A3			A4 – A5		B1 – B7							C1 – C4				D
PRODUCT STAGE			CONSTRUCTION PROCESS STAGE		USE STAGE							END OF LIFE STAGE				BENEFITS & LOADS BEYOND SYSTEM BOUNDARY
A1	A2	A3	A4	A5	B1	B2	B3	B4	B5	B6	B7	C1	C2	C3	C4	D
Raw material supply	Transport	Manufacturing	Transport	Construction – Installation process	Use	Maintenance	Repair	Replacement	Refurbishment	Operational energy use	Operational water use	Deconstruction demolition	Transport	Waster processing	Disposal	Reuse, Recovery, Recycling, Potential

Figure 2: Environmental product declaration stages and modules according to EN 15804 [11]

Previous studies on this matter do not utilize this structured approach of EN 15804, often only address individual parameters of the asphalt mix production or rely on data from individual sources and databases.

In this context, the benefit of this work is the identification of influential production factors and the comprehensive validation of emission impacts using a variety of sources for both asphalt and concrete mixes. Subsequently, based on a 30-year life cycle, the GHG emissions of two road sections of concrete and asphalt mix with different traffic volumes are evaluated. This concluding assessment offers potential approaches that indicate precisely where GHG reduction can be achieved and allow further assessment of ecological and economic improvements.

Winter maintenance as part of road operations is responsible for a large part of the allocable workload in road services and is therefore a good starting point for far-reaching ecological and economic improvements. With a variety of issues ranging from the suitability of deicing agents and equipment to the implementation of plowing and spreading operations to the question of law and environment, this dissertation focuses on the in-depth research on the development of suitability criteria of deicing agents, aiming for a safer and more sustainable winter maintenance. Particularly worth highlighting is the development of a new test method for temperature- and time-dependent determination of deicing performance in **Paper II**. Comparisons on a theoretical and practical basis confirm the results obtained and, by knowing the exact effect, pave the way for efficient and resource-conserving use.

However, deicing agents such as sodium chloride (SC) are highly corrosive and, when applied during winter maintenance, cause high consequential damage to metal-based infrastructure due to corrosion. Therefore, the investigation of corrosion in **Paper III** represents a further part of the overall evaluation of deicing agents. Since comparison of existing test methods for corrosion assessment shows unsatisfactory results, as the methods are either cost-intensive or cause little effect, a cost-effective test method is presented. This alternating immersion (AI) method allows good repeatability, comparability and efficiency while maintaining high test rates. The obtained results provide optical and analytical comparison of different deicing agents on unalloyed steel (Fe) and further investigate the suitability of low-cost, sugar-based corrosion inhibitors. Additionally, this dissertation evaluates the combination of low-cost deicing agents with further corrosion inhibitors on Fe as well as on galvanized steel (Fe(Zn)) and copper (Cu). Together with the consideration of health hazards to humans, a recommendation is made. The findings provide both scientific and practical additional value through an unprecedented range of investigations. Currently, the recommendations are already being applied to preserve or extend the life of critical structures and are thus already actively contributing to the achievement of the circular economy.

Another example of the approach to the field is the research on the storability of deicing agents, because caking in silos can under certain circumstances prevent smooth road operation. The effect of

anticaking agents (ACA) and the influence of moisture are well known, but their quantitative assessment is not. For this reason, an in-depth consideration of this aspect in **Paper IV** is part of this dissertation. Along with the hygroscopic properties of deicing agents, the evaluation of pourability is the most important characteristic of storability. An easy to perform and illustrative test method of pourability shows repeatable results and demonstrates the suitability as well as limitations of ACAs as a function of material moisture.

In the course of considering the cross-section of road operations, snow plowing quality can be identified as another influential factor for effective and safe winter maintenance. The developed practice-oriented test method enables a quantifiable assessment of the residual snow quantity after plowing and thus allows a comparison of different plowing systems and equipment. The durability of snowplow blades (mounted at the lower edge of the snow shield as seen in Figure 3) is also of importance for a circular economy analysis, as it determines the material consumption and clearing quality. Using a specially developed field test method, the wear under winter conditions is tested and the resistance of different snowplow blades is measured.

In summary, this dissertation provides answers to ecological and economic questions on both a scientific and practical basis by systematically examining the wide-ranging field of road construction and operation using selected cases.

Figure 3: Removable snowplow blades (denoted by down arrows) on the snowplow

1.2   Objectives and overview

The objectives of this dissertation can be separated into five research questions (RQs), which, together with the concept of circular economy, form the framework of this dissertation.

RQ1   With the increased prevalence of weather events, the need to reduce the GHGs responsible for climate change is in sharp focus.

- o How can the GHG emissions be reduced in road construction?
- o What are the influencing factors in asphalt mix and concrete production?
- o What is the potential of RAP in terms of GHG reduction?
- o How do asphalt and concrete pavements compare at a functional level (i.e., pavement design in dependence of traffic volume) in terms of climate change?
- o What is the proportion of construction- to traffic-related GHGs?

Paper I—"Life cycle assessment of greenhouse gas emissions from recycled asphalt pavement production" addresses part of RQ1 concerning asphalt mix and asphalt pavements. The impact of climate change on the concrete production and the comparison of both pavement materials at a functional level (i.e., pavement design in dependence of traffic volume) are also discussed in this dissertation.

Author contribution: Conceptualization, methodology investigation, data analysis and curation, writing, editing, visualization.

RQ2 Climate change triggers more severe weather events and could lead to more (severe) snowfall in some areas, thus strongly affecting the usage of deicing agents in winter maintenance as a part of road operation.

- o Can alternative deicing agents with better performance reduce the consumption of conventional deicing agents?
- o How can the deicing performance be evaluated?
- o What is the theoretical background of deicing?

Paper II—"Deicing performance of common deicing agents for winter maintenance with and without corrosion-inhibiting substances" answers RQ2 by testing different deicing agents with a newly developed test method for deicing performance (i.e., cryostat-based evaluation of deicing agents (CEDA)). This dissertation additionally compares the results of CEDA with those of the commonly used test method from our tests and the literature.

Author contribution: Conceptualization, methodology investigation, data analysis and curation, writing, editing, visualization.

RQ3 Deicing agents, such as SC, are highly corrosive and reduce the life cycle of metals in transport infrastructure.

- o How can corrosion due to deicing agents be reduced?
- o How can corrosion be tested? What are the laboratory test methods?
- o Is there an inexpensive method to achieve both good deicing performance and low corrosion?

Paper III—"Analysis of metal corrosion methods and identification of cost-efficient and low-corrosion deicing agents" answers RQ3 by comparing three different corrosion test methods and different deicing agents with and without corrosion inhibitors on unalloyed steel. This dissertation further evaluates more inhibitors on unalloyed steel, galvanized steel and copper. Along with the evaluation of the possible hazardous effects on humans, recommendations are presented.

Author contribution: Conceptualization, methodology investigation, data analysis and curation, writing, editing, visualization.

RQ4 If there is less residual snow after clearing with a snowplow, fewer deicing agents need to be spread.

- o How can snow removal quality or the amount of residual snow be evaluated?
- o What is the performance of different snowplow blades in terms of wear and tear?

RQ5 The pourability of deicing agents stored in silos is highly influenced by moisture.

- o How can pourability be evaluated?
- o Are there ways to enhance pourability to stop clogging in silos?

Paper IV—"Optimization potential in operational winter maintenance" addresses both RQ4 and RQ5. RQ4 is answered by introducing an evaluation method for the snow removal patterns using different snowplow equipment and comparing snowplow blades for abrasion and resistance. RQ5 is answered with the help of the "Auslaufbox nach Sonntag" (discharge box) and by reevaluating and summarizing all data in this dissertation.

Author contribution: Conceptualization, methodology investigation, data analysis and curation, writing, editing, visualization.

2   Paper I—Life Cycle Assessment of Greenhouse Gas Emissions from Recycled Asphalt Pavement Production

2.1   General

The paper is attached in the Annex. Additional analysis on GHG emissions of concrete pavements and a comparison of asphalt and concrete road sections beyond the contents of the paper is presented as well.

Abstract: With the growing impact of climate change, there is an increasing need and obligation to reduce the responsible greenhouse gases (GHG) in road construction as well. Using life cycle assessment (LCA) methods, several studies have already separately analyzed individual parameters of the asphalt production process and illustrated potential improvements in terms of GHG reduction. However, the data of most assessments originate from single sources and databases, and as such can offer little validation against unreliable assumptions. For this reason, in addition to conducting separate assessments at quarries, batch asphalt mixing plants, and construction sites in order to collect energy and material consumption data with which to calculate GHG emissions, this work relies on the results of multiple sources found in the literature. Using the structure for environmental product declarations (EPDs) in EN 15804, the results are divided into the different stages of a life cycle and the corresponding modules. This allows for systematic comparison of different products and eliminates previous uncertainties regarding the inclusion of benefits beyond the system boundary. The results show the dominance of asphalt binder in the material footprint and the corresponding advantage of substituting virgin material with recycled material, as well as the influence of material moisture on GHG emissions in the production process. In addition to evaluating the material itself, two road sections with increasing traffic volume (and increasing share of electric mobility) were examined and compared with the traffic-related GHG emissions over a 30-year lifetime. It is confirmed that traffic has a substantially higher share of the total GHG emissions (>95%); however, as its regulation is the responsibility of governments, the construction industry can only bring about improvements in its own sphere in seeking to further climate protection.

2.2   Summary

Many studies on the environmental impact of asphalt mix production can be found in the literature. However, these publications are often based on values from individual databases, focus only on certain factors influencing the production process, or present only results related to specific scenarios, making it impossible to compare construction materials.

This was the decisive point in examining the ecological footprint of the raw materials of asphalt mix production through multiple sources and, where possible, through our investigations of material and energy flows. This was the foundation for conducting an LCA as shown in Figure 4, which provides the framework for calculating the LCI, i.e., the material and energy resources related to the life cycle.
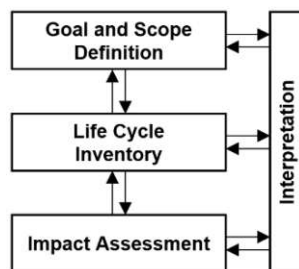
Figure 4: Life cycle assessment framework according to ISO 14040 [12]

The LCI was created using the software STAN [14], which enables material flow analysis according to ÖNORM S2096 [13]. Figure 5 shows the flow diagram consisting of material flows, four input flows (i.e., hot virgin asphalt binder, virgin filler, aggregates, and RAP), and one output flow (i.e., asphalt pavement). The obtained results are then analyzed in detail with the help of a clear structural specification for construction products according to EN 15804.
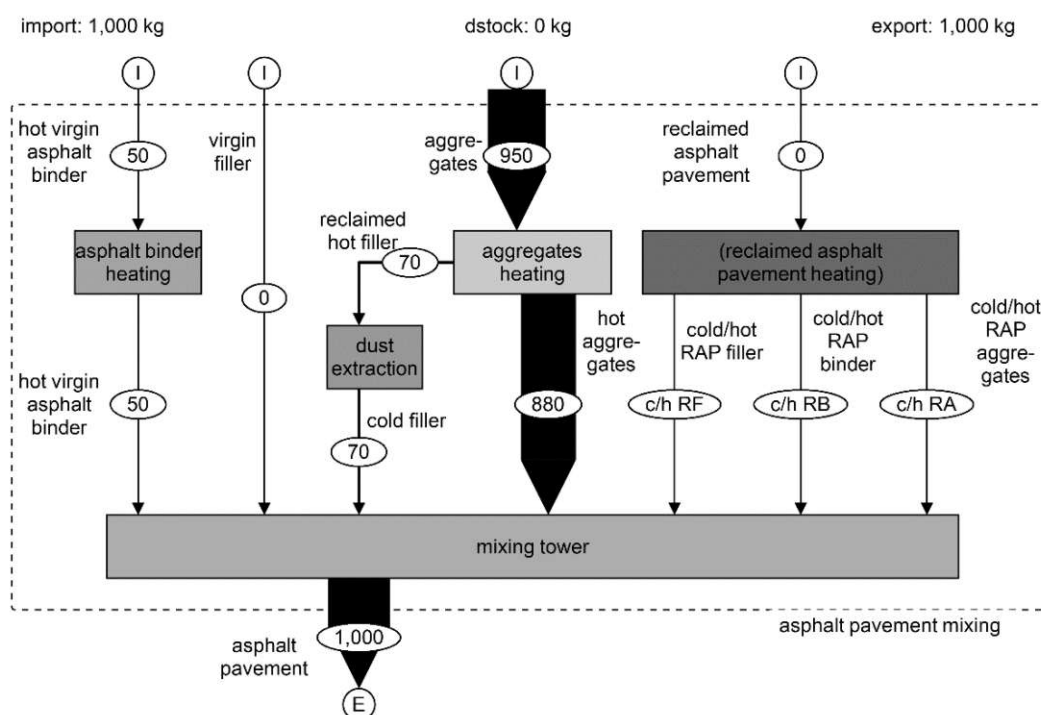
Figure 5: Life cycle inventory of asphalt pavement mixing (software: STAN) [14]

The GHG emissions of asphalt mix production (180°C mix temperature, 5% asphalt binder, 88% aggregate, 7% filler) are shown in Table 1 as a function of mineral aggregate moisture content (0%–5%) and are subdivided into modules according to EN 15804 [11], as shown in Figure 2. Module A1 (extraction of raw materials) has a large share of the total emissions with 20.6 kg CO_2e/t asphalt mix. A breakdown of the individual raw materials within Module A1 is presented in the original article and shows a strong influence of asphalt binder with 18.25 kg CO_2e/t asphalt mix for 50 kg asphalt binder and 2.38 kg CO_2e/t asphalt mix for 950 kg mineral aggregates.

Together with Modules A2 and A3, the cradle-to-gate approach can be formed (A1–A3) and totals between 36.6 and 47.1 kg CO_2e/t asphalt mix, depending on the moisture content of the mineral aggregates. If other life cycle stages are included (i.e., transport, installation, removal, and landfill) apart from the use stage (B1–B7: repair, maintenance, and operational road service), the GHG impact increases to 44.0–54.5 kg CO_2e/t. The transport distance of materials was assumed to be 25 km (except for the transport distance of the asphalt binder to the mixing plant, which is 100 km).

Table 1: GHG [kg CO₂e/t of asphalt pavement] of all modules according to EN 15804 [Paper I]

Moist. Aggr.	A1	A2	A3	A4	A5	B1– B7	C1	C2	C3	C4*	D	GHG Total
0%			13.8									44.0
1%			15.9									46.1
2%	20.6	2.2	18.0	1.9	1.4	-	2.1	1.9	0	0.1	-	48.2
3%			20.1									50.3
4%			22.2									52.4
5%			24.3									54.5

Therefore, the total transport share of GHG is 6 kg CO_2e/t (for A2, A4, and C2) for the aforementioned distances. If the distance is increased to 100 km for all materials and modules (A2, A4 and C2), then the GHG impact increases to 22.5 kg CO_2e/t and will become the dominating factor of GHG emissions in the production process. The GHGs of the reuse, recovery, recycling, and potential stage were calculated for a mix containing 30% RAP. The assumed composition of RAP (i.e., 3% asphalt binder, 88% aggregate, and 9% filler) substitutes 291 kg mineral aggregates and 9 kg asphalt binder, thus reducing the emissions by 3.90 kg CO_2e/t (of which 3.29 kg CO_2e/t accounts for the saved virgin asphalt binder).

Based on the results of the initial scenario, as shown in Table 1 (5% moisture and 25 km distance = 54.5 kg CO_2e/t), two two-lane road sections with different traffic volumes (7 m total width without shoulder) were considered. One section was designed for a traffic load of 1 million equivalent single-axle loads (ESALs), and the other section was designed for a traffic load of 52.5 million ESALs, which resulted in design type LK1.3 asphalt pavements (for 0.4–1.3 million ESALs) and LK82 (for 42–82 million ESALs) according to the Austrian guidelines [15].

The total GHG impact also includes the production and construction of unbound base layers and amounts to 284–408 kg CO_2e/m road. In comparison, the traffic on these road sections with a 2% increase p.a. leads to 9,800 and 135,000 kg CO_2e/m road sections cumulatively for 30 years. Although traffic cannot be directly linked to the asphalt (road) product, a comparison helps in estimating the orders of magnitude. Irrespective of this and the fact that the industry sector in Austria has already reduced its GHG footprint by 11% in the last 30 years, the emissions of the transport sector increased by 50% [16]. Thus, measures to reduce GHG emissions and improve the material cycle (keyword: circular economy) must be taken now in asphalt mix production to be able to continue producing low-cost and high-quality materials in the future.

2.3　Additional results—comparison of asphalt and concrete pavements

As mentioned previously, the published article includes an evaluation of the GHG emissions of asphalt mix production and two road sections with different traffic volumes. Given that the concrete pavement is used, particularly in the high-level road networks, a comparison of both asphalt and concrete design types seemed reasonable.

For asphalt pavements, no distinction was made in different mix designs for individual layers (i.e., surface layer, binder layer, or base layer) because their characteristics, particularly the asphalt binder content, with its high impact on GHG emissions, differ only slightly. Assuming an average asphalt binder content of 5 m% (usually ranging between 3.5 and 6.5 m%), each additional percentage point would lead to an increase of approximately 3.7 kg CO_2e/t asphalt mix.

However, concrete mix designs for pavements are more strongly differentiated into highly resistant top-layer concrete with a higher cement content (usually 450 kg/m³ concrete or 19.5 m%) and low cement-containing bottom-layer concrete (usually 350 kg/m³ concrete or 14.6 m%). This differentiation ensures cement savings through thin top-layer concrete slabs on the road surface and thicker bottom-layer concrete slabs underneath. A list of typical top- and bottom-layer concrete mix designs is given in Table 2.

Table 2: Mix design of 1 m³ concrete

	Top-layer concrete [kg/m³]	Bottom-layer concrete [kg/m³]
Coarse aggregates	1,162.00	1,136.00
Fine aggregates	522.00	757.00
Cement	450.00	350.00
Water	175.00	152.00
Air-entraining agent	0.68	0.63
Superplasticizer	1.80	0.00
Total	2,311.48	2,395.63

Analogous to the approach for asphalt pavements in the article, the functional unit cubic meter is used for the production of concrete for concrete pavements, and its life cycle from cradle to grave is represented by Modules A1–A5, as well as Modules C1–C4, according to EN 15804 [11]. This assumes an untreated, unreinforced, and undoweled construction method without slab formation. Only the materials (i.e., anchors, dowels, joint filling material, and evaporation protection agent) and processes (i.e., application of evaporation protection agent, joint cutting, and brushing surface) related to the concrete surface of the road sections are included in the calculation.

Module A1—Raw material supply

The footprint of coarse and fine aggregates is assumed as per the original article, 2.51 kg CO_2e/t aggregate with a standard deviation of 0.49 kg CO_2e/t. Table 3 shows the CO_2e footprint of cement from different sources. Removing the lowest and highest values, a mean value of 696 kg CO_2e/t cement was calculated, with a large deviation of 92 kg CO_2e/t presumably because of different production efficiencies and transport distances, similar to the asphalt binder.

Table 3: List of different sources for the GHG footprint of cement

Source	ID [Reference]	kg CO_2e/t
IBU—Average Austrian cement	EPD-VOZ-20200025-IAG1-DE [17]	493.0
Cemsuisse—Swiss CEM II/B	Cem-13-01 CEM II/B [18]	557.0
Cemsuisse—Average Swiss cement	Cem-13-01 Durchschnitt [18]	573.0
Ökobaudat—Average German cement	d2e01b0a-bfdf-412a-996e-20d592df0d5f [19]	587.0
Cemsuisse—Swiss CEM II/A	Cem-13-01 CEM II/A [18]	589.0
IBU—Portland Fly Ash CEM II/A-V 42.5 N	EPD-HCG-20160235-CAD1-EN [17]	678.0
Ökobaudat—CEM II/B	df40fb5f-9a10-422d-8d95-69a3af9d0d96 [19]	719.8
IBU—Portl. Comp. CEM II/A-M (T-L) 42.5 R	EPD-KNT-20200211-CAA1-EN [17]	728.0
ProBas—Cement	587C9D45-B4CF-4912-9939-CA438D91E543 [20]	752.0
IBU—Portland Limestone CEM II/A-LL 42.5 R	EPD-HCG-20190045-CAA1-EN [17]	759.0
Ökobaudat—CEM II 32.5	63f50bbb-8257-47fe-93d5-ca5ad26e5187 [19]	782.7
Ökobaudat—CEM II 42.5	08d59fb4-e75c-4f31-82f2-caa0bcaa5f04 [19]	795.2
IBU—UK Average Portland Cement	EPD-MPA-20170159-CAG1-EN [17]	830.0
Ökobaudat—Cement CEM II/A	bff1b0ac-5d16-4cce-9e5d-a3269eff093c [19]	875.5
Mean		695.9
SD		92.3

Drinking water production is strongly dependent on location because, in some regions, water is taken directly from springs, whereas in other regions, it needs to be treated. Although drinking water treatment is rarely necessary in Austria; the average value for Europe with and without treatment of 0.15 kg CO_2e/t water is used, as shown in Table 4.

Table 4: GHG footprint of drinking water

Source	ID [Reference]	kg CO_2e/t
Ökobaudat—Thinkstep—Tap water	ce3057d1-3371-47b4-a982-a1c42c2c6a85 [19]	0.13
Ecoinvent—Tap water production	Underground water w/o treatm. (Europe w/o CH) [21]	0.17
Ecoinvent—Tap water production	Underground water without treatment (CH) [21]	0.04
Ecoinvent—Tap water production	Conventional treatment (Europe w/o CH) [21]	0.27
Ecoinvent—Tap water production	Conventional treatment (CH) [21]	0.12
Mean		0.15
SD		0.07

Because special agents and materials are rarely assessed ecologically, only one source for the GHG footprint of air-entraining agents and superplasticizers could be identified as shown in Table 5. Calculations based on only one source are unsatisfactory, but the influence on the overall result is small because of the small amounts added. For example, the addition of 1.68 kg superplasticizer with 1,530 kg CO_2e/t leads to 2.6 kg CO_2e/m³ concrete (or 1.1 kg CO_2e/t concrete).

Table 5: GHG footprint of special agents for concrete

Source	ID [Reference]	kg CO_2e/t
IBU—Air Entrainers Europe	EPD-EFC-20210193-IBG1-EN [17]	439
IBU—Plasticizers and Superplasticizers	EPD-EFC-20210198-IBG1-EN [17]	1,530

A summary of the GHG footprint (i.e., min, mean, and max) for all raw materials is shown in Table 6.

Table 6: Summary of GHG emissions including bandwidth

	CO_2e footprint in kg CO_2e/t		
	Min	Mean	Max
Coarse aggregates	2.02	2.51	3.00
Fine aggregates	2.02	2.51	3.00
Cement	603.65	695.89	788.14
Water	0.07	0.15	0.22
Air-entraining agent	329.25	439.00	548.75
Superplasticizers	1,147.50	1,530.00	1,912.50

By multiplying the data (i.e., mean) in Table 6 with the masses of the concrete mix design in Table 2, the data presented in Table 7 and Figure 6 can be derived. Thus, the possible range of GHG emissions for bottom-layer concrete is 215–282 kg CO_2e/m³ and 277–364 kg CO_2e/m³ for top-layer concrete. The conversion of these values (i.e., mean) using the corresponding density of the layers of 2,311 and 2,396 kg/m³ results in 103.8 and 138.6 kg CO_2e/t concrete, respectively.

Table 7: Total GHG emissions of concrete including bandwidth

	Top-layer concrete in kg CO_2e/m³			Bottom-layer concrete in kg CO_2e/m³		
	Min	Mean	Max	Min	Mean	Max
Coarse aggregates	2.35	2.92	3.49	2.29	2.85	3.41
Fine aggregates	1.05	1.31	1.57	1.53	1.90	2.27
Cement	271.64	313.15	354.66	211.28	243.56	275.85
Water	0.01	0.03	0.04	0.01	0.02	0.03
Air-entraining agent	0.22	0.30	0.37	0.21	0.28	0.35
Superplasticizers	2.07	2.75	3.44	0.00	0.00	0.00
Total [kg CO_2e/m³]	277.34	320.46	363.57	215.32	248.61	281.91
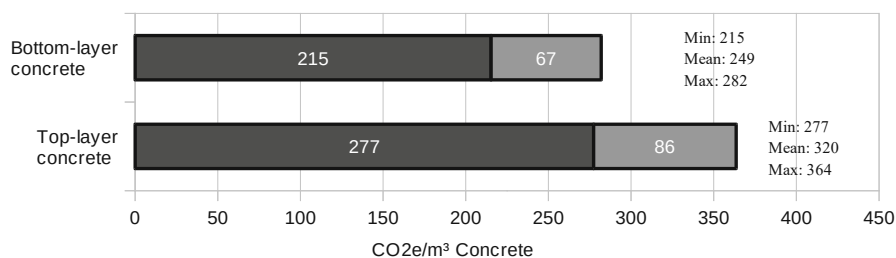
Figure 6: Comparison of the GHG emissions of concrete

Module A2—Transport of raw materials

For Module A2, the same transport distances as in the original article are specified for asphalt mixes, i.e., 25 km for mineral aggregates and 100 km for cement and admixtures, analogous to the asphalt binder. Compared with asphalt binder, cement has a higher influence on the footprint of concrete because of its higher share in the mix. Based on the general transport emissions of 0.075 kg CO_2e/t-km, the consequent results of the individual materials are shown in Table 8.

Table 8: Transport distances and GHG emissions of Module A2

		CO_2e footprint in kg CO_2e/t	
	Transport [km]	Top-layer concrete [kg CO_2e/t]	Bottom-layer concrete [kg CO_2e/t]
Coarse aggregates	25	2.18	2.13
Fine aggregates	25	0.98	1.42
Cement	100	3.38	2.63
Water	0	0.00	0.00
Air-entraining agent	100	0.01	0.00
Superplasticizers	100	0.01	0.00
Total [kg CO_2e/t]	–	2.83	2.58
Total [kg CO_2e/m³]	–	6.55	6.18

Modules A3–A5—Construction, transport to the building site, and paving

Module A3 represents the concrete production and is, in contrast to asphalt mix production, a simple process as the materials are only mixed and not heated. This process is usually done on-site using a mobile mixer powered by diesel generators. With an average mixing capacity of 180 m³/h and a consumption of 80 L diesel/h, a specific consumption of 0.44 L diesel/m³ concrete is obtained. For the top-layer and bottom-layer concrete, GHG emissions of 1.39 kg CO_2e/m³ or 0.60 and 0.58 kg CO_2e/t, respectively, are detected.

Because the concrete is mixed at the construction site, the transport distance of 5 km in Module A4 is quite short, leading to GHG emissions of 2.00 and 2.15 kg CO_2e/m³ (0.87 and 0.90 kg CO_2e/t) for the top-layer and bottom-layer concrete, respectively.

In Module A5, the concrete is paved with slipform pavers, with the bottom-layer concrete being placed and vibrated first, followed directly by the top-layer concrete. At the same time, the dowels and tie bars are placed, and the surface is smoothed afterward. Because the installation of dowels and anchors cannot be modeled separately from paving the concrete, Module A5 includes the placement process (or the associated energy input) but not the materials anchors and dowels. An overview of the results is given in Table 9.

Table 9: GHG emissions of Modules A3–A5

Module	Top-layer concrete [kg CO_2e/m³]	Bottom-layer concrete [kg CO_2e/m³]
A3	1.39	1.39
A4	2.00	2.15
A5	1.19	1.19

Modules C1–C4—Deconstruction, transport, waste processing, and disposal

For the removal of concrete pavement, which is represented by Module C1, a suitable breaker machine (consuming 11 L diesel/h) is used to break up the concrete slabs into small fragments, one excavator (consuming 23 L diesel/h) is used to further crush the material, and one is used to load the trucks. At a removal rate of 80 m³/h (8–9 trucks/h) and a consumption of 57 L diesel/h, the specific GHG emissions of the deconstruction module are calculated to be 2.24 kg CO_2e/m³ (0.97 and 0.93 kg CO_2e/t for the top-layer and bottom-layer concrete, respectively). The transportation (with a transport distance of 25 km) of the material to the landfill results in 10.02 and 10.76 kg CO_2e/m³ (4.33 and 4.49 kg CO_2e/t) of top-layer and bottom-layer concrete, respectively.

Waste treatment is unnecessary because reclaimed concrete can be completely landfilled. Only one wheel loader is needed for landfilling (250 t/h, 18.5 L diesel/h), emitting 0.23 kg CO_2e/t. Reclaimed concrete is nearly completely reused as RCA; therefore, only 1% of the volume is landfilled [22]. This leads to an average GHG impact of 0.02 kg CO_2e/m³ or 0.01 kg CO_2e/t. A summary of this module can be found in Table 10.

Table 10: GHG emissions of Modules C1–C4

Module	Top-layer concrete [kg CO_2e/m³]	Bottom-layer concrete [kg CO_2e/m³]
C1	2.24	2.24
C2	10.02	10.76
C3	0.00	0.00
C4	0.02	0.02

Summary of Modules A1–C4

Table 11 summarizes the results presented in the previous subchapters.

Table 11: GHG emissions of Modules A1–C4 of concrete

Module	Top-layer concrete [kg CO_2e/m³]	Bottom-layer concrete [kg CO_2e/m³]
A1	320.46	248.61
A2	6.55	6.18
A3	1.39	1.39
A4	2.00	2.15
A5	1.19	1.19
B1–B7	NA	NA
C1	2.24	2.24
C2	10.02	10.76
C3	0.00	0.00
C4	0.02	0.02
Total A1–C4 [kg CO_2e/m³]	343.87	252.55
Total A1–C4 [kg CO_2e/t]	148.77	113.77

Surface-related processes and materials

When concrete is paved, anchors and dowels are also set, the surface is cured, evaporation protection agent is applied, and joints are cut and filled. These processes and materials are area-related and, therefore, dealt with separately in this subsection. For this purpose, 1 m of a two-lane road with a total width of 7 m is assumed, analogous to the cross-section considered in the original paper. First, the individual processes are discussed in detail. Then, a clearer presentation of the results in tabular form is provided.

Anchors and dowels

As shown in Figure 7, dowels (steel bar, 25 × 500 mm, 1.93 kg) are installed at 25 cm intervals in the transverse joint, and 3 anchors (steel bar, 14 × 700 mm, 0.85 kg) are installed in the longitudinal joint for each field length (usually 5 m) [23]. For a 7 m-wide road of length 1 m, there will be 28 dowels and 0.60 anchors, i.e., 54.45 kg steel. With a CO_2e footprint of 435 kg CO_2e/t reinforcing steel according to Table 12, the GHG impact from the production of anchors and dowels (Modules A1–A3) is 23.69 kg CO_2e/m road cross-section. Transporting the materials to the construction site (with a transport distance of 25 km), installing them into the fresh concrete and removing them together with concrete (already considered in concrete pavement and removal, discussed previously), and disregarding landfilling lead to a CO_2e footprint of 23.73 kg CO_2e/m road cross-section.

Table 12: GHG footprint of reinforcing steel/rebar

Source	ID [Reference]	kg CO_2e/t
Bau EPD GmbH—Austrian reinf. steel/rebar	00001158 [24]	442
ift Rosenheim GmbH—German reinf. steel/rebar	EPD-BS-10.2 [25]	240
The International EPD System—Cold rolled rebars	S-P-01086 [26]	395
Ecoinvent 3.7—Reinforcing steel production AT	Reinforcing steel production (AT) [21]	464
Ökobaudat—Reinforcing steel/rebar	e9ae96ee-ba8d-420d-9725-7c8abd06e082 [19]	635
Mean		435
SD		127
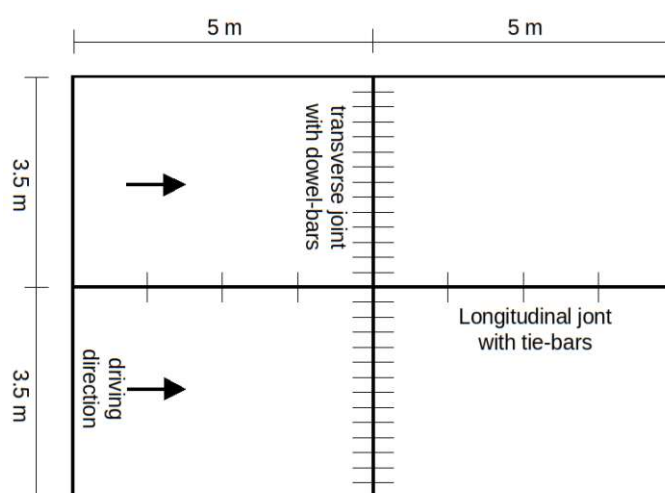
Figure 7: Concrete field dimensions [23]

Surface treatment

To produce an exposed aggregate concrete surface, after the application of the evaporation protection agent (paraffin-based retarder, 200 g/m²), the surface is brushed and again treated with the evaporation protection agent (paraffin-based retarder, 200 g/m²). For this particular agent, no calculations of the CO_2e footprint could be found in the literature; thus, the results of paraffin production were used, which is 654 kg CO_2e/t according to the ecoinvent database (paraffin production in Europe [21]).

A consumption of 2.8 kg evaporation protection agent for the total cross-section, transport distance of over 100 km to the construction site, and application utilizing a curing truck (1,000 m²/h, 5 L diesel/h) result in 1.95 kg CO_2e/m road cross-section. The exposed aggregate concrete surface is produced by a special sweeper (1,000 m²/h, 10 L diesel/h) and results in a 0.22 kg CO_2e/m road cross-section.

Joint production and filling

Two joint cutters (8 L diesel/h each) and one grout pot for heating the asphalt binder (5 L diesel/h) are used to cut and fill the joints. At a cutting rate of 50 m/h and a filling rate of 0.252 kg asphalt binder/m (30×8 mm joint filling with an asphalt binder density of 1,050 kg/m³), the CO_2e footprint of the asphalt binder according to the article (365 kg CO_2e/t [Paper I]) results in a total impact of 3.39 kg CO_2e/m road cross-section. The average joint length results from the geometry of a field with 5 m length (2×3.5 m) and 7 m width to $1 + {}^7/_5 = 2.4$ m.

Overview

A comprehensive list of all surface-related materials and processes is given in Table 13, which altogether results in a GHG impact of 29.29 kg CO_2e/m road cross-section.

Table 13: GHG emissions of Modules A1–C4 of surface-related processes and materials

Module	Dowel and tie-bars [kg CO_2e/m section]	Surface retarder [kg CO_2e/m section]	Surface brushing [kg CO_2e/m section]	Joint cutting and filling [kg CO_2e/m section]
A1–A3	23.69	1.83	0.00	0.22
A4	0.04	0.01	0.00	0.00
A5	0.00*	0.11	0.22	3.16
B1–B7	Not considered	Not considered	Not considered	Not considered
C1*	0.00	0.00	0.00	0.00
C2*	0.00	0.00	0.00	0.00
C3*	Not considered	Not considered	Not considered	Not considered
C4*	Not considered	Not considered	Not considered	Not considered
Total A1–C4	23.73	1.95	0.22	3.39

*Already included in concrete production.

Comparison of construction-type asphalt with construction-type concrete

The previous findings provide a basis for the comparison of both asphalt and concrete pavement construction materials. Because of the different material properties, a comparison at the functional level must be made. For this purpose, two road sections with different traffic volumes are compared, and based on their traffic load expressed by ESALs, the corresponding construction type to withstand the calculated traffic load according to the Austrian guidelines [15] was selected, as follows:

- A low-traffic-volume section with an annual average daily traffic (AADT) increase of 2% p.a. from 2,600 to 4,700 in 30 years. This is equivalent to 1 million accumulated ESALs and leads to the asphalt pavement construction type AS1-LK1.3, which is designed for 0.4–1.3 million ESALs, and concrete pavement construction type BE1-LK2.1, which is designed for 0.6–2.1 million ESALs.
- A high-traffic-volume section with an AADT increase of 2% p.a. from 30,000 to 54,000 in 30 years. This is equivalent to 52.5 million accumulated ESALs and leads to the asphalt pavement construction type AS1-LK82, which is designed for 42–82 million ESALs, and concrete pavement construction type BE1-LK89, which is designed for 40–89 million ESALs.

The composition of the construction type defined in each case is shown in Figure 8.
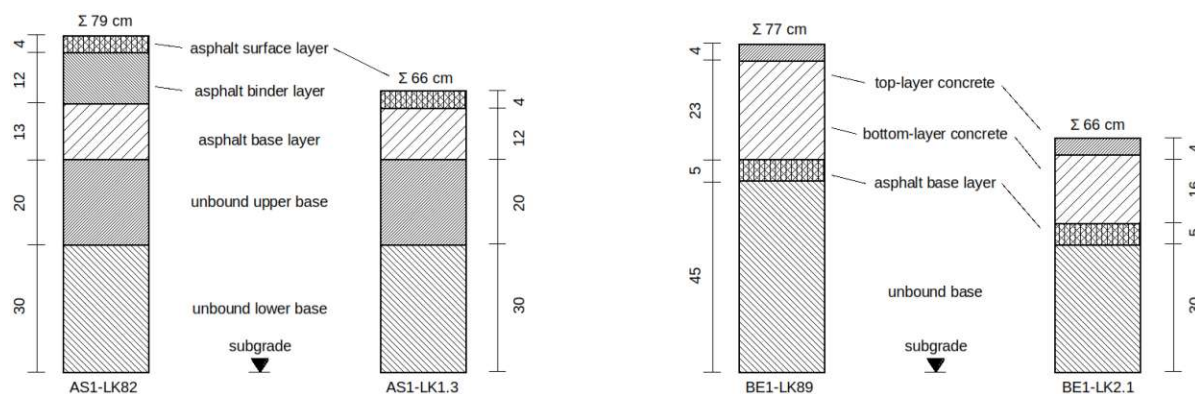
Figure 8: Composition of the construction types for asphalt and concrete pavements (height in cm) [15]

In the original article, for the asphalt pavement construction types AS1-LK82 and AS1-LK1.3 with two renewal measures each (i.e., replacement of the asphalt surface layer of 4 cm every 10 years), the GHG emission impact for a life cycle of 30 years is 408 and 284 kg CO_2e/m road cross-section with 7 m width, respectively.

It is assumed that no maintenance measures are required for the concrete pavement construction types BE1-LK89 and BE1-LK2.1 and improvements to reinstate friction of the concrete surface are neglected. Before a comparison can be made, the layers below the concrete pavement must be considered. For the 5 cm-thick asphalt mix layer, a CO_2e footprint of 54.5 kg CO_2e/t (modules A1–C4, as in the article considering the asphalt pavement) was assumed. Emissions for the unbound base course (density of 2,100 kg/m³) were calculated by paving aggregates (A1–A3 = 2.51 kg CO_2e/t), as in the original article. For this purpose, the aggregates are transported 25 km to the construction site and compacted there with 0.19 L diesel/t. The excavation is done by an excavator (144 t/h and 20 L diesel/h) and transported with 6 trucks/h to a landfill 25 km away, where only a small part is landfilled as nonreusable. An overview of the individual modules is given in Table 14.

Table 14: GHG emissions of Modules A1–C4 of the unbound base layer

Module	Unbound base layer [kg CO_2e/m³]
A1–A3	5.27
A4	3.94
A5	1.25
B1–B7	Not considered
C1	0.92
C2	3.94
C3	Not considered
C4	Not considered
Total A1–C4	15.41

With the help of the data provided in Table 12 to Table 14, the total GHG emissions of the concrete pavement construction types BE1-LK89 and BE1-LK2.1 can be calculated, as depicted in Table 15.

Table 15: GHG emissions of the concrete construction types BE1-LK89 and BE1-LK2.1

Module	Height [cm]	BE1-LK89 [kg CO_2e/m]	Height [cm]	BE1-LK2.1 [kg CO_2e/m]
Surface-based	–	29.29	–	29.29
Top-layer concrete	4	96.28	4	96.28
Bottom-layer concrete	23	438.80	16	305.25
Asphalt base layer	5	47.69	5	47.69
Unbound base layer	45	48.55	30	32.37
Total A1–C4	77	660.62	55	510.89

The analogous procedure with data from the original article leads to Table 16, which shows the total GHG emissions of the asphalt pavement construction types AS1-LK82 and AS1-LK1.3.

Table 16: GHG emissions of the asphalt construction types AS1-LK82 and AS1-LK1.3 [Paper I]

Module	Height [cm]	AS1-LK82 [kg CO_2e/m]	Height [cm]	AS1-LK1.3 [kg CO_2e/m]
2× surface rehabilitation	–	76.30	–	76.30
Asphalt surface layer	4	38.15	4	38.15
Asphalt binder layer	12	114.45	–	–
Asphalt base layer	13	123.99	12	114.45
Unbound base layer	50	54.83	50	54.83
Total A1–C4	79	407.72	66	283.73

A graphical comparison of the results shown in Table 15 and Table 16 is depicted in Figure 9. Notably, asphalt pavement construction emits approximately 40–50% of GHGs compared with concrete pavement construction: 207–511 and 331–661 kg CO_2e/m road cross-section with a width of 7 m.

When considering a 30-year service life, renewal measures for asphalt pavements are being considered, as described previously (twice in this period). The balance of the asphalt pavement worsens by 76 to 284 or 408 kg CO_2e for the aforementioned sections. For concrete pavements, it is assumed that no significant rehabilitation is required. Maintenance of the joints by recutting (assumption: 25% expense of new production) and refilling every 10 years emits only approximately 2 kg CO_2e/m road cross-section and is, therefore, neglected.
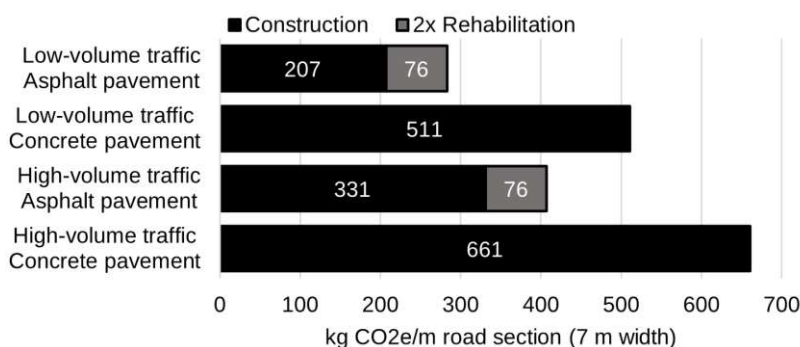
Figure 9: Comparison of the GHG emissions of asphalt and concrete pavements

2.4   Conclusion and outlook

An ecological assessment of GHG emissions is presented in the original article for asphalt pavements and in this dissertation for concrete pavements. The basis for this comparative assessment is the modular structure for EPDs of EN 15804 [11], which provides subdivision into production, transport, paving, and removal and handling of the material.

If considering the GHG emissions caused by traffic on this road section, then the major influence of the transport sector becomes apparent, which is also supported by the findings in the literature [27]: As calculated in the article, in 30 years, depending on the electromobility share, 8–10 t CO_2e/m road cross-section will be emitted on the low-traffic-volume section or 109–135 t CO_2e/m road cross-section will be emitted on the high-traffic-volume section. For comparison, construction emissions of asphalt and concrete pavements are between 0.28 and 0.51 t CO_2e/m road cross-section for the low-traffic-volume section and between 0.41 and 0.66 t CO_2e/m road cross-section for the high-traffic-volume section.

Therefore, it makes sense not only to consider the GHGs of the construction itself but also to look at the impact of the construction design in terms of GHG emissions on the transport sector (i.e., on the vehicles driving over it). In this context, two components influence fuel consumption, i.e., the longitudinal evenness of the road surface and the rolling resistance due to the surface structure and

deflections [28]. However, the results in the literature regarding this vary from having a negligible impact on fuel consumption and GHG emissions [29] to mildly indicating an advantage of (rigid) concrete pavements due to higher stiffness [30]. Regardless of the magnitude of the influence, asphalt pavement constructions show lower stiffness, particularly in the hot summer months, causing higher deflections and thus higher fuel consumption [30]. Building on this work, the next step is to assess the impact of these materials on the transport sector.

3   Paper II—Deicing Performance of Common Deicing Agents for Winter Maintenance with and without Corrosion-Inhibiting Substances

The paper is attached in the Annex. Additional comparisons of the test results with results from literature as well as a detailed experimental description of the newly developed method, which go beyond the content of the paper, are also presented.

Abstract: Sodium chloride is by far the most cost-effective deicing agent in winter road maintenance and therefore is used by road authorities worldwide. However, chloride ions foster high corrosivity which significantly reduces the service lifetime of metals and reinforced concrete of transport infrastructures. Hence, a holistic evaluation with the main criteria of deicing performance and corrosion is demanded and, if possible, alternatives should be considered. This paper focuses on the deicing performance of sodium chloride and other common acetate-, carbonate-, chloride- and formate-based deicing agents. A newly developed test method is presented enabling high volume testing at good repeatability. From its results a nonlinear model is derived to predict deicing performance up to five hours after application. Subsequently, this model is compared with both existing empirical and theoretical approaches for evaluating the deicing performance. In addition, the impact of added corrosion-inhibiting substances like sugars on deicing performance is investigated. Finally, a comparison of all tested substances in terms of corrosivity and deicing performance is presented, with corrosion being separately investigated in detail in another paper.

3.1   Summary

Worldwide, sodium chloride (SC) is commonly used for removing snow and ice or preventing both from sticking to the road surface. However, particularly in areas with metallic infrastructure, SC leads to problems in the long term because of its corrosive effect. Alternative deicing agents can reduce this circumstance, but they must be evaluated holistically to enable safe use in winter road maintenance. To this end, the properties of alternative deicing agents in terms of skid resistance, storability, environmental impact, corrosiveness, deicing performance, and costs must be investigated.

Nevertheless, deicing performance is the most important characteristic of deicing agents. For this reason, the original article compares the theoretical approach for assessing deicing performance with the results of practical methods. The theoretical approach is based on the freezing point depression, which is determined based on the colligative properties (molar mass) and dissociative properties (Van't Hoff factor) of the deicing agent solution. For practical evaluation, the SHRP H-205.1 test [31], [32] is usually used, wherein ice plates are prepared, a certain amount of deicing agent is applied, and the thawed liquid is drained off after a certain time. The quotient of the deiced quantity and the applied quantity of the deicing agent gives the deicing performance as a function of temperature and exposure time. Because this test underestimates the deicing performance (which has also been reported in the literature [36]–[39]) and is time-consuming, a new test method (i.e., CEDA) was codeveloped with the Institute of Materials Chemistry, TU Wien to increase both the accuracy and test speed.

In this test, a defined amount of water is filled into the small wells of a reaction plate and frozen to a specific temperature using a cryostat. Then, different amounts of deicing agent are applied to each well and the condition of the samples is photographed every minute. For the evaluation, the images are manually reviewed, and the condition of each sample is marked as "completely deiced" or "(partly) frozen". With the observed time from adding the deicing agent to the state "completely deiced" and the amount of deicing agent applied, the deicing performance can be represented in mass deiced per mass deicing agent [g/g]. Thus, as in the SHRP test, the time curve of the deicing performance can be shown selectively. Using a nonlinear regression model, the relationship between deicing performance and exposure time can be described quantitatively, and a 95% confidence interval and 95% prediction interval can be calculated.

The direct comparison of the regression model of both methods for SC at a temperature of −5°C shows that, for long exposure times (>3 h), the CEDA method with 12.7 g/g (= 12.7 times the deicing agent is deiced) is closer to the theoretical maximum of the deicing performance (11.7 g/g) than the results of the SHRP test with 9.5 g/g.

Given the suitability of the newly developed method, other deicing agents (in the article, magnesium chloride (MC), calcium chloride (CC), potassium carbonate (PC), as well as acetates and formates of potassium and sodium) were tested.

SC shows the best deicing performance (12.7 g/g), followed by sodium formate (SF; 11.4 g/g) and potassium acetate (PA; 10.6 g/g). Because SC is the cheapest of these agents, simple sugars that inhibit the corrosive effect (refer Paper III) have been added. The influence of these sugars on the deicing performance is noticeable but reduced only by the expected factor by which the mass of SC has been replaced by sugar (i.e., instead of 100% SC, e.g., 92% SC + 8% sugar). However, the fact that the combination of SC and mannose (SC + Man) shows lower deicing performance than other sugars (i.e., maltose, arabinose, and glucose) is unknown. A summary of all tested agents is provided in Table 17.

Table 17: Maximum deicing performance at 300 min [Paper II]

Agent	Chemical formula	Abbreviation	DP at −5°C [g/g]
Sodium chloride	$NaCl$	SC	12.75
SC + 8% maltose monohydrate	$NaCl + C_{12}H_{22}O_6 \cdot H_2O$	SC + Mal	11.75
SC + 8% arabinose	$NaCl + C_5H_{10}O_5$	SC + Ara	11.63
SC + 8% glucose	$NaCl + C_6H_{12}O_6$	SC + Glu	11.62
Sodium formate	$HCOONa$	SF	11.41
Potassium acetate	CH_3COOK	PA	10.59
SC + 8% mannose	$NaCl + C_6H_{12}O_6$	SC + Man	10.37
Calcium chloride dihydrate	$CaCl_2 \cdot 2H_2O$	CC	8.28
Sodium acetate	CH_3COONa	SA	8.16
Magnesium chloride hexahydrate	$MgCl_2 \cdot 6H_2O$	MC	6.83
Potassium carbonate	K_2CO_3	PC	6.74
Potassium formate	$HCOOK$	PF	6.38

3.2 Additional results

As mentioned previously, the SHRP H-205.1 method underestimates the actual deicing performance. In the article, this has already been described using SC; this circumstance will also be demonstrated using sodium acetate (SA) and MC. Figure 10 shows the comparison of the results of the SHRP method with that of the CEDA method at −5°C. The results of the CEDA method are taken from the article. The regression model is based on Equation (1), and the parameters of the model are shown in Table 18.

$$y(t) = b_0 \times \left(1 - e^{(-b_1 \times t)}\right) \tag{1}$$

Table 18: Parameters of the regression models at −5℃

Agent–Model	b_0	b_1	$t = 60$ min	$t = 120$ min
SC–SHRP	9.48	0.015	5.63	7.91
SC–CEDA	12.75	0.018	8.42	11.28
SA–SHRP	6.07	0.023	4.54	5.69
SA–CEDA	8.16	0.010	3.68	5.70
MC–SHRP	2.92	0.048	2.76	2.91
MC–CEDA	6.83	0.017	4.37	5.94

Thus, the maximum deicing capacity is underestimated by the SHRP method: for SC and SA by 26% (9.48 g/g instead of 12.75 g/g and 6.07 g/g instead of 8.16 g/g, respectively) and for MC even by 57% (2.92 g/g instead of 6.83 g/g). The underestimation of the deicing performance is further complicated by the fact that the climate chamber (Binder MKF-720) that was used for the SHRP method has different temperature zones inside the chamber. This means that, despite setting the air conditioning to −5℃, the temperature in the left rear area is on average −7.4℃ and that in the right front area is −3.1℃. In principle, this is not unusual (the magnitude of the differences here is unusual) and can be accounted for by temperature mapping. However, given that the temperatures also fluctuate within the same zone presumably because of the airflow in the climate unit, the deicing process is temperature sensitive, and repeatability is rather low, the climate chamber is therefore unsuitable for this experiment. This may also be a result of the change or simplification of the SHRP test method: A climate chamber with arm inlets was used instead of a separate box inside an upright freezer following the specific requirements for testing in an upright freezer in the appendix of SHRP H-205.1 [32]. This appendix also states that the preferred environment for testing is a walk-in cold room with a separate temperature-regulated box.
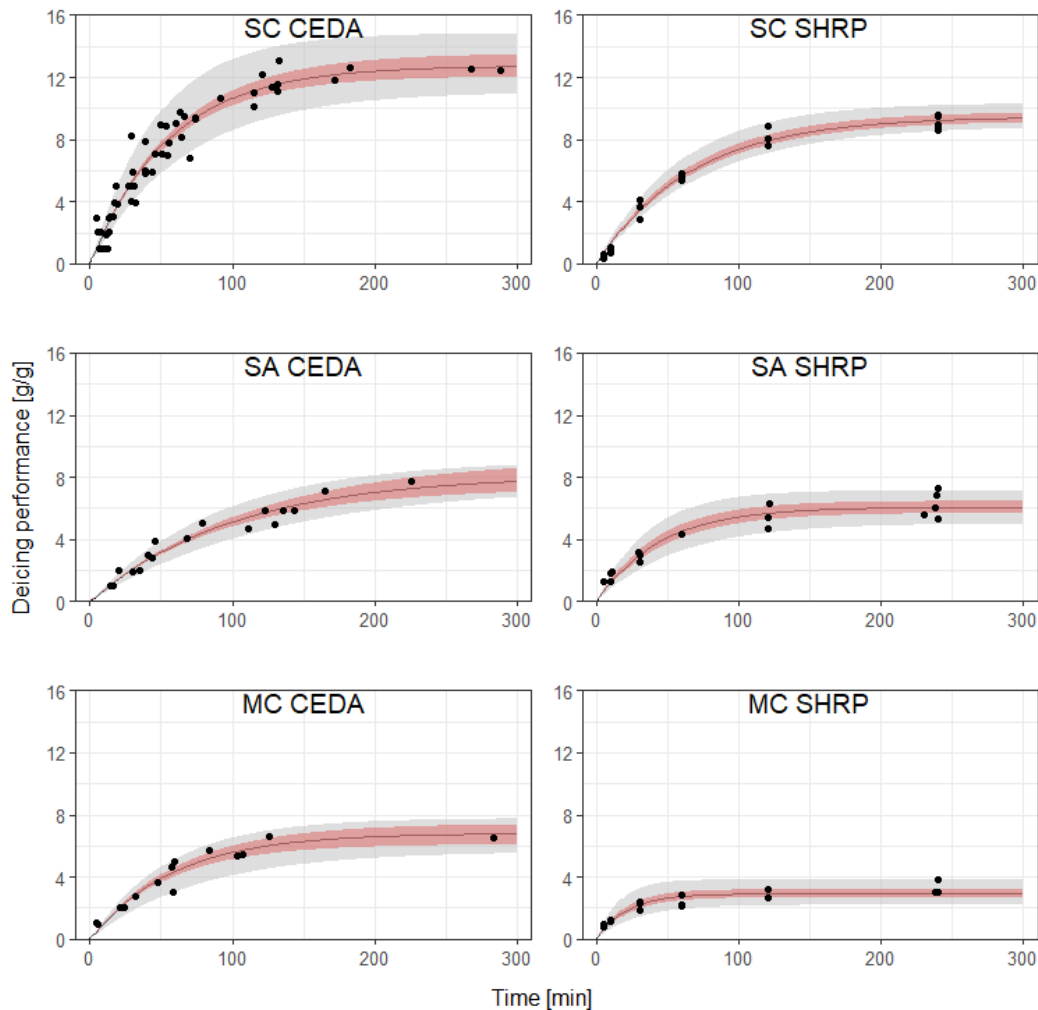
Figure 10: Nonlinear models of the CEDA and SHRP methods at −5℃

Comparison with results from the literature

In addition to the comparison of test methods already made in the article, further results of the deicing performance of SC from the literature will be discussed. Some of the referenced reports strictly follow the SHRP test regime, whereas others are slightly modified. Table 19 shows a selection of results and their test conditions for solid SC. Given that SHRP H-205.1 [32] specifies to aspirate the thawed amount with a syringe and note the result in milliliters, some of the results are converted from milliliters thawed per gram deicing agent [mL/g] to grams thawed per gram deicing agent [g/g]. The conversion factor depends on the density, concentration, and temperature of the SC solution. According to SHRP H-205.1 [32], approximately 0.97 g H_2O/mL solution can be assumed. Furthermore, some results were tested at temperatures different from −5°C, i.e., 15°F (−9.4°C), 20°F (−6.7°C), 25°F (−3.9°C), and 30°F (−1.1°C). For comparison, these results were linearly interpolated to −5°C, although the relationship between deicing performance and temperature is quite likely nonlinear.

Table 19: Deicing performance (DP) found in the literature

Source	Method	Temperature	DP at −5°C [g/g]
Shi et al. 2013 [37]	Modified SHRP—mL/g to g/g	−1.1°C and −9.4°C*	4.3
Alger and Haase 2006 [38]	SHRP—mL/g to g/g	−3.9°C and −6.7°C*	5.1
SHRP TU Wien (TUW)	Modified SHRP—g/g	−5°C	5.6
Fay and Shi 2011 [35]	SHRP—g/g	−5°C	8.5
CEDA TU Wien (TUW)	CEDA—g/g	−5°C	8.4
Autelitano et al. 2019 [39]	Modified SHRP—g/g	−6°C	9.0

* Temperature linearly interpolated to -5°C

As shown in Figure 11, the deicing performance after 60 min determined by the CEDA and (modified) SHRP methods presented in [35] and [39] is similar with 8.4–9 g/g.

At 4.3–5.6 g/g, the deicing performance determined by the (modified) SHRP method in [40], [41] and TU Wien is significantly lower. As previously indicated, the reason is probably the different boundary conditions of the SHRP test with the following possible influencing factors:

- Temperature control of the test chamber: Melting of ice is an endothermic process (i.e., heat is required from the environment). SC lowers the freezing point of water, thereby causing ice to melt even at less than 0°C. Therefore, the ambient temperature of the samples is lower, and a possible counter-control of the (small) climate chamber could lead to large deviations.
- Air movement in the test chamber: Specimens exposed to direct airflow could be affected by sublimation and evaporation, depending on their aggregate state.
- Uneven distribution of solid SC: The application of SC to the specimens could be uneven. As a result, SC may be overrepresented at some points, i.e., incompletely dissolved within the exposure time; thus, the deicing potential may not be fully exploited.
- Penetration influence: Single salt grains of different sizes could (completely) penetrate the ice plate and retain the meltwater in the resulting channels, thus falsifying the result.
- Incomplete aspiration: Meltwater could remain in the sample because of adhesion despite careful aspiration or draining.
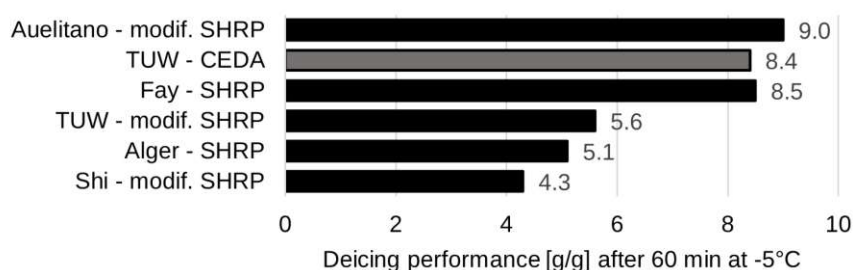
Figure 11: Comparison of deicing performance found in the literature

This circumstance shows that the correct performance of the SHRP test depends on many factors; therefore, the comparability of the results from different tests is difficult to achieve. For this reason, the CEDA method has been developed as its setup is easier to reproduce and enables better handling of the desired temperature. The process will be briefly presented.

A defined amount of distilled water (i.e., 400 µL or 399.28 µg at 20°C) is filled into the wells of the reaction plates and frozen. For this purpose, the reaction plate is placed in a cryostat (Huber Ministat 240) so that the wells are completely surrounded by the cooling liquid, as shown in Figure 12.
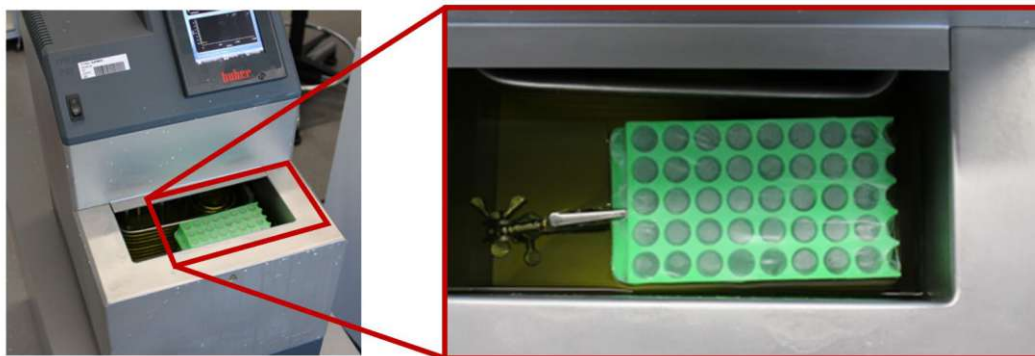
Figure 12: New method: Cryostat with reaction plate [Paper II]

The wells, which are open at the top, are covered and brought to the desired temperature (in the article, −5°C) overnight; meanwhile, the temperature of the cooling liquid is monitored. To start the deicing process, a certain amount of deicing agent (between 30 and 500 µg) is applied to each of the wells, and the automatic photography process (Canon EOS 2000d, one photo per minute) is started. After 300 min at the latest, the experiment is finished, and the photos are optically evaluated manually. The status of the individual wells is visually evaluated as "(partly) frozen" or "completely deiced" based on the photo.

The "(partly) frozen" state is represented by the presence of ice in the well, which can be detected by noncentered or multiple reflections of the light source above. The time of the "completely deiced" state is noted and used for the calculation of the deicing performance: Within the start of the deicing process to the aforementioned time, the amount of deicing agent in the corresponding well that has "completely deiced" the defined amount of ice. This procedure enables the testing of many samples at the same time, thereby ensuring a better estimation of the deicing performance than the SHRP test with a smaller number of samples. An example of the procedure for evaluating the state is shown in more detail in Figure 13, where images of four wells are examined at four different times. From left to right, the exposure time becomes longer so that the ice changes from the "(partly) frozen" state (denoted by the blue circles) to the "completely deiced" state (denoted by the red circles).
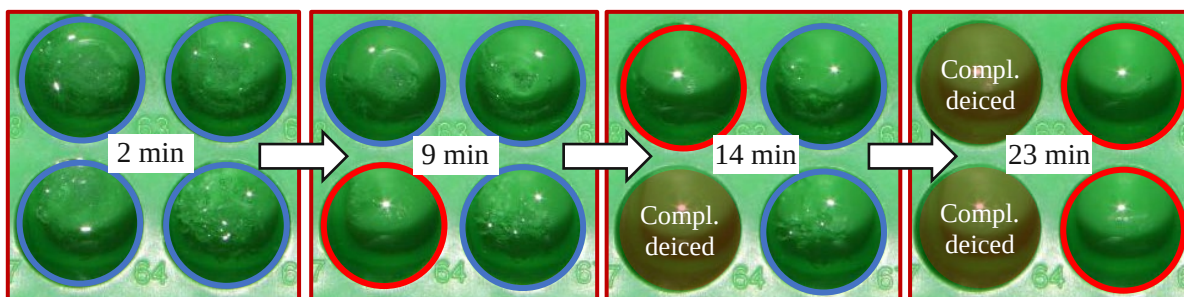
Figure 13: Distinction of the deiced state (from left to right: 2, 9, 14, and 23 min after adding SC)

3.3   Conclusion and outlook

Although the SHRP H-205.1 test [32] is a practice-oriented test for solid deicing agents, the replication of the setup and the reproduction of the results can be challenging. The problems presented in this chapter and the different results in the literature confirm this conclusion, leading to the development of a new test method (i.e., CEDA) with fewer requirements, significantly lower space consumption, and higher test volume. The results of this new method are compared with the theoretically calculated and empirical test results. With the results showing good repeatability, several deicing agents were tested, and the results were analyzed with the help of a nonlinear regression model, enabling the calculation at a 95% confidence interval and 95% prediction interval. Notably, SC has the best deicing performance at −5°C, being able to deice 12.75 times its weight (12.75 g/g). Other tested agents, such as SF (11.41 g/g) and PA (10.59 g/g), show similar performance, whereas PC (6.74 g/g) and PF (6.38 g/g) deice only half of the amount of SC. Before testing the corrosion rate of the presented agents (see Paper III), a possible influence of inhibitors added to SC on the deicing performance has to be evaluated. Substituting 8% SC with sugars (i.e., arabinose, glucose, mannose, or maltose), only a small difference in deicing performance can be observed because of the lower amount of SC, precluding the detrimental effect on deicing performance.

These experiments were only conducted at a temperature of −5°C; thus, a sufficient performance of the deicing agents at other temperatures cannot be predicted. Therefore, the temperature range relevant for winter maintenance (i.e., −15°C to 0°C) needs to be tested; consequently, a model that considers both time and temperature needs to be designed.

A further step would be the automation of the test evaluations. With CEDA, the evaluation and state detection of the samples are done based on the photos taken every minute. However, this leads to two problems, i.e., time consumption and different perceptions of the data evaluator as to when a sample can be specified as "completely deiced." Although the latter usually only leads to clear optical differences in the range of minutes, it is a factor of uncertainty. Therefore, the test setup should be adapted to allow an automated determination of the condition of the sample (e.g., by thermography).

4   Paper III—Analysis of Metal Corrosion Methods and Identification of Cost-Efficient and Low-Corrosion Deicing Agents

The paper is attached in the Annex. Additional analysis on further inhibitors and metals, as well as the health hazard assessment of these agents beyond the content of the paper, are presented as follows.

Abstract: Deicing agents in winter maintenance are critical in providing safe roads at all times. Sodium chloride is the most common, efficient, and favorable agent but has a drawback of high corrosiveness, thus substantially shortening the service life of metal-based transport infrastructures. This work focuses on corrosion and addresses approaches for the following corrosion test methods that quantify the mass loss of metals for different deicing agents: standardized neutral salt spray test (ISO 9227), salt solution immersion test (ASTM G31-72), and alternate immersion test (ISO 11130). A wide range of different deicing agents with and without corrosion inhibitors are tested on unalloyed steel, and an analytical and visual comparison is made. Results reveal a substantially reduced corrosion effect at reasonable costs by selecting the appropriate deicing agent with or without corrosion inhibitors. For the final selection of deicers, deicing performance and cost effectiveness are compared.

4.1   Summary

To ensure the safe usability of roads and paths in winter, sodium chloride (SC) is the preferred deicing agent for preventive and curative snow and ice control worldwide [16], [43]. As shown in Paper II, SC is one of the most effective deicing agents (with good availability). However, because of its high corrosivity, the use of SC leads to high follow-up costs, particularly for metal-based infrastructure [40], [44]–[49]. Therefore, alternative deicing agents, in addition to being tested for their suitability as deicing agents (deicing performance, see Paper II), are also tested for their corrosivity in this article.

To detect meaningful differences in corrosion of different deicing agents, the aim was to find a method as simple and inexpensive as possible to obtain a large measure of corrosion products. To this end, the following test methods for producing corrosion on unalloyed steel plates by a 5 m% SC solution were investigated:

- Salt solution immersion test according to ASTM G31-72 [48],
- Standardized neutral salt spray test according to ISO 9227 [49], and
- Alternate immersion test according to ISO 11130 [50].

Notably, the test methods applied are only based on standardized methods but do not strictly follow them. The exact modifications to the standard can be found in the article, but a short presentation will be given here. The metal plates on which corrosion is tested are made of unalloyed steel (S235JR according to EN 100025 [51]) and have the dimensions of 150 × 100 × 1 mm, with a weight of 235 ± 2.4 g. An example is shown in Figure 14.

Figure 14: Unalloyed steel specimen

Regardless of the test method, corrosion damage is quantified by specifying the mass loss of the metal plates. For this purpose, after completion of the test, the corrosion products are removed and the change in the weight of the plate in relation to the original weight (relative mass loss) is assessed.

For the removal of corrosion products, the recommendations of the ISO 8407 [52] standard were applied: Light mechanical cleaning (washing off the plate with tap water) and subsequent chemical–physical cleaning in an ultrasonic bath at 50°C in a 20 m% diammonium hydrogen citrate solution. Treatment in the ultrasonic bath is conducted until no change in mass can be detected.

Salt solution immersion test

As shown in Figure 15, this test method is based on simplicity. This is explicitly provided for in ASTM G31-72 [48], which also states that the specifications contained therein are not intended to be a mandatory standard but rather a recommendation. Under certain conditions, aeration or heating of the test liquid is proposed. To maintain the simplicity of the experiment, these options are omitted. The resulting disadvantage is a low corrosive effect because the corrosion process is hindered by the low oxygen supply. Tests at room temperature (RT) show only a corrosion-related mass loss of 0.2 m% or 0.5 g after 21 days of exposure in a 5 m% SC solution, see also Figure 16.

Figure 15: Salt solution immersion test [Paper III]

Figure 16: Specimen after 21 days fully immersed

Standardized neutral salt spray test

According to ISO 9227 [49], this test method is significantly more complex to reproduce. To keep costs and effort low, reproducing the test exactly according to the standard was avoided, and some modifications were made, particularly to the spray device and ambient temperature. The samples are sprayed directly via four commercially available atomizing nozzles (each approximately 0.3 L/h), and the test solution is reused after spraying. The off-standard reuse of the test solution was adopted because of the uneconomically high material requirement for such a high throughput of the atomizing nozzles (30 L/day) and a continuous operation of 21 days. According to the standard, very fine atomizing nozzles

with a throughput of 1–2 mL/h on an area of 80 cm² are intended, which would lead to a throughput of 3 L/day for the manufactured test chamber (dimensions of 100 × 50 cm).

In contrast to the standard, humidification is noncontinuous but in a cycle of 115–117 min spraying and 3–5 min aeration. The exact duration is controlled to ensure a throughput of approximately 30 L/day. A second essential change concerns the testing temperature: According to the standard, 35°C is intended, but given that, on one hand, the aerosols produced by spraying the deicing agent solution could also attack the environment and, on the other hand, the available climate chamber is too small for the built corrosion setup with space for several samples, the test is conducted at RT. A picture of the chamber is shown in Figure 17.
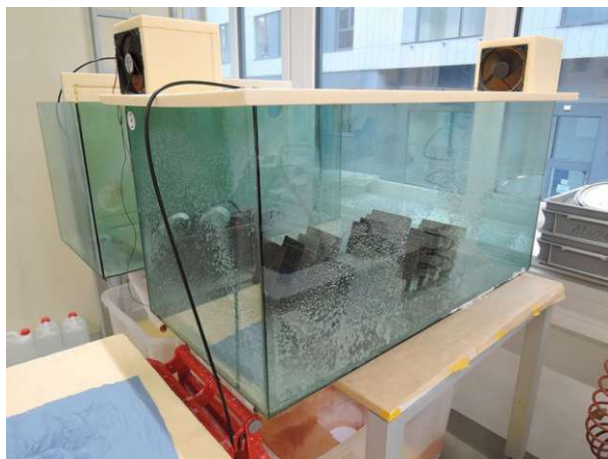
Figure 17: Experimental setup of the spray test [Paper III]

As shown in Table 20, these simplifications led to low corrosion on the metal specimens. Still, the median value of the relative weight loss in the neutral salt spray test is significantly higher than that in the salt solution immersion test, amounting to 2.1 m% (approximately 4.9 g) and, as will be shown subsequently, is lower than expected because of the temperature selection.

Table 20: Progress of corrosion on metal plates in the spray test

0 days	4 days	7 days	11 days

14 days	18 days	21 days	Cleaned

Regardless of the temperature, the follow-up tests showed that the flow of the atomizing nozzles was severely impaired at irregular intervals, or the nozzles were clogged completely. This finding can be attributed to several factors: On one hand, the test solution is circulated, and in the process (despite the fine particle filter), small particles could be sucked in and clog the nozzles. On the other hand, the specification and quality of the atomizing nozzles could have played a role. Therefore, the replicated test setup is too unreliable to produce repeatable results. These problems are presumable because of the changes to the standard, and not due to the general test execution of the neutral salt spray test according to the standard.

Alternate salt solution immersion test

This test based on ISO 11130 [50] is simpler than the neutral salt spray test, and modifications in the replica mainly concern the temperature of the test solution or the environment. The specimens are alternately immersed in the test solution for 10 min and dried for 50 min. The standard specifies a temperature of $25 \pm 2°C$ for the solution and $70 \pm 2°C$ for the air temperature with a relative humidity (RH) of $\leq 50\%$. However, in the replicated test setup, the test solution is stored at ambient temperature and not separately tempered. Initial experiments were conducted at RT ($19 \pm 1°C$; RH $32 \pm 5\%$) and in the climate chamber (CC) at elevated temperatures ($34 \pm 1°C$; RH $\geq 70\%$), as shown in Figure 18 and Figure 19, respectively. The results for unalloyed steel samples in 5 m% SC solution show median values of 3.7 m% (approximately 8.7 g) mass loss because of corrosion at RT and 11.7 m% (approximately 27.4 g) at elevated temperatures, i.e., 1.8 and 5.6 times the corrosion products of the spray test, respectively. However, the results in the climate chamber show a high scatter (interquartile range (IQR) of 4.7 m%), which is probably caused by the strong airflow of the climatic unit on the samples.

Figure 18: Alternate immersion at room temperature

Figure 19: Alt. immersion in the climate chamber

At elevated temperatures, high-level corrosion is produced, enabling good differentiation of various test solutions without other factors (e.g., uneven cleaning and small differences in metal plates) significantly affecting the results.

After proving the suitability of the test method, a climate container (CT) was used to test three test setups at elevated temperatures ($34 \pm 1°C$; RH $80 \pm 10\%$) simultaneously. As shown in Figure 20, the size of the container ensures that the specimens can be positioned so that they are not directly affected by the conditioned airflow from the floor. This also reflects in the test results: a (median) loss of 14.2 m% (33.2 g) after 21 days with a significantly lower scatter (IQR of 0.8 m%).

Figure 20: Alternate immersion in a temperature-controlled container [Paper III]

Comparison of different deicing agents and inhibitors

As mentioned previously, high corrosion and low scatter enable the comparison of different deicing agents and inhibitors. Each deicing agent is tested as a 5 m% solution (e.g., 5 g SC + 95 g H_2O). When

adding inhibitors to SC, 8 m% is added based on the dry mass of SC (i.e., 8 m% of 5 g = 0.4 g). A comprehensive list of the deicing agents and inhibitors included in the experimental program is given in Table 21. Notably, nontechnical abbreviations were utilized to ensure readable figures (e.g., CH_3COOK = potassium acetate = PA). The results of the experimental program are shown in Figure 21, where corrosion caused by water without the addition of deicing agents is also shown. As mentioned in the article, only PC is less corrosive than water as it forms an alkaline solution, which leads to the passivation of the steel surface.

Table 21: Tested deicing agents and inhibitors

Agent	Abbreviation	Formula
Calcium chloride	CC	$CaCl_2$
Magnesium chloride	MC	$MgCl_2$
Potassium acetate	PA	$C_2H_3KO_2$
Potassium carbonate	PC	K_2CO_3
Potassium formate	PF	$CHKO_2$
Sodium acetate	SA	$C_2H_3NaO_2$
Sodium chloride	SC	NaCl
Sodium chloride + arabinose	SC + Ara	$NaCl + C_5H_{10}O_5$
Sodium chloride + glucose	SC + Glu	$NaCl + C_6H_{12}O_6$
Sodium chloride + maltose	SC + Mal	$NaCl + C_{12}H_{22}O_{11}$
Sodium chloride + mannose	SC + Man	$NaCl + C_6H_{12}O_6$
Sodium formate	SF	$CHNaO_2$
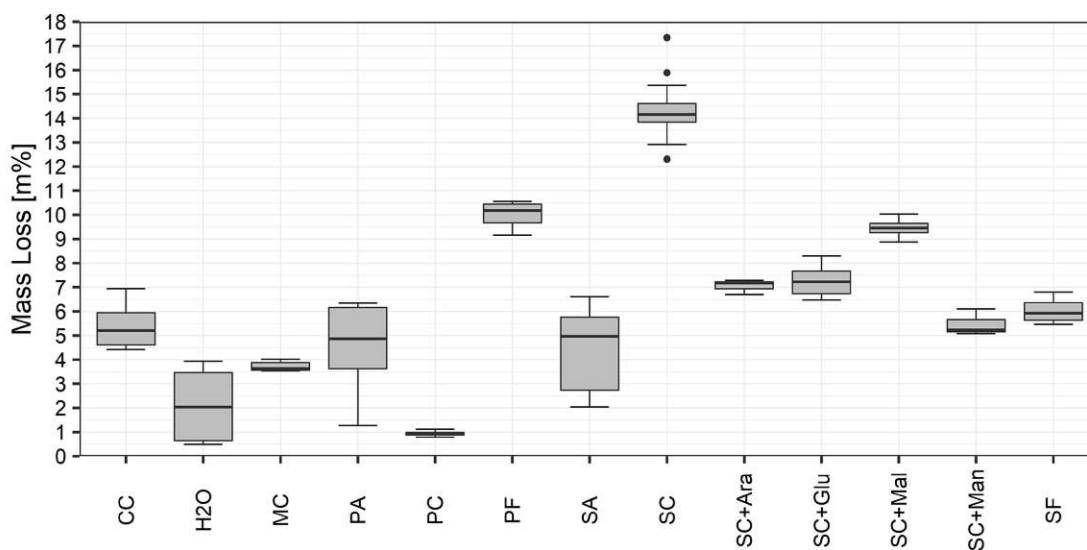
Figure 21: Mass losses of all tested deicing agents and inhibitors [Paper III]

4.2   Additional results

Previous tests have focused on unalloyed steel; however, different metallic materials are used in the infrastructure sector. For this reason, corrosion tests with different deicing agents with and without inhibitors were also tested and compared on galvanized steel (Fe(Zn)) and copper (Cu). In addition to the results previously presented in Paper III, different inhibitors were also tested on all metals. Before this, however, the process of oxygen corrosion and the possible effects of inhibitors are discussed.

Corrosion process and corrosion reduction

In simple terms, (electrochemical) corrosion occurs when electrons migrate from the metal atoms on the surface via an electrolytic transport medium (in this case, water) to the electron receivers (in this case, oxygen). Generally, small damages on the metal surfaces lead to more free energy available in these areas. Thus, a potential difference is formed between such areas and the undamaged areas. This potential

difference is enhanced by SC (NaCl: Na^+ and Cl^-). The area with more free energy (negatively charged) is called the anode, whereas the area with positively charged area is called the cathode. The redox reaction according to [53] proceeds as follows: At the anode, iron oxidizes to Fe^{2+} and the electrons released in the process migrate to the cathode, where they react with water (H_2O) and oxygen (O_2, which is reduced in the process) and combine to form hydroxide ions (OH^-). The positively charged Fe^{2+} reacts with the negatively charged OH^- to form iron(II) hydroxide ($Fe(OH)_2$), and further reaction with O_2, H_2O, and OH^- leads to the subsequent oxidation stage, forming iron(III) oxide-hydroxide ($FeO(OH)$). With the release of water, $Fe(OH)_2$ and $FeO(OH)$ become a mixture of iron(II) oxide and iron(III) oxide, which is called rust. The complete reaction is expressed in Equations 2−5 [53].

The corrosion rate in atmospheric environments is generally determined by the diffusion rate of oxygen through any barrier on the reactive steel surface, i.e., it depends strongly on oxygen exposure. The ambient temperature also plays a significant role as it affects the oxygen content in water (i.e., 14 mg O_2/L H_2O at 0°C and 7 mg O_2/L H_2O at 35°C). The higher the temperature is, the less O_2 can be dissolved and the less corrosion will occur. Also, a higher temperature multiplies the Arrhenius activation energy, which is required to start the process. However, the exact quantitative influence is unknown. Both phenomena are contradictory; therefore, no general rule can be established.

$$2Fe \rightarrow 2Fe^{2+} + 4e^- \tag{2}$$
$$2H_2O + 2O^{2-} + 4e^- \rightarrow 4OH^- \tag{3}$$
$$2Fe^{2+} + 4OH^- \rightarrow 4Fe(OH)_2 \tag{4}$$
$$4Fe(OH)_2 + 2O_2 \rightarrow 4FeO(OH) + H_2O \tag{5}$$

Corrosion in the environment of winter maintenance can be reduced, on one hand, by constructive protection of the metal surface by painting and using galvanized zinc coatings or, on the other hand, by adding inhibitors (to the deicing agent). Both methods can prevent oxygen access by attaching themselves to the surface or by forming a compound with O_2 by themselves. The former could be a possible explanation of the effectiveness of sugars because reducing sugars (such as glucose, mannose, and maltose) act as anodic inhibitors, i.e., they can prevent the oxidation of Fe (at the anode) [54].

Test program of different inhibitors

Corrosion reduction of the sugars tested in the article is promising; thus, additional agents that might have a possible preventive effect on the corrosion process are investigated. A list of the substances identified and additionally tested is provided in Table 22. These substances were added at 8 m% (based on the dry weight of SC), exactly as in the article. Notably, less corrosive deicing agents were also added to SC as inhibitors. The sugars already tested in the original article are listed for completeness and marked with an asterisk (*).

Table 22: Tested deicing agents and inhibitors [55]

Agent	Abbreviation	Formula
Sodium chloride + arabinose*	SC + Ara	$NaCl + C_5H_{10}O_5$
Sodium chloride + calcium nitrite	SC + CaNi	$NaCl + Ca(NO_2)_2$
Sodium chloride + glucose*	SC + Glu	$NaCl + C_6H_{12}O_6$
Sodium chloride + glycerin	SC + Gly	$NaCl + C_3H_8O_3$
Sodium chloride + maltose*	SC + Mal	$NaCl + C_{12}H_{22}O_{11}$
Sodium chloride + mannose*	SC + Man	$NaCl + C_6H_{12}O_6$
Sodium chloride + disodium phosphate	SC + DiPh	$NaCl + Na_2HPO_4$
Sodium chloride + sodium metasilicate	SC + NaSi	$NaCl + Na_2SiO_3$
Sodium chloride + potassium acetate	SC + PA	$NaCl + C_2H_3KO_2$
Sodium chloride + potassium carbonate	SC + PC	$NaCl + K_2CO_3$
Sodium chloride + potassium formate	SC + PF	$NaCl + CHKO_2$
Sodium chloride + sodium acetate	SC + SA	$NaCl + C_2H_3NaO_2$
Sodium chloride + sodium formate	SC + SF	$NaCl + CHNaO_2$
Sodium chloride + tetrabutylammonium bromide	SC + TbAb	$NaCl + C_{16}H_{36}BrN$

Notably, glucose and mannose have the same chemical molecular formula, i.e., $C_6H_{12}O_6$. In the present case, the term epimer is used, which is a special form of diastereoisomers as it differs only at one stereocenter and has different physical properties (Classification: Isomerism–Stereoisomerism–Diastereoisomerism–Epimerism) [56].

The results of relative mass loss due to the alternating immersion tests at elevated temperatures after 21 days are shown in Figure 22. The evaluations in the article are based on at least six replicates; however, only three replicates were tested in the additional investigations presented here. For this reason, only the individual values for these results are shown as gray dots, and their median values (to be consistent with the presentation of the data from the article) are shown as black crossbars.

The combinations of SC and other deicing agents as inhibitors (SC + PA/PC/PF/SA/SF) are in the upper range of mass loss with a median value between 9 m% and 13 m%. Sodium metasilicate (SC + NaSi), at 5.6 m%, is at the same level as mannose (SC + Man = 5.3 m%), below this is calcium nitrite (SC + CaNi = 4.2 m%), whereas disodium phosphate (SC + DiPh) performs better with 1.5 m%.
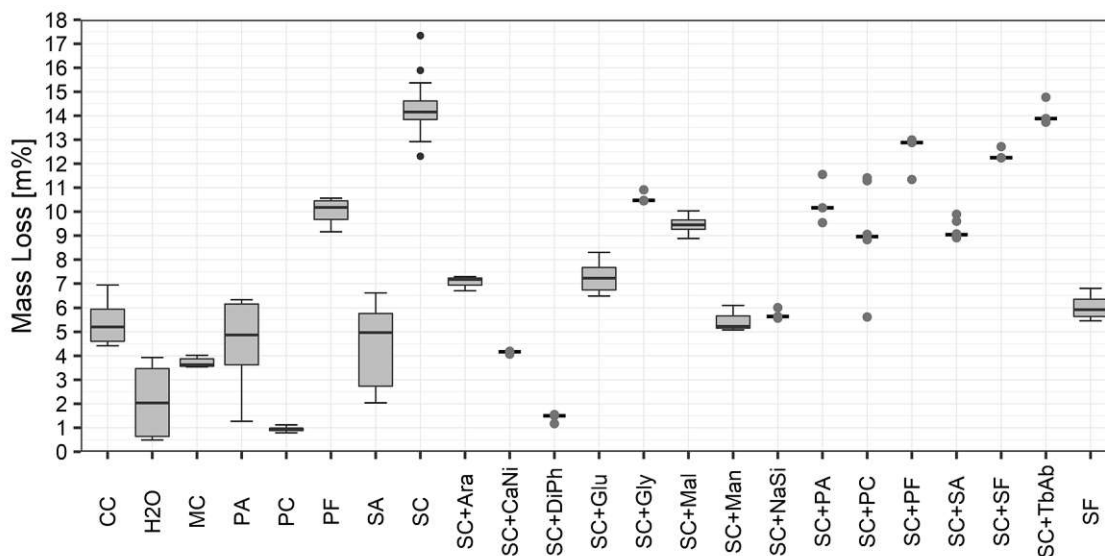
Figure 22: Relative mass losses of all tested substances [including data from Paper III]

Alternating immersion test with FeZn and Cu

In addition to Fe, different metals are used in the infrastructure sector; two of them, i.e., galvanized (zinc-coated) steel (Fe(Zn)) and copper (Cu), are shown in Figure 23 and Figure 24. Cu is frequently

used in the railroad sector. For this reason, all basic deicing agents, as well as SC as a deicing agent in combination with less corrosive agents, were also tested as a 5 m% solution on different metals (i.e., metal plates = 150 × 100 × 1 mm, Fe(Zn) = 231.1 ± 2.8 g, Cu = 264.1 ± 2.8 g). Analogous to the previous procedure, three metal plates each were tested with the alternate immersion test method at elevated temperatures in the temperature-controlled container for 21 days.
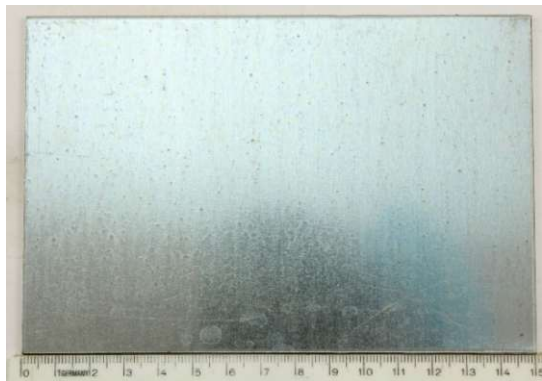
Figure 23: Galvanized steel (Fe(Zn)) specimen

Figure 24: Copper (Cu) specimen

The mass losses of all tested combinations are shown in Figure 25 for Fe(Zn) and Figure 26 for Cu. Given that only single testing (i.e., one test run with three replicates each) is conducted, incorrect results are more difficult to identify. Therefore, the following results should be considered the preliminary indication of the corrosive effects.

On Fe(Zn), the corrosion rates of all deicing agents are approximately 2 m% and thus on the same level as water (H_2O), showing the low corrosive effect on Fe(Zn). Only SC and its combination with glucose, glycerin, and maltose (SC + Glu/Gly/Mal) seem to have a higher impact. By contrast, SC combined with mannose (SC + Man) shows slightly fewer corrosive effects with a median mass loss of 1.4 m%. The results of PC are quite scattered and should therefore be treated with caution.

On Cu, the corrosion rates of all deicing agents are even lower than 0.2 m%. Notably, MC has the highest mass loss of 0.27 m% probably because MC inhibits the formation of copper(I) dioxide, which can then lead to higher corrosion rates [57]. As mentioned previously, these results are considered the preliminary indication of the corrosive effects. Therefore, the details of the electrochemical corrosion process on Cu (or materials other than Fe) will be investigated in detail in a future study.
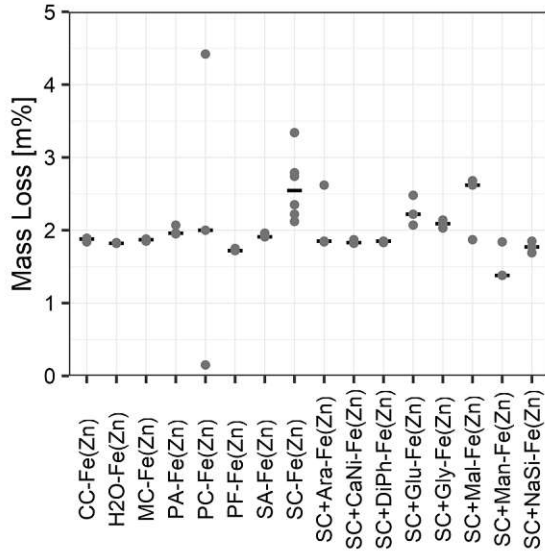
Figure 25: Relative mass loss of Fe(Zn) specimen
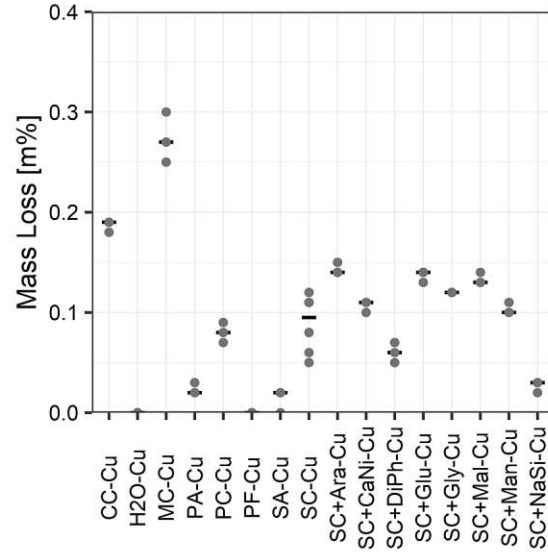
Figure 26: Relative mass loss of Cu specimen

Analogous to the visual representation of the tested specimens on Fe, the results of the additional tested inhibitors on Fe and of all results on Fe(Zn) and Cu are depicted in Table 23 to Table 28.

For comparison, the photos of the Fe specimens in H_2O and SC from the original article are also included in Table 23. Notably, the extent of corrosion can only be roughly estimated from the photos, and it is impossible to make an exact visual distinction, particularly with the low corrosion rates of Fe(Zn) and Cu.

Photo documentation of the alternate corrosion test of Fe (added to Paper III)

Table 23: Photo documentation of unalloyed steel specimen [55]
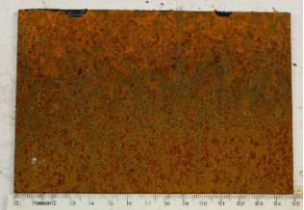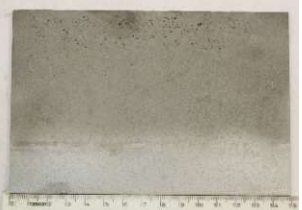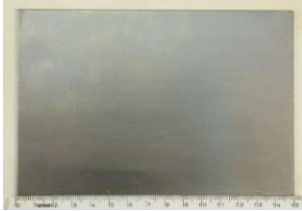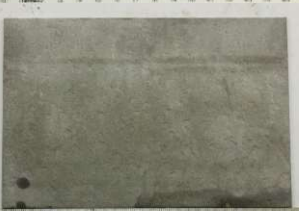
Fe	0 days	21 days	21 days + cleaned
H₂O [Paper III]			
SC [Paper III]			
SC + CaNi			
SC + DiPh			
SC + Gly			
SC + NaSi			
SC + PA			
SC + PC			

Table 24: Photo documentation of unalloyed steel specimen [55]

Fe	0 days	21 days	21 days + cleaned
SC + PF			
SC + SA			
SC + SF			
SC + TbAb			

Photo documentation of the alternate corrosion test of galvanized steel

Table 25: Photo documentation of galvanized steel specimen [55]
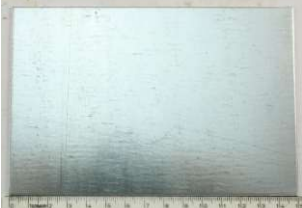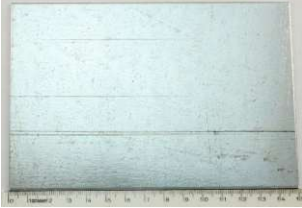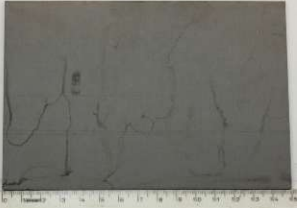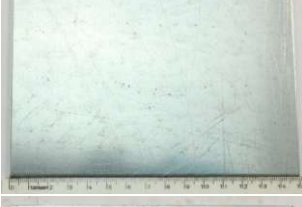
Fe(Zn)	0 days	21 days	21 days + cleaned
CC			
H$_2$O			
MC			
PA			
PC			
PF			
SA			
SC			

Table 26: Photo documentation of galvanized steel specimen [55]
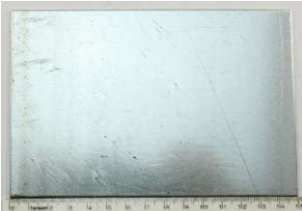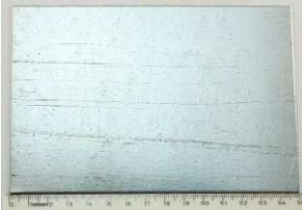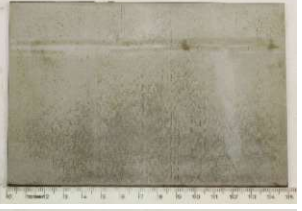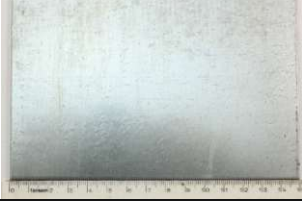
Fe(Zn)	0 days	21 days	21 days + cleaned
SC + 8% Ara			
SC + 8% CaNi			
SC 8% Glu			
SC + 8% Gly			
SC + 8% Mal			
SC + 8% Man			
SC + 8% DiPh			
SC + 8% NaSi			

Photo documentation of the alternate corrosion test of copper

Table 27: Photo documentation of copper specimen [55]
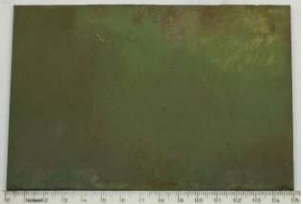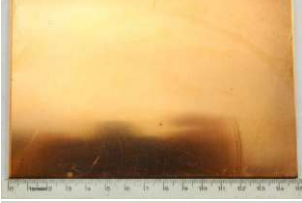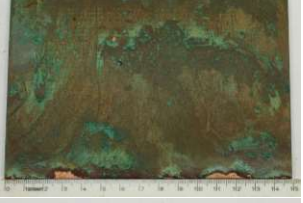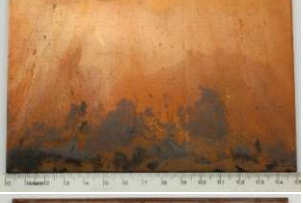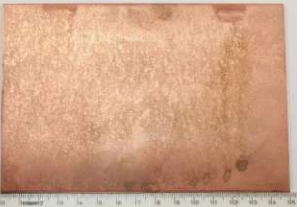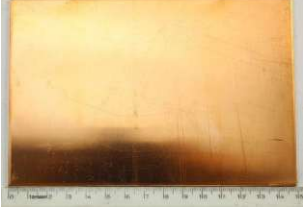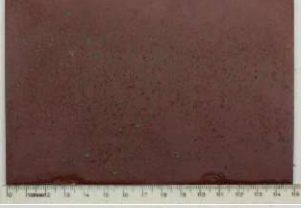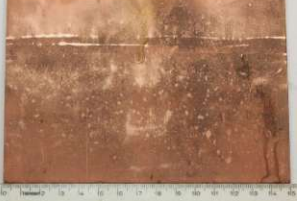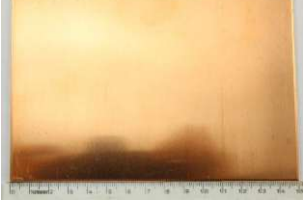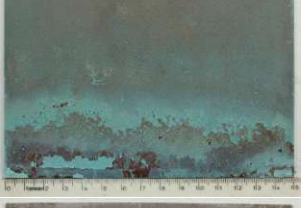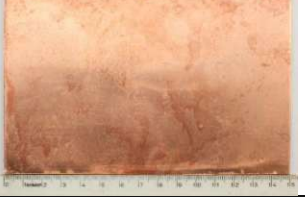
Cu	0 days	21 days	21 days + cleaned
CC			
H$_2$O			
MC			
PA			
PC			
PF			
SA			
SC			

Table 28: Photo documentation of copper specimen [55]

Cu	0 days	21 days	21 days + cleaned
SC + 8% Ara			
SC + 8% CaNi			
SC 8% Glu			
SC + 8% Gly			
SC + 8% Mal			
SC + 8% Man			
SC + 8% DiPh			
SC + 8% NaSi			

Hazard classification of the tested substances

Thus far, a large number of agents capable of reducing corrosion were investigated. However, not all of them can be used in winter maintenance without further investigation of their hazardous effects on humans. A selection of these effects is listed in the United Nation's "Globally Harmonized System of Classification and Labelling of Chemicals (GHS)." The GHS is a worldwide system for classifying chemicals and is printed on the packaging of the agents or specified in their safety data sheets.

For the tested agents, all occurring health hazards (H-numbers) found in the literature (from the German Social Accident Insurance (DGUV) database [58] and the supplier's safety data sheets [59]) are summarized in Table 29. Marked with an "x" in the corresponding column, CC and PC can cause serious eye irritation (H319). In the case of a combination (e.g., SC + PC), the hazardous effect is assumed to affect the entire mixture, which is indicated with an "(x)," although a detailed study needs to be conducted for such small amounts added to (nonhazardous) SC. The following substances most likely do not affect human health (see also "x" in the first column of Table 29):

- Main deicing agents: MC, PA, PF, SA, SC, SF, and their combinations with SC;
- Inhibitors: Ara, Glu, Gly, Mal, Man, DiPh, and their combinations with SC.

Table 29: GHS hazard statements according to Sigma-Aldrich and GESTIS Substance DB [59], [60]

Abbrev.	No GHS hazard statement	Toxic if swallowed H301	Harmful if swallowed H302	Skin/eye damage H314	Skin irritation H315	Eye damage H318	Serious eye irritation H319	Respiratory irritation H335	Other GHS hazard statements
CC							x		
MC	x								
PA	x								
PC					x		x	x	
PF	x								
SA	x								
SC	x								
SC + Ara	x								
SC + CaNi		(x)				(x)			
SC + Glu	x								
SC + Gly	x								
SC + Mal	x								
SC + Man	x								
SC + DiPh	x								
SC + NaSi					(x)	(x)		(x)	H290
SC + PA	x								
SC + PC					(x)		(x)	(x)	
SC + PF	x								
SC + SA	x								
SC + SF	x								
SC + TbAb			(x)		(x)		(x)		H361fd, H412
SF	x								

4.3 Conclusion and outlook

For winter maintenance, SC is the most widely used deicing agent because it is readily available, relatively inexpensive, and effective. However, SC causes high economic damage because of its highly corrosive effect on metals [45], [61], [62]. To quantify corrosion, three different corrosion test methods, i.e., the full immersion test, neutral salt spray test, and alternate immersion test, were compared. Because the alternate immersion test was determined to have the greatest effect at elevated temperatures and after 21 days of testing, many deicing agents, as well as inhibitors that can reduce the corrosion process, were tested on three different metals (i.e., Fe, Fe(Zn), and Cu).

Compared with SC with a relative mass loss of approximately 14 m% due to corrosion on Fe, PC with only approximately 1 m% mass loss is particularly outstanding. In combination with (inexpensive) SC, the following inhibitors are suitable for reducing corrosion of Fe: DiPh, CaNi, Man, and NaSi. On all other metals, only a slight difference in corrosive effects is measured. Only MC can cause higher corrosion rates on Cu.

However, because PC, CaNi, and NaSi can negatively affect human health (i.e., skin/eye damage and respiratory irritation), their use as deicing agents (or as additives to them) must be investigated more closely. DiPh and the sugar Man have no hazardous effects on humans and are suitable for winter maintenance; however, their effects on flora and fauna have not been investigated.

5 Paper IV—Optimization Potential in Operational Winter Maintenance

The paper is attached in the Annex. A more detailed analysis on the pourability of SC and the wear and tear of snowplow blades beyond the content of the paper is presented as well.

Abstract: Based on the fact that cleared snow does not have to be thawed, a good clearing pattern is essential for an economic winter maintenance. The development of suitable procedures for comparing the snow removal efficiency and durability of different snowplow systems was therefore one of the focal points of a research project on behalf of ASFINAG, BMVIT and the federal states in Austria. Based on extensive preliminary tests to determine the amount of remaining snow, a procedure for large-scale field tests was developed. In addition, tests were carried out on the wear and tear of snowplow blades. The obtained results enable reliable conclusions to be drawn about the durability and economy of steel and combi blades. A future long-term trial in co-operation with road and highway maintenance departments will also enable a comparison by manufacturer. The recommendations of ÖNORM EN 16811-1: 2016-11 regarding a (minimum) moisture content of sodium chloride may impair the pourability leading to observed blockages in salt silos. A wide range of deicing agents were therefore tested using the test method for pourability with the "discharge box after Sonntag". The discharge rate and the discharge angle have confirmed the observations and, according to the results, are suitable for demonstrating the influence of the anticaking agent and moisture content in a practical manner.

5.1 Summary

As shown in the previous chapters, extensive research in the field of deicing efficiency has been conducted. However, the step before deicing, i.e., clearing the snow from the roads and pavements, usually receives little attention. To address this issue, a method to quantitatively evaluate the clearing quality of residual snow after plowing was developed. In the future, this should enable a comparison of different snow removal systems and additional equipment.

For the evaluation of the snowplow blades (these are the bars on the lower edge of the snow shield on a snowplow, see Figure 3), a comparative abrasion test was conducted with the help of a snowplow system manufacturer. Segments of snowplow blades were tested under the same surface load on asphalt pavement (share of snow on track approximately 30%) and the corresponding abrasion was measured in millimeters after every run with a length of 13 km (78 km total test length). To ensure that every segment was subjected to the same degree of exposure, its position was swapped within the test rack after each run, ensuring that each segment was placed in a slot position. Pictures of the test are shown in Figure 27 and Figure 28.

Figure 27: Test rack with snowplow blade segments [Paper IV]

Figure 28: Panorama Hinterstoder–Höss [Paper IV]

In total, nine different steel blades (each with a thickness of 20 mm) and five combination blades (mostly steel and corundum; each with a thickness of 50 and 36 mm) were examined. Figure 29 shows the results and a linear regression model including the 95% confidence interval according to Equation (6), where y describes the abrasion as a function of the driven distance x. The descriptive coefficient β for the slope is shown in Table 30. Given the boundary conditions of 0 mm abrasion at 0 km, the coefficient α for the intercept is 0. The last column of Table 30 shows the distance to a 100 mm abrasion of the blade. The results certainly show too much wear because of heavy stress during the test (70% wet asphalt pavement surface). Thus, the difference between the blades is relevant: For the same amount of abrasion, a 50 mm-thick combination blade can be driven 1.7 times as far as a 36 mm-thick combination blade or 5.8 times compared with a 20 mm-thick steel blade. The comparison of the 36 mm combination blades with the 20 mm steel blades results in 3.4 times the operating distance with the same wear.

$$y(x) = \alpha + \beta \times x \qquad\qquad (6)$$

Table 30: Coefficients of the linear regression of the wear of scraper blades

Type of scraper blade	β	km of wear of 100 mm
Combination blades 50 mm	0.03704	2,700
Combination blades 36 mm	0.06410	1,560
Steel blades 20 mm	0.21636	460

The extent to which the use of combination blades is more effective than the use of steel blades depends on several factors. For example, the significantly higher purchase costs are offset by the lower follow-up costs because of blade replacement. The clearing quality must also be considered because "softer" materials (such as steel in this case) ensure better clearing performance in the case of icy road surfaces because of high contact pressure on the road. Thus, knowledge of the quantitative clearing quality is required for a holistic assessment. The aforementioned method was developed for this purpose; however, tests are still pending.
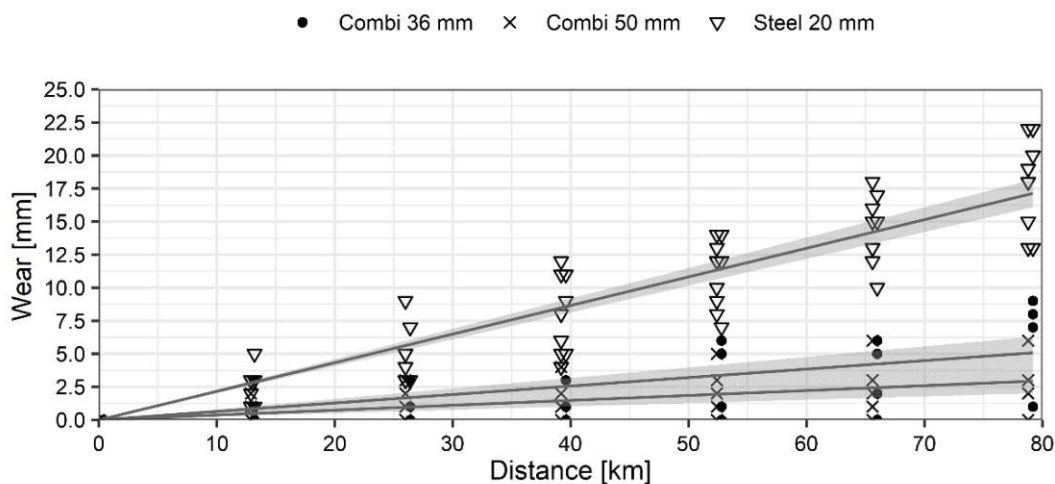
Figure 29: Wear of scraper blades as a function of driven distance

After problems with salt storage in silos due to clogging were repeatedly reported, the "Auslaufbox nach Sonntag" (discharge box), which was originally designed to determine the pourability of agglomerates in the plastics recycling industry [62], was used to determine the pourability of salt types with different moisture contents. The salt (here solid SC) to be tested is carefully filled into the discharge box, and the front flap is opened so that the salt can discharge. The discharge rate, i.e., the mass discharged as a function of the total filling mass, and the angle enclosing the horizontal and fracture surfaces (more precisely, the mean value of the angles of each side) are recorded. The discharge box is shown in Figure 30 with a low discharge rate and large discharge angle and in Figure 31 with a high discharge rate and small discharge angle.

Figure 30: Discharge box with a large discharge angle

Figure 31: Discharge box with a small discharge angle

In the original article, different types of salt (i.e., rock salt and vacuum salt) with different anticaking agents (ACAs) and moisture contents were tested. The test program is shown in Table 31, where sodium ferrocyanide was mainly used as ACA, except for one sample. The results are shown here again in simplified form but are based on the results of the original article.

Table 31: Test program for the discharge rates of different types of salt [Paper IV]

Type	ACA	ACA content [mg/kg]	Abbreviation
Rock salt	None	0	RS-0
Rock salt	Sodium ferrocyanide	70	RS-70
Vacuum salt	None	0	VS-0
Vacuum salt	Sodium ferrocyanide	8	VS-8
Vacuum salt	Cyanide-free, organic	12	VS-12-Bio
Vacuum salt	Sodium ferrocyanide	22	VS-22
Vacuum salt	Sodium ferrocyanide	80	VS-80

If all of the results of the discharge rate and discharge angle are compared in a graph, then a linear relationship between the two descriptive variables can be observed, i.e., the larger the discharge angle, the lower the discharge rate. The simple linear regression can be described using Equation (6) and the coefficients $\alpha = 81.3466$ and $\beta = -0.683672$. The resulting regression line is shown in Figure 32 as a continuous line. The regression line resulting from the theoretical boundary conditions (i.e., maximum at 100% discharge rate and 0° discharge angle and minimum at 0% discharge rate and 90° discharge angle) is shown as a straight dashed line.
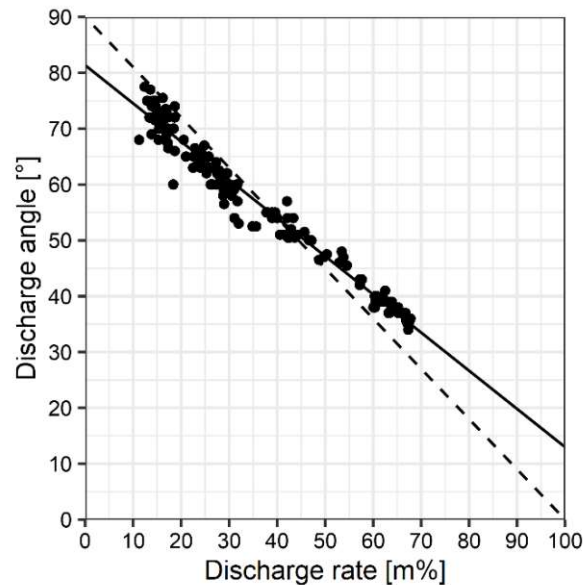
Figure 32: Discharge angle vs discharge rate of all types of tested salt [Paper IV]

If the discharge rate is plotted as a function of moisture content and salt type or ACA content, then Figure 33 is obtained. For completely dry salt (denoted by the color red), the discharge rate is always more than 60 m%. If a moisture content of 0.25 m% is added to the salt (denoted by the color green), then salts without an ACA bake together strongly and the discharge rate is reduced to approximately 20 m%, whereas salts with an ACA perform significantly better. Notably, a moisture content of 0.25 m% is low, i.e., only 2.5 g water is added per kilogram of salt. Higher moisture contents of 0.50 m% and 0.75 m% (denoted by the colors cyan and purple) further reduce the pourability of salts with ACA, although the discharge rate is still better than without ACA.

Furthermore, the organic ACA shows no effect at all, an ACA (sodium ferrocyanide) content of (less than) 8 mg/kg shows only a slight effect, and an ACA content of more than 22 mg/kg shows no significant improvement.
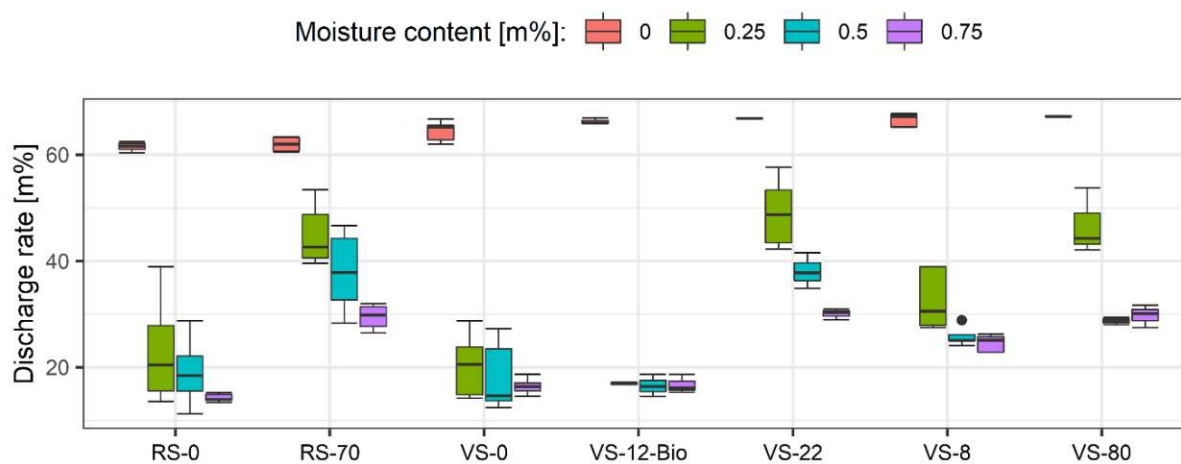
Figure 33: Discharge rate as a function of moisture content [63]

5.2 Conclusion and outlook

Because cleared snow and ice do not have to be deiced, the efficiency of snowplows is one of the most important factors in winter maintenance but does not seem to be the focus of research. Therefore, a comparison of snowplows in terms of efficiency and blade wear was conducted. For efficiency, preliminary tests were conducted to develop a suitable method for quantifying residual snow after clearing. The method presented lays the foundation for conducting practical tests in the future.

For evaluating the abrasion of snowplow blades, extensive field testing was conducted, which shows significant differences between materials and manufacturers under heavy-duty conditions. With this method, a maximum abrasion of 22 mm after 78 km was achieved with 20 mm-thick steel snowplow blades, whereas combination blades (steel and corundum) only show 5 mm (36 mm thickness) and 2.5 mm (50 mm thickness) for the same distance.

In combination with the snow-clearing quality, which is still to be investigated, a model that will provide a recommendation for the selection of snowplow blades according to boundary conditions (e.g., snow or ice frozen to the surface, temperature, and consistency of snow) needs to be developed.

Because deicing agents, such as SC, have to be spread eventually and clogging of salt silos has been repeatedly reported, tests investigating the effects of different moisture contents and ACA (sodium ferrocyanide) on the pourability of SC were conducted. The effectiveness of the "Auslaufbox nach Sonntag" (discharge box) was proven and the results show significant differences in discharge rate and discharge angle depending on the ACA and moisture content. A minimum of 22 mg ACA/kg salt is required for adequate pourability, with only a slight improvement when increased to 80 mg/kg. A biological alternative to sodium ferrocyanide was determined to be ineffective in improving pourability, even at low moisture content.

In addition to the analysis of the moisture and ACA contents, future studies should focus on the influence of the grading curve on pourability. This also includes a critical review of the grading curves for SC specified in ÖNORM EN 16811-1 [64], particularly the amount of extra fine grains. Nevertheless, the effectiveness of countermeasures seems to be limited even at moderate moisture contents of 0.75 m%. Thus, the moisture content should always be kept as low as possible during delivery and storage.

6   Conclusions and outlook

The transition from a linear economy to a circular economy is crucial to handle the Earth's resources with more care and thus also to comply with the European regulations (Waste Framework Directive 2008/98/EC) and to reach the targets of the "Sustainable Development Goals of the United Nations". The circular economy is a far-reaching concept but can be comprehensively represented in the research field of road construction and operation in four steps, i.e., ecological and economic use of resources and materials, increasing service life through more durable materials, utilization of resources in recycled products, and direct and indirect reduction of environmental impacts. Considering this framework of circular economy, several topics are selected, answering specific research questions (RQs).

The first part of this dissertation and the first paper tackle RQ1 and present the asphalt mix and concrete production factors that affect climate change or greenhouse gas (GHG) emissions. The use of lifecycle assessment and the structure of environmental product declarations according to EN 15804 enable the systematic comparison of different products and eliminate previous uncertainties regarding the inclusion of benefits beyond the system boundary. For asphalt mix production, the results show the dominance of asphalt binder in the material footprint and the corresponding advantage of substituting virgin material with recycled material, as well as the influence of material moisture on GHG emissions in the production process. Because concrete production is not influenced by moisture and does not require heat, the only dominant factor is the material footprint of cement. The comparison of both materials, at all stages of EN 15804 (except for the use stage (B1–B7)), shows that a typical asphalt mix (180°C mix temperature, 5% asphalt binder, 88% aggregate, 7% filler, no RAP) yields a CO_2e footprint of 54.5 kg CO_2e/t, whereas a typical concrete mix (depending on its cement content) yields CO_2e footprint between 103.8 kg CO_2e/t (350 kg cement/m³) and 138.6 kg CO_2e/t (450 kg cement/m³).

In addition to evaluating the material, two road sections (1 m long, 7 m wide) for low- and high-traffic-volume sections are compared. Over a 30-year lifetime, two surface layer replacements for asphalt pavements are included and yield 284 and 408 kg CO_2e/m for the low-traffic-volume and high-traffic-volume asphalt pavement cross-sections, respectively. For concrete construction, no rehabilitation measures are included, leading to 511 and 661 kg CO_2e/m for the low- and high-traffic-volume concrete pavement cross-sections, respectively.

When additionally accounting for the traffic-related GHG emissions over a 30-year lifetime, a major share of the transport sector in comparison to the construction itself is apparent. Depending on the share of electromobility, 8,000–10,000 kg CO_2e/m road cross-section will be emitted on the low-traffic-volume section or 109,000–135,000 kg CO_2e/m road cross-section will be emitted on the high-traffic-volume section.

Therefore, not only the GHG of the construction itself but also the impact of the construction design in terms of GHG emissions on transport need to be considered. In this context, two components influence fuel consumption, i.e., the longitudinal evenness of the road surface and the rolling resistance due to the surface structure and deflections. As the results from the literature vary on the magnitude of this influence, the next step is to assess the impact of those parameters on the transport sector.

The second part of this dissertation focuses on winter maintenance, as it is responsible for a large part of the allocable workload in road services and thus represents a good starting point for far-reaching ecological and economic improvements. A foundation for resource-conserving use of deicing agents is provided by answering RQ2 and evaluating the performance of deicing agents in Paper II. The deicing performance is usually determined using the SHRP H-205.1 test; however, because problems regarding the repeatability of this test method have been reported, a new test method for deicing performance (i.e., CEDA) was developed. As the results of CEDA show good repeatability, several deicing agents were tested, and the results were analyzed with the help of a nonlinear regression model, enabling the calculation at the 95% confidence interval and 95% prediction interval. Notably, sodium chloride (SC) has the best deicing performance at −5°C, being able to deice 12.75 times its weight (12.75 g/g). Other

tested agents, such as sodium formate (SF; 11.41 g/g) and potassium acetate (PA; 10.59 g/g), show similar performance, whereas potassium carbonate (PC; 6.74 g/g) and potassium formate (PF; 6.38 g/g) deice only half of the amount of SC. Moreover, the influence of corrosion inhibitors added to SC on the deicing performance was evaluated. By substituting 8% SC with sugars (i.e., arabinose, glucose, mannose, or maltose), only a slight difference in deicing performance was observed because of the lower amount of SC, precluding a detrimental effect on the deicing performance.

Since the experiments were only conducted at a temperature of −5°C, a sufficient suitability at other temperatures cannot be predicted. Therefore, the temperature range relevant for winter maintenance (i.e., −15°C to 0°C) needs to be tested, and a model that considers both time and temperature needs to be designed. A further step would be the automation of the test evaluations.

Based on the deicing performance, knowledge of the corrosive effects of the deicing agents should assist in selecting the right agent. This topic is defined with RQ3 and tackled by the third paper. Although SC is a cost-effective deicing agent, it causes high economic damage because of its highly corrosive effect on metals. To quantify corrosion, three different corrosion test methods were compared, i.e., the full immersion test, neutral salt spray test, and alternate immersion test. Because the alternate immersion test had the greatest effect at elevated temperatures (34°C) after 21 days of testing, many deicing agents, as well as inhibitors that potentially reduce the corrosion process, were tested on three different metals (i.e., unalloyed steel (Fe), galvanized steel (Fe(Zn)), and copper (Cu)).

Compared with SC with a relative mass loss of approximately 14 m% due to corrosion on Fe, PC with only approximately 1 m% mass loss is particularly outstanding. In combination with (inexpensive) SC, the following inhibitors are suitable for Fe: Disodium phosphate (DiPh), calcium nitrite (CaNi), mannose (Man), and sodium metasilicate (NaSi). On Fe(Zn) and Cu, only a slight difference in corrosive effects is measured. Only magnesium chloride (MC) can cause higher corrosion rates on Cu. However, because PC, CaNi, and NaSi can negatively affect human health (i.e., skin/eye damage and respiratory irritation), their use as deicing agents (or as additives) must be investigated more closely. DiPh and the sugar Man have no hazardous effects on humans and are suitable for winter maintenance; however, their effects on flora and fauna have not been investigated.

Because cleared snow and ice do not have to be deiced, the efficiency of snowplows and snowplow blades ensures the resource-conserving use of deicing agents and snowplow blades, thereby contributing to the circular economy. The fourth paper provides answers to RQ4 by developing a suitable method for quantifying residual snow after clearing and evaluating the wear of snowplow blades in a field test. Therefore, three different types of snowplow blades were tested, with 20 mm-thick steel blades showing a maximum abrasion of 22 mm after 78 km, whereas combination blades (steel and corundum) only show 5 mm (36 mm thickness) and 2.5 mm (50 mm thickness) for the same distance.

However, as stated in RQ5, even the best deicing agent and best snowplow blade are useless when clogging of deicing agents in storage silos occurs. Therefore, the fourth paper additionally focuses on the suitability of additives for increasing the initial and long-term pourability by investigating the discharge rate and discharge angle with the help of the "Auslaufbox nach Sonntag" (discharge box). The results show significant differences in discharge rate and discharge angle depending on the anticaking agent (ACA) and moisture content (0 m% to 0.75 m%). A minimum of 22 mg ACA/kg salt is required to achieve adequate pourability, with only a slight improvement when increased to 80 mg/kg. However, the effectiveness of countermeasures seems to be limited even at a moderate moisture content of 0.75 m%. Thus, the moisture content should always be kept as low as possible during delivery and storage.

As shown, there are multiple improvement potentials in the field of road construction and road operation, which can help achieve the concept of the circular economy. This dissertation provides concise answers to the RQs posed, lays the groundwork, and points the way to further investigation of more environmentally compatible road construction and operation.

7   References

[1] W. R. Stahel, "The circular economy," *Nature*, vol. 531, no. 7595, pp. 435–438, Mar. 2016, doi: 10.1038/531435a.

[2] F. Pomponi and A. Moncaster, "Circular economy for the built environment: A research framework," *J. Clean. Prod.*, vol. 143, pp. 710–718, Feb. 2017, doi: 10.1016/j.jclepro.2016.12.055.

[3] B. C. Guerra *et al.*, "Circular economy applications in the construction industry: A global scan of trends and opportunities," *J. Clean. Prod.*, vol. 324, p. 129125, Nov. 2021, doi: 10.1016/j.jclepro.2021.129125.

[4] G. L. F. Benachio, M. D. C. D. Freitas, and S. F. Tavares, "Circular economy in the construction industry: A systematic literature review," *J. Clean. Prod.*, vol. 260, p. 121046, Jul. 2020, doi: 10.1016/j.jclepro.2020.121046.

[5] United Nations, "Sustainable Development Goals of the United Nations," Apr. 13, 2023. https://sdgs.un.org/goals/goal12

[6] European Commission, "Circular economy action plan." Apr. 11, 2023. [Online]. Available: https://environment.ec.europa.eu/strategy/circular-economy-action-plan_en

[7] European Parliament and Council, "Directive 2008/98/EC on waste and repealing certain Directives." 2018. Accessed: Apr. 11, 2023. [Online]. Available: http://data.europa.eu/eli/dir/2008/98/2018-07-05

[8] Eurostat, "Guidance on classification of waste according to EWC-Stat categories." 2010.

[9] BGBl. II Nr. 290/2016, "Verordnung des Bundesministers für Land- und Forstwirtschaft, Umwelt und Wasserwirtschaft über die Pflichten bei Bau- oder Abbruchtätigkeiten, die Trennung und die Behandlung von bei Bau- oder Abbruchtätigkeiten anfallenden Abfällen, die Herstellung und das Abfallende von Recycling-Baustoffen (Recycling-Baustoffverordnung – RBV)." 2016. [Online]. Available: https://www.ris.bka.gv.at/eli/bgbl/II/2016/290/20161027

[10] International Organization for Standardization, "ISO 14025:2006 -Environmental labels and declarations - Type III environmental declarations - Principles and procedures." 2006. [Online]. Available: https://www.iso.org/standard/38131.html

[11] CEN-CENELEC, "EN 15804:2012+A2:2019 - Sustainability of construction works - Environmental product declarations - Core rules for the product category of construction products." 2020.

[12] International Organization for Standardization, "ISO 14040:2006 - Environmental management - Life cycle assessment - Principles and framework." 2006. [Online]. Available: https://www.iso.org/standard/37456.html

[13] Austrian Standards Institute, "ÖNORM S 2096-2 -Material flow analysis - Part 2: Application in waste management - Methodology." 2005.

[14] "STAN - SubsTance flow ANalyis." TU Wien, Institute for Water Quality, Resource and Waste Management. [Online]. Available: https://www.stan2web.net/

[15] Österreichische Forschungsgesellschaft Straße - Schiene - Verkehr, "RVS 03.08.63 - Pavement Design (Oberbaubemessung)." 2021.

[16] Umweltbundesamt, *Klimaschutzbericht 2022*, vol. 0816. Wien, 2022.

[17] IBU (Institut Bauen und Umwelt e.V.), "IBU EPD Database," Apr. 13, 2023. https://ibu-epd.com/

[18] cemsuisse (Verband der Schweizerischen Cementindustrie), "Cemsuisse EPD Database," Apr. 13, 2023. https://www.cemsuisse.ch/umweltdeklarationen/

[19] Deutsches Bundesministerium für Wohnen, Stadtentwicklung und Bauwesen, "Oekobaudat EPD Database," Apr. 13, 2023. https://www.oekobaudat.de/

[20] Deutsches Umweltbundesamt, "Probas EPD Database," Apr. 13, 2023. https://www.probas.umweltbundesamt.de/

[21] ecoinvent Association, "ecoinvent LCI Database v 3.7," Apr. 13, 2023. https://ecoinvent.org/

[22] Bundesministerium für Nachhaltigkeit und Tourismus, "Die Bestandsaufnahme der Abfallwirtschaft in Österreich - Statusbericht 2019," Wien, 2019.

[23] R. Blab *et al.*, "Betonstrassen - Das Handbuch, Leitfaden für die Praxis," Wien: Zement + Beton Handels- u. Werbeges.m.b.H., 2012.

[24] Bau EPD GmbH, "Bau EPD Database," Apr. 13, 2023. https://www.bau-epd.at/

[25] ift Rosenheim GmbH, "ift Rosenheim EPD Database," Apr. 13, 2023. https://www.ift-rosenheim.de/

[26] EPD International AB, "International EPD System Database," Apr. 13, 2023. https://www.environdec.com/home

[27] J. P. C. Araújo, J. R. M. Oliveira, and H. M. R. D. Silva, "The importance of the use phase on the LCA of environmentally friendly solutions for asphalt road pavements," *Transp. Res. Part Transp. Environ.*, vol. 32, pp. 97–110, Oct. 2014, doi: 10.1016/j.trd.2014.07.006.

[28] A. Louhghalam, M. Akbarian, and F.-J. Ulm, "Carbon management of infrastructure performance: Integrated big data analytics and pavement-vehicle-interactions," *J. Clean. Prod.*, vol. 142, pp. 956–964, Jan. 2017, doi: 10.1016/j.jclepro.2016.06.198.

[29] R. E. Kim, S. Kang, B. F. Spencer, I. L. Al-Qadi, and H. Ozer, "Impact of Pavement Roughness and Deflection on Fuel Consumption Using Energy Dissipation," *J. Eng. Mech.*, vol. 145, no. 10, p. 04019080, Oct. 2019, doi: 10.1061/(ASCE)EM.1943-7889.0001653.

[30] S. Pouget, C. Sauzéat, H. D. Benedetto, and F. Olard, "Viscous Energy Dissipation in Asphalt Pavement Structures and Implication for Vehicle Fuel Consumption," *J. Mater. Civ. Eng.*, vol. 24, no. 5, pp. 568–576, May 2012, doi: 10.1061/(ASCE)MT.1943-5533.0000414.

[31] C. C. Chappelow and A. D. McElroy, "SHRP-H647 - Evaluation Procedures for Deicing Chemicals and Improved Sodium Chloride," vol. Strategic Highway Research Program, 1993.

[32] Chappelow, Cecil C. and Darwin, David, *Handbook of Test Methods for Evaluating Chemical Deicers*, vol. SHRP-H-332. in Strategic Highway Research Program, no. 332, vol. SHRP-H-332. Washington, DC: National Academy of Sciences, 1992.

[33] K. Nilssen, A. Klein-Paste, and J. Wåhlin, "Accuracy of Ice Melting Capacity Tests: Review of Melting Data for Sodium Chloride," *Transp. Res. Rec. J. Transp. Res. Board*, vol. 2551, no. 1, pp. 1–9, Jan. 2016, doi: 10.3141/2551-01.

[34] M. Akin and X. Shi, "Development of Standard Laboratory Testing Procedures to Evaluate the Performance of Deicers," *J. Test. Eval.*, vol. 40, no. 6, p. 103615, Nov. 2012, doi: 10.1520/JTE103615.

[35] L. Fay and X. Shi, "Laboratory Investigation of Performance and Impacts of Snow and Ice Control Chemicals for Winter Road Service," *J. Cold Reg. Eng.*, vol. 25, no. 3, pp. 89–114, Sep. 2011, doi: 10.1061/(ASCE)CR.1943-5495.0000025.

[36] S. Koefod, J. Adkins, and M. Akin, "Alternative Approaches to Measuring Deicer Ice-Melting Capacity: Optimization of Test Accuracy and Precision," *Winter Maint. Surf. Transp. Weather*, no. E-C162, pp. 432–442, 2012.

[37] X. Shi, K. Fortune, R. Smithlin, M. Akin, and L. Fay, "Exploring the performance and corrosivity of chloride deicer solutions: Laboratory investigation and quantitative modeling," *Cold Reg. Sci. Technol.*, vol. 86, pp. 36–44, Feb. 2013, doi: 10.1016/j.coldregions.2012.10.011.

[38] R. Alger and J. Haase, "Analysis of the Benefits of Bulk Pre-Wetting Solid NaCl with Several Different Liquids," Michigan Department of Transportation, Jul. 2005.

[39] F. Autelitano, M. Rinaldi, and F. Giuliani, "Winter highway maintenance strategies: Are all the sodium chloride salts the same?," *Constr. Build. Mater.*, vol. 226, pp. 945–952, Nov. 2019, doi: 10.1016/j.conbuildmat.2019.07.292.

[40] D. H. Hanke *et al.*, "International Development of Application Methods of De-icing Chemicals - State of the Art and Best Practice," PIARC - Technical Committee B.2 Winter Serivce, La Defense, 2019R08EN, 2019. [Online]. Available: https://www.piarc.org/en/order-library/30548-en-International%20Development%20of%20Application%20Methods%20of%20De-icing%20Chemicals%20-%20State%20of%20the%20Art%20and%20Best%20Practice

[41] "The Snow and Ice Data Book 2018," PIARC - Technical Committee B.2 Winter Serivce, SIDB2018EN, 2019.

[42] X. Shi, D. Veneziano, N. Xie, and J. Gong, "Use of chloride-based ice control products for sustainable winter maintenance: A balanced perspective," *Cold Reg. Sci. Technol.*, vol. 86, pp. 104–112, Feb. 2013, doi: 10.1016/j.coldregions.2012.11.001.

[43] G. H. Koch, M. P. H. Brongers, N. G. Thompson, Y. P. Virmani, and J. H. Payer, "Cost of corrosion in the United States," in *Handbook of Environmental Degradation of Materials*, Norwich, NY: Elsevier, 2005, pp. 3–24. doi: 10.1016/B978-081551500-5.50003-3.

[44] X. Shi *et al.*, "Evaluating Snow and Ice Control Chemicals for Environmentally Sustainable Highway Maintenance Operations," *J. Transp. Eng.*, vol. 140, no. 11, p. 05014005, Nov. 2014, doi: 10.1061/(ASCE)TE.1943-5436.0000709.

[45] J. Petkuvienė and D. Paliulis, "The Impact of Road Maintenance Substances on Metals Surface Corrosion," *Moksl. - Liet. Ateitis*, vol. 1, no. 4, pp. 92–96, Apr. 2011, doi: 10.3846/mla.2009.4.18.

[46] X. Shi and S. Jungwirth, "The Search for 'Greener' Materials for Winter Road Maintenance Operations," in *Sustainable Winter Road Operations*, X. Shi and L. Fu, Eds., Chichester, UK: John Wiley & Sons, Ltd, 2018, pp. 378–401. doi: 10.1002/9781119185161.ch17.

[47] X. Shi, L. Fay, Z. Yang, T. A. Nguyen, and Y. Liu, "Corrosion of Deicers to Metals in Transportation Infrastructure: Introduction and Recent Developments," *Corros. Rev.*, vol. 27, no. 1–2, pp. 23–52, Apr. 2009, doi: 10.1515/CORRREV.2009.27.1-2.23.

[48] "ASTM G31-72(2204) - Standard Practice for Laboratory Immersion Corrosion Testing of Metals," ASTM International, West Conshohocken, PA, 2004. [Online]. Available: https://www.astm.org/

[49] "ISO 9227:2017 - Corrosion tests in artificial atmospheres-Salt spray tests," International Organization of Standardization, 2017. [Online]. Available: www.iso.org

[50] "ISO 11130:2017 - Corrosion of metals and alloys-Alternate immersion test in salt solution," International Organization of Standardization, 2017. [Online]. Available: www.iso.org

[51] "OENORM EN 10025-1:2004: Hot rolled products of structural steels - Part 1: General technical delivery conditions," 2004. [Online]. Available: www.austrian-standards.at

[52] "ISO 8407:2021 - Corrosion of metals and alloys-Removal of corrosion products from corrosion test," International Organization of Standardization, 2021. [Online]. Available: www.iso.org

[53] R. Benedix, *Bauchemie: Einführung in die Chemie für Bauingenieure und Architekten*. Wiesbaden: Springer Fachmedien Wiesbaden, 2015. doi: 10.1007/978-3-658-04144-1.

[54] A. Y. El-Etre, "Inhibition of C-steel corrosion in alkaline solution using some reducing sugars," *Corros. Prev. Control*, pp. 92–99, 2005.

[55] M. Hoffmann, M. R. Gruber, B. Hofko, T. Seifried, A. N. Koyun, and H. Grothe, "WinterLife - Endbericht WINTERdienst mit effektiven, nachhaltigen und nicht aggressiven Taumitteln sowie optimalen LIFE Cycle Costs der Bahn," TU Wien, Wien. [Online]. Available: http://hdl.handle.net/20.500.12708/40385

[56] T. Schmiermund, *Einführung in die Stereochemie: Eine Hilfe für Studierende und Auszubildende*. in essentials. Wiesbaden: Springer Fachmedien Wiesbaden, 2019. doi: 10.1007/978-3-658-28087-1.

[57] C. Pan, M. Guo, and Z. Wang, "Effect of MgCl2 on the Corrosion Behavior of Copper Under Periodic Wet/Dry Cycle Condition," *J. Mater. Eng. Perform.*, vol. 28, no. 5, pp. 2562–2572, May 2019, doi: 10.1007/s11665-019-04058-3.

[58] German Social Accident Insurance (DGUV), "GESTIS Substance Database," Apr. 13, 2023. https://gestis-database.dguv.de/

[59] Sigma-Aldrich, "Safety Data Sheet," Apr. 13, 2023. https://www.sigmaaldrich.com/AT/en

[60] J. Kruger, *Uhlig's corrosion handbook*. Hoboken, NJ: John Wiley & Sons, Ltd.

[61] N. G. Thompson, M. Yunovich, and D. Dunmire, "Cost of Corrosion and Corrosion Maintenance Strategies," *Corros. Rev.*, vol. 25, no. 3–4, pp. 247–262, Aug. 2007, doi: 10.1515/CORRREV.2007.25.3-4.247.

[62] A. Sonntag and S. Bosewitz, "Die Bestimmung der Rieselfähigkeit von Agglomeraten mit einer Auslaufbox," Fa. Alfred Sonntag Kunststoffe, Schimberg, 2006.

[63] M. R. Gruber, B. Hofko, M. Hoffmann, and W. Kluger-Eigl, "Endbericht zum Forschungsprojekt Wirkmodell Winterdienst," TU Wien, Wien, 2019. [Online]. Available: http://hdl.handle.net/20.500.12708/39833

[64] Austrian Standards Institute, "ÖNORM EN 16811-1 - Winter service equipment and products - De-icing agents - Part 1: Sodium chloride - Requirements and test methods." 2016.

8   List of Figures

9   List of Tables

Paper I

sustainability

MDPI

Article

Life Cycle Assessment of Greenhouse Gas Emissions from Recycled Asphalt Pavement Production

Michael R. Gruber * and **Bernhard Hofko**

Institute of Transportation, TU Wien, Karlsplatz 13/E230-3, A-1040 Vienna, Austria
* Correspondence: michael.gruber@tuwien.ac.at

Abstract: With the growing impact of climate change, there is an increasing need and obligation to reduce the responsible greenhouse gases (GHG) in road construction as well. Using life cycle assessment (LCA) methods, several studies have already separately analysed individual parameters of the asphalt production process and illustrated potential improvements in terms of GHG reduction. However, the data of most assessments originate from single sources and databases, and as such can offer little validation against unreliable assumptions. For this reason, in addition to conducting separate assessments at quarries, batch asphalt mixing plants, and construction sites in order to collect energy and material consumption data with which to calculate GHG emissions, this work relies on the results of multiple sources found in the literature. Using the structure for environmental product declarations (EPDs) in EN 15804, our results are divided into the different stages of a life cycle and the corresponding modules. This allows for systematic comparison of different products and eliminates previous uncertainties regarding the inclusion of benefits beyond the system boundary. The results show the dominance of asphalt binder in the material footprint and the corresponding advantage of substituting virgin material with recycled material, as well as the influence of material moisture on GHG emissions in the production process. In addition to the evaluating the material itself, two road sections with increasing traffic volume (and increasing share of electric mobility) were examined and compared with the traffic-related GHG emissions over a 30-year lifetime. We can confirm that traffic has a substantially higher share of the total GHG emissions (>95%); however, as its regulation is the responsibility of governments, the construction industry can only bring about improvements in its own sphere in seeking to further climate protection.

1. Introduction

With the increasing impact of climate change, the reduction of greenhouse gas (GHG) emissions is becoming increasingly important on a global scale. Road infrastructure is particularly vulnerable to the consequences of climate change, such as severe weather and extreme temperatures, as it was not originally designed with these factors in mind. It is therefore crucial to identify the factors in the road infrastructure production chain that contribute to climate change and to find ways to reduce the environmental impact of these materials. One approach to achieve this is to use life cycle assessment (LCA) methods, which provide a structured way to compare the production of road pavements under different boundary conditions.

Many LCA studies have been conducted to date, most of them specialised on certain aspects of the production, construction, or use stage of asphalt pavements [1–7]. For the production stage, which is dominated by the energy demand for heating and drying of materials, a substantial reduction of GHG emissions is possible when using dry aggregates and natural gas [8]. In particular, the influence of moist aggregates on the energy demand

is quite high, ranging from 7 to 8 kWh/t asphalt pavement per 1% increase of moisture content [9,10]. A practical study has found that the calculated theoretical energy demand used in most literature exceeds the actual energy consumption by 11 to 13% [9].

Another factor in reducing energy demand and GHG emissions is lowering the production temperature, which can lead to energy savings of 2.6 kWh/t asphalt pavement per 10 °C decrease (between 150 °C and 200 °C asphalt pavement temperature) [10]. A more drastic measure to reduce production temperatures is using warm mix asphalt (in general <150 °C), which reduces energy demand and emissions (not only GHG emissions) [11]; however, the consequent use of the necessary additives may offset this advantage [12]. A combination of reduced temperatures and reclaimed asphalt pavement (RAP) added in the range of 10–50% has proven to be beneficial for GHG emissions, with a decrease of 12–17%. The primary advantage of RAP is the reduction in the amount of virgin materials (especially asphalt binder) required for production [12–14]. In contrast to Austria, countries with low resources of qualitatively suitable aggregates must use RAP or recycled aggregates (RCA) to avoid long-distance transport of virgin aggregates. This can make the use of RAP/RCA even more beneficial, as in certain cases GHG emissions are reduced by up to 65% when using RCA compared to virgin material [15]. It should be noted that RAP should be preferred solely in asphalt pavements due to its binder content; RCA, on the other hand can replace virgin aggregate in both asphalt pavements and in concrete pavements and subgrade layers.

In addition to asphalt binder having a large carbon footprint in general, quite large differences in energy demand, and consequently GHG emissions, are observed due to the different system boundaries, technological efficiencies, and regulations in different countries [16]. A reduction in GHG emissions of up to 8% can be achieved by replacing 10% of virgin binder with bio-based binders [17].

A more holistic view of road systems shows that the use stage with traffic cannot be neglected over a certain lifetime, as traffic-related GHG emissions are more than 1000 times higher than the sum of production, construction, and rehabilitation [14]. The urgency of reducing GHG emissions is even clearer when additionally accounting for faster deterioration of roads due to climate change, primarily higher temperatures. This may lead to more road rehabilitation work being required, which, when combined with traffic, leads to higher fuel consumption due to increased road roughness [18].

The use of individual databases to assess the effect of specific processes and materials on GHG emissions has been performed in many studies presented to date. While this is common, it makes the results vulnerable to false assumptions and uncertainties in these values. For example, high variance has been found in on-site emission measurements, with CO and CH_4 emissions particularly affected (CH_4 is a GHG), mainly because they both depend on the combustion efficiency of gas burners [19]. Therefore, relying on single sources can be problematic. The present work mitigates this problem by using multiple sources and using the structure for environmental product declarations (EPD) according to EN 15804 [20]. This ensures better comparability of products and processes under different boundary conditions by clearly dividing the results into the stages and corresponding modules (see Section 2.2), which additionally removes uncertainties with respect to the allocation and especially the inclusion of benefits beyond the system boundary.

Hence, the aim of this study is to: (i) investigate the GHG emissions of the asphalt pavement production, (ii) the extent to which different factors are influential during production, and (iii) the comparison of GHG emissions during a 30-year lifetime (according to Austrian regulations [21]) of asphalt pavements, including rehabilitation works, in both a low traffic volume and a high traffic volume road section. The results provide information on the environmental impact of common road materials, and in particular provide clarification about how different settings of the asphalt production process (moisture of aggregates, adding RAP, etc.) influence energy demand and GHG emissions.

2. Materials and Methods

To assess the environmental impact of processes and products, we conducted an LCA based on the standard ISO 14040 and consisting of the following main modules: goal and scope definition, inventory analysis, impact assessment, and interpretation of results, as shown in Figure 1 [22]. The following subsections provide an overview of which processes are included for the production of one ton of asphalt pavement.
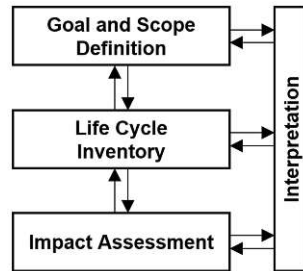
Figure 1. Framework of LCA according to ISO 14040 [22].

2.1. LCA—Goals and Scope

The aim of this first part is to investigate the GHG emissions of the asphalt pavement production and their influencing factors. The system boundaries, include materials and energy inputs and outputs, are shown for asphalt production in Figure 2, illustrating the options for adding hot or cold RAP. This material flow analysis was performed using STAN software (https://www.stan2web.net/, accessed on 1 March 2023) [23]. The inputs were as follows:

- hot virgin asphalt binder (delivered hot);
- virgin filler (produced when drying aggregates—see Section 3.3);
- virgin mineral aggregates;
- RAP.

The materials and energy input for the production of mixing plants, trucks etc., or wear and tear of used products was not taken into account. One ton (=1000 kg) was used as functional unit; wherever possible, data originating from Europe were preferred. To ensure good structure and clarity, the results were divided into modules according to EN 15804.

There are a total of 24 indicators for an LCA according to EN 15804+A2:2019 (compared to seven indicators in EN 15804:2012). These are divided into the categories of environmental impact, resource use, waste and output flows. The first category, environmental impact, consists of thirteen indicators: climate change (total, fossil, biogenic, LULUC), ozone depletion, acidification, eutrophication (aquatic freshwater, aquatic marine, terrestrial), photochemical ozone formation, abiotic depletion (minerals and metals, fossil resources), and water use. Additionally, there are other categories, e.g., resource use, waste, and output flows; however, this study only concentrates on the global warming potential GWP (now: climate change total) as expressed by GHG emission in kg CO_2-equivalents per ton of asphalt pavement (kg CO_2e/t).

2.2. LCA—Modules

To standardise EPDs, each step in the life cycle of a product can be summarised in a stage consisting of different modules. For instance, the product stage (A1–A3) is a combination of the modules raw material supply (A1), transport (A2), and manufacturing (A3). A summary of all stages and modules, which in this work include modules A1–A5, C1–C4, and D (marked with x), can be found in Figure 3.
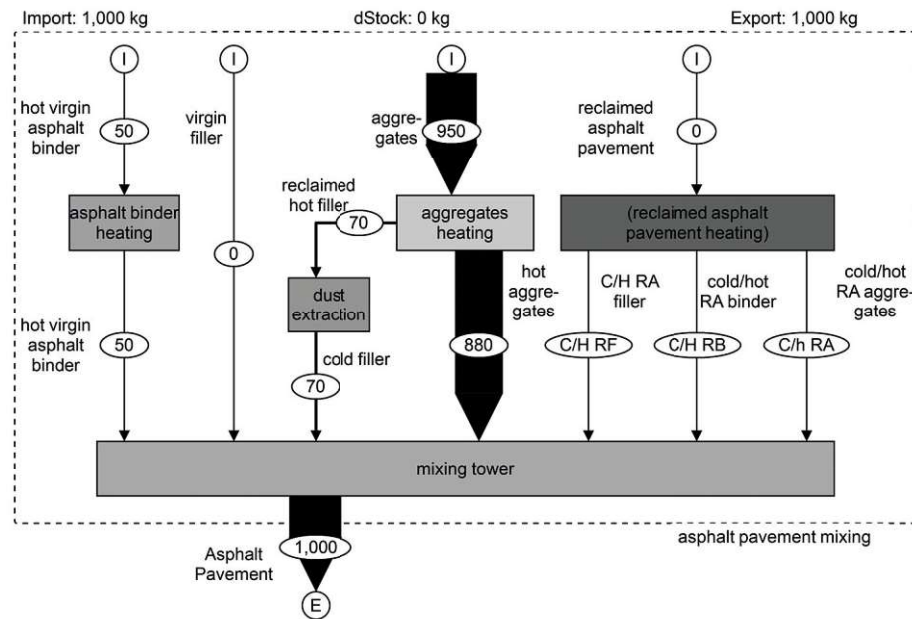
Figure 2. System boundaries of asphalt pavement production with 0% RAP (STAN) [23].

Figure 3. Product stages and modules of EPD according to EN 15804 [20].

3. Results and Discussion

3.1. Module A1—Raw Material Supply

The following subsections provide information on how much GHG emissions must be associated with base materials of asphalt pavements, i.e., mineral aggregates (coarse, fine) and asphalt binder.

3.1.1. Module A1—Mineral Aggregate Production in Quarry

This module section is part of the module raw material supply (A1) of the asphalt production, and represents a cradle-to-gate approach for mineral aggregates. Processes include drilling holes for explosives, blasting, internal transport, crushing, and screening to make the product (mineral aggregate in different sizes) ready for sale.

Data collection for coarse mineral aggregates was divided into measured data from quarries and data from the literature. Because the former data represent the actual use of resources for these activities, they were further used to calculate emissions, while data from the literature were only used to validate the data collected from quarries.

Data from Quarries

Three quarries supplied the consumed amount of diesel and electricity, explosives (ammonium nitrate and fuel oil, or ANFO), fuel oil, and water for up to five years for the production of mineral aggregates (see Table A1 in the Appendix A). All these energy resources produce emissions while being used or when being produced; hence, we multiplied the resource's emission factor by the amount used (see Table A1), resulting to obtain the GHG emissions of 2.51 kg CO_2e per ton of mineral aggregate, which is shown in Table 1.

Table 1. GHG—production of coarse mineral aggregates in quarry.

Type	ANFO	Elect.	Diesel	Heat. Oil	Liq. Gas	Water	Total
Unit				kg CO_2e/t			
n	7	10	10	4	4	2	-
Mean	0.14	0.68	1.62	0.069	0.01	0.00	2.51
SD	0.03	0.23	0.23	0.004	0.00	0.00	0.49
Share	5.55%	26.99%	64.42%	2.74%	0.30%	0.01%	100%

Data from the Literature

The mineral processing industry has published EPDs in many European countries, and as such is already a step further ahead than construction industries in other jurisdictions. In addition to these EPDs, the GHG emissions can be extracted from various databases, such as e.g., Ecoinvent, ProBas, or Oekobaudat. The crushing of aggregates produces fine aggregates such as sand; however, sand is often extracted from quarry ponds, which may explain the difference in GHG emissions from the production of fine mineral aggregates.

The mean value for coarse mineral aggregates is 2.79 kg CO_2e per ton, while for fine mineral aggregates (0/2 and 0/4 fraction) it is 2.06 kg CO_2e per ton. Detailed calculations can be found in the Tables A2 and A3 in the Appendix A.

Because data obtained from quarries do not distinguish between fine and coarse mineral aggregates, it is plausible that the mean value lies between the values for fine and coarse aggregates extracted from the literature. Here, the combined value for fine and coarse mineral aggregates (2.51 kg CO_2e/t) obtained from quarries in Austria is used for further calculations.

3.1.2. Module A1—Asphalt Binder

This module section is part of the module raw material supply (A1) of asphalt production, and represents a cradle-to-gate approach for asphalt binder (bitumen). This work is limited to standard asphalt binder (bitumen), and does not consider polymer-modified asphalt binders (PmB). Because asphalt binder is a byproduct of the oil refining industry, isolating the energy and resources required is a complex process, and companies may be reluctant to disclose their exact production steps.

Therefore, only data from the literature are used here; because there are already substantial geographically related differences in the quality of crude oil and refining efficiency, high variation is to be expected. Production processes include crude oil drilling, transport to refinery, production of asphalt binder, and provisioning in tanks at the refinery. Table 2 lists all sources found for GHG emissions produced by asphalt binder, along with the mean of 365 kg CO_2e per ton and standard deviation of 142 kg CO_2e/t, formed by dropping the highest and lowest numbers to obtain a more robust result.

Table 2. GHG—production of asphalt binder in refinery.

Source	Reference	kg CO_2e/t
Eurobitume v3.1—European Bitumen Association	[24]	~~150~~
Butt—KTH Royal Institute	[25]	173
Stripple—IVL Swedish Environm. Res. Inst.	[26]	173
Yang—CEE U Illinois	[27]	324
GaBi DB—Mean of EU/US Bitumen at Refinery (Thinkstep)		327
Hakkinen—Techn. Res. Center of Finland	[28]	330
Mukherjee—CEE Michigan TU	[29]	390
Athena Sust. Mat.—Inst. f. Cement Assoc. Canada	[30]	400
Samieadel—NC State U	[17]	534
Thinkstep—LCA of Asphalt Binder f. Asphalt Inst.	[31]	637
Jungbluth—ESU Switzerland	[32]	~~720~~
Mean ~~(n = 11)~~ (n = 9)		365
SD		142

3.1.3. Module A1—Reclaimed Asphalt Pavement Processing

This section is part of the module raw material supply (A1) of asphalt production, and represents a cradle-to-gate approach for processing RAP.

According to EN 15804, the life cycle of asphalt pavement ends with the end of life stage (C1 to C4), including the modules deconstruction (C1) and transport (C2) to storage in a landfill (or already to an asphalt mixing plant). This means that the accounting of GHG emissions for RAP begins with transportation to a processing facility, where it is crushed, screened, and stored for further use. These processes are usually conducted at the landfill itself or in the asphalt mixing plant at which it is ultimately used. In both scenarios, the transport distance is the same regardless of whether unprocessed RAP or processed RAP is transported.

It is assumed that processing takes place at the landfill, which results in allocating the transport to the mixing plant to the transport (A2) module of the asphalt pavement production process. If processing in the mixing plant were assumed, the transport module A2 would be 0, as the transportation (C2) module of the end of life stage would account for the transport of RAP from the extraction site to the mixing plant where it is processed. However, as mentioned above, RAP is transported to the landfill (module C2), where it is processed.

In summary, RAP processing includes crushing (electric) and feeding the crusher with a wheel loader (diesel), resulting in emissions of GHGs amounting to 0.37 kg CO_2e per ton of RAP, as seen in Table 3.

Table 3. GHG—production/processing of RAP in landfill.

Source	Crusher (Electr.E.)		Wheel Loader (Diesel)		Total GHG
Unit	kWh/t	kg CO_2e/t	L/t	kg CO_2e/t	kg CO_2e/t
n	2	2	2	2	-
Mean	0.63	0.14	0.07	0.21	0.37
SD	0.03	0.01	0.01	0.02	0.03
Share	-	37.4%	-	62.6%	100%

3.1.4. Summary of Module A1

A summary of the masses and GHG emissions of the raw material supply in the production stage for a common mix design for asphalt pavements can be seen in Table 4. As is be explained later, the filler supply (70 kg) is not imported; rather, it is provided by the dust extraction system of the drying drum (see Figure 2). Therefore, this import stream coincides with the mineral aggregate stream (880 kg), meaning that 950 kg of mineral

aggregates are accounted for. The total GHG emissions of this module, A1, are 20.6 kg CO_2 per ton of asphalt pavement.

Table 4. Asphalt pavement mix design.

Category	Unit	Filler	Min. Aggr.	Asph. Bin.	Total
Mix Design	%	7	88	5	100
Mix Design	kg	70	880	50	1000
Mix Design	kg		950	50	1000
GHG (Mat.)	kg CO_2e/t		2.51	365	-
GHG (Total)	kg CO_2e/t		2.38	18.25	20.6

3.2. Modules A2, A4, and C2—Transport

The transport (A2) module of asphalt production includes the transport of all required raw materials (from module A1) from gate to gate, which in the case of mineral aggregates is from the quarry to the batch asphalt mixing plant. The transport (A4) module represents the transport of ready-to-use asphalt pavement from the mixing plant to the construction site, while module transport (C2) characterises the transport of reclaimed (deconstructed) asphalt pavement from building site to the landfill.

It is assumed that the truck has a maximum loading capacity of 25 tons and delivers the cargo (with a consumption of 35 L Diesel/100 km) from A to B (which is represented by a certain distance), then returns empty (with a consumption of 25 L Diesel/100 km) to A; consequently, the truck makes a round trip with an average consumption of 30 L Diesel/100 km, resulting in 0.075 kg CO_2e per ton and one kilometre of transported material from A to B. This value is slightly below the Austrian Environmental Agency (Umweltbundesamt) indications of 0.085 kg CO_2e/tkm [33].

Summary of Modules A2, A4, and C2

As Austria is a small country and has large deposits of natural mineral aggregates, transport distances are quite short. Table 5 provides an overview of the average transport distances and their corresponding GHG emissions. All distances are set to 25 km except for asphalt binder, which on average is transported about 100 km to the mixing plant. Not taken into account in this calculation is the mass of water contained in the mineral aggregates, which is transported as well.

Table 5. Transport distances and GHG emissions.

Module	Category	Mass kg	Distance km	GHG E. kg CO_2e/t	Total GHG kg CO_2e/t
A2	Min. Aggr.	950	25	1.8	Total A2
A2	Asph. Bin.	50	100	0.4	2.2
A4	Asph. Pav.	1000	25	1.9	1.9
C2	Asph. Pav.	1000	25	1.9	1.9
					$\sum$ 6.0

For modules A2, A4, and C2, transportation of all materials (except asphalt binder) for a distance of 25 km results in 6.0 kg CO_2e per ton of asphalt pavement. Increasing this distance directly increases the GHG emissions (by a factor of 1.9 per 25 km) to 11.4 kg CO_2e/t for 50 km and to 22.5 kg CO_2e/t for 100 km (without alteration of the distance to the asphalt binder supply). Apparently, these transport modules A2, A4, and C2 can quickly become the driving factor in the GHG emissions of the asphalt pavement production process.

3.3. Module A3—Production

As part of the product stage, the production (A3) module represents the main process of batch mixing asphalt pavements: a pair of cold feeders supply a conveyor belt with different sizes of mineral aggregates, which are then directly delivered to the drying drum, where they are dried and brought to the desired temperature. After this, the hot aggregates are lifted by the hot elevator to the mixing plant, where they are separated into different size fractions by the hot screen and stored in compartments. Hoppers in the bottom of these compartments ensure that precisely the mass of the size fraction required for the asphalt pavement's mix design is supplied to the batch mixer, where the asphalt binder (bitumen) is added. After the surface of all mineral aggregates is covered with a thin film of asphalt binder inside the mixer, the process is finished and the ready-mixed asphalt pavement is filled into storage compartments for storage until it is loaded onto trucks.

Two techniques are commonly used for the addition of RAP, namely, cold addition and hot addition. When using cold addition, RAP is not dried or heated before entering the batch mixer via a by-pass to evade the hot screen; instead, it is co-heated by the hot virgin aggregates directly inside the mixer. However, this means that the virgin aggregates have to be superheated in order to co-heat and dry the RAP, which takes a lot more energy than heating. Because this superheating is limited and the addition of cold and moist RAP to very hot virgin aggregates causes sudden evaporation with an associated pressure increase, the total amount of RAP added in this cold addition technique is limited to between 10% RAP at 8% moisture content and 40% RAP at 2% moisture content, according to current Austrian regulations [34].

Hot addition of RAP allows for gentle heating of RAP, which should reduce temperature-induced ageing of the asphalt binder in the RAP. There are two sub-techniques: In the first, the virgin aggregates and RAP are dried and heated together in the drying drum, which is less common; in the second technique, all processes are the same as for cold addition except that the RAP is dried and heated in a separate dryer drum (called a parallel drying drum). This latter method theoretically allows RAP ratios of up to 100%, although currently in Austria only 30–60% RAP is added hot.

Each type of asphalt pavement and each asphalt layer has certain requirements (in addition to the requirements for mineral aggregates and asphalt binder): grading curve, asphalt binder content, void content, bulk density, Marshall stability, etc. There are many different mix designs for asphalt pavements, which of course affect the need for more or less asphalt binder and other materials that significantly influence GHG emissions. For simplicity, a typical mix design according to Table 6 was chosen, indicating a 30% addition of RAP (300 kg). According to EN 15804, any benefits (such as adding RAP) are not included in the process itself, and are instead reported in thereuse potential (D) module of the benefits and loads beyond the system boundary stage.

Table 6. Asphalt pavement mix design, composition of RAP and substitution of virgin materials.

Category	Filler	Mineral Aggr.	Asph. Bin.	Total
Mix Design	7%	88%	5%	100%
Mix Design	70 kg	880 kg	50 kg	1000 kg
RAP	9%	88%	3%	100%
RAP	27 kg	264 kg	9 kg	300 kg
Substituted Mat.	27 kg	264 kg	9 kg	300 kg
Virgin Mat.	43 kg	616 kg	41 kg	700 kg

The evident processes for module A3 with the different recycling techniques (hot/cold) are shown in Figure 2; these do not affect the material flow analysis or calculations, and the same is true for figures in Table 6). In this figure the four input streams of the subsystem boundary of the production (A3) module are visible, representing the sum of the raw material supply (A1) and transport (A2) modules, which include 50 kg of asphalt binder,

0 kg of filler, and 950 kg of mineral aggregates. Because in many cases filler is not imported and is instead reclaimed by a dust extraction system when the aggregates are heated in the drying drum, this import stream is modelled as 0 kg and the reclaimed filler (70 kg) is allocated to the input stream of mineral aggregates (70 + 880 = 950 kg). The reclaimed filler is stored and added cold into the mixer when needed, which means that while the filler consumes energy when produced in the drying drum, it does not contribute positively to the temperature of the asphalt pavement. The input stream of RAP is only indicated here, and is not considered in the material flow calculation in this module, as its benefitting from substitution of virgin materials is taken into account later in the case of module D.

The next step in this flow chart is the heating and drying process of mineral aggregates and RAP, if applicable. Heating the asphalt binder does not usually need much energy, as it is delivered hot at around 160 °C and only needs to be kept at a constant temperature. On the other hand, heating and drying mineral aggregates and RAP generally consumes large amounts of energy, especially considering the enormous amount of energy (2257 kJ/kg of water) needed to evaporate the physically bound water content in the material.

3.3.1. Drying and Heating Process of Module A3

As mentioned above, the energy required for heating, and especially for drying, is directly influenced by the desired temperature and water content of the aggregates and RAP. A comparison of the specific heat capacity of the asphalt pavement's ingredients is shown in Table A4 in Appendix A. To emphasise the high energy requirement for the evaporation process, to heat 1 kg of water from 0 °C to 100 °C ($\Delta T = 100$ K) around 418 kJ are needed, while to evaporate the same amount of 100 °C water more than five times this energy (2257 kJ) is necessary.

It is therefore of utmost importance to keep all materials, especially the fine aggregate fraction (which absorbs a particularly large amount of water), as dry as possible by covering or roofing it. RAP, on the other hand, has poor absorption characteristics due to containing asphalt binder. Even if RAP is exposed to precipitation, the moisture content does not increase to such an extent that the energy needed in the drying process is substantially affected. However, it is recommended to cover RAP anyhow.

Using the specific heat capacity provided in Table A4 of the Appendix A, the following Table 7 shows the theoretical energy demand for heating and drying a ton (dry mass) of mineral aggregates by 180 K (from 15 °C to 195 °C) in dependence of moisture content. The water contained is, of course, only heated by 85 K (from 15 °C to 100 °C) and subsequently evaporated.

Table 7. Influence of moisture in mineral aggregates on energy demand.

Mineral Aggregates			Water in Mineral Aggregates				Total
Mass kg	ΔT K	E Heat. kJ	Mass kg (%)	ΔT K	E Heat. kJ	E Vapor. kJ	Energy $\sum$ kJ
1000	180	153,000	0 (0)	85	0	0	153,000
1000	180	153,000	10 (1)	85	3556	22,570	179,126
1000	180	153,000	20 (2)	85	7111	45,140	205,251
1000	180	153,000	30 (3)	85	10,667	67,710	231,377
1000	180	153,000	40 (4)	85	14,222	90,280	257,502
1000	180	153,000	50 (5)	85	17,778	112,850	283,628
1000	180	153,000	60 (6)	85	21,333	135,420	309,753

Considering the asphalt pavement mix design presented previously in Table 6; assuming fairly moist mineral aggregates with a water content of 5%, Table 8 shows the energy required to bring asphalt pavement to a temperature of 180 °C by heating and additionally evaporating its containing water. It is assumed that the initial temperature of all materials is 15 °C, except for asphalt binder, which is stored at 160 °C. It is further assumed that only the mineral aggregates are heated and dried in the drying drum. As mentioned earlier, filler

is added cold, even though it is reclaimed at a hot stage in the dust extraction process, as it is not used immediately. Consequently, while the energy for heating the filler is included in module A3, the filler does not contribute to the mixture's temperature; this is indicated with the asterisk (*) in Table 8.

Table 8. Calculation of module A3 for given asphalt pavement mix design.

Category	Filler	Mineral Aggr.	Asph. Bin.	Total
Mass Material	7%	88%	5%	100%
Mass Material	70 kg	880 kg	50 kg	1000 kg
Mass Material		950 kg	50 kg	1000 kg
ΔT		180 K	0 K	-
Temp.		195 °C	160 °C	180 °C *
E Heat.		145,350 kJ	0 kJ	145,350 kJ
Mass Water		47.5 kg (5%)	0 kg	48 kg
ΔT		85 K	0 K	-
Temp.		100 °C	-	-
E Heat.		124,096 kJ	0 kJ	24,096 kJ
Total			Σ	269,446 kJ
Total (85%)			85% Efficiency	316,996 kJ [1]

[1] 316,996 kJ = 88.1 kWh.

Table 8 shows that the energy demand for this specific asphalt pavement mix design is 316,996 kJ or 88.1 kWh, assuming 85% efficiency of the mixing plant (which accounts for differences in calculated and real consumption; see [9]). Knowing the GHG emissions of different energy sources [33], the calculation of the specific emissions can be conducted using the figures in Table A5 in the Appendix A. It is evident that natural gas has the lowest emissions, at 22.9 kg CO_2e, while lignite has the highest, at per ton of asphalt pavement. As the most common energy source for the heating and drying process in Austrian asphalt mixing plants is natural gas, all further calculation are based on the use of natural gas.

Dividing the required energy of 88.1 kWh by the average heating value of natural gas (imported from Russia) of 11.3 kWh/m³ results in a consumption of 7.8 m³ per ton of asphalt pavement. These figures (and the assumed efficiency of 85%) appear to be legitimate when compared to the average natural gas consumption of Austrian asphalt mixing plants (more precisely, the drying drums) at between 6 and 8 m³ per ton asphalt pavement, with a water content of 5% in mineral aggregates being on the disadvantageous side in terms of energy demand. As shown later, a water content of 2% would lead to an energy demand of 63.7 kWh, and consequently of 5.6 m³ natural gas per ton, which is in the lower range of the average consumption.

Impact of Varying Moisture Content of Mineral Aggregates

Below, Table 9 lists the different GHG emissions with varied moisture contents of the mineral aggregate. As already indicated by Table 7, it is evident that the water content in the mineral aggregate is the driving factor in energy consumption during the heating and drying process. This table provides greater understanding of the effects of moisture content; in all further calculations, we assume a moisture content of 5%.

Table 9. Impact of moisture content on GHG emissions.

Water Content in Min. Aggr. %	Energy kWh	Total GHG kg CO_2e
5	88.1	22.9
4	79.9	20.8
3	71.8	18.7
2	63.7	16.6
1	55.6	14.5
0	47.5	12.4

3.3.2. Electrical Energy Usage of Module A3

Although many parts of the asphalt mixing plant require electrical energy, it is not reasonable to measure each electrical consumer individually. Therefore, only the electrical energy of the entire plant is evaluated daily, showing a decrease depending on the daily mixing quantity; mixing between 1000 and 3000 tons of asphalt daily consumes between 4 and 2 kWh/t of electrical energy. A low daily mixing quantity of 500 tons can result in a consumption rate of up to 6 kWh/t. Apart from the fact that a plant has a certain baseline consumption, this relation is most likely due to the fact that high mixing quantities often imply that a certain mix design is produced with a high proportion of the daily production. In other words, the likelihood of high electrical energy consumption is high when many different mix designs are produced and the mixing plant needs to be permanently adjusted to the requirements of the product.

Estimation of the GHG emissions based on the electrical energy consumption of the asphalt mixing plant in module A3, assuming 4 kWh/t and electrical energy emissions of 0.345 kg CO_2e/kWh (ecoinvent: Austrian industrial mix), results in an average 1.38 kg CO_2e per ton of asphalt pavement.

3.3.3. Summary of Module A3

In summary, the GHG emissions of module A3 consist of consumption of natural gas (for heating, drying, and vaporising the water content of mineral aggregates) at 22.9 kg CO_2e/t and of electrical energy (for operation of plant components) at 1.4 kg CO_2e/t. For the asphalt pavement mix design used before, this amounts to 24.3 kg CO_2e per ton of asphalt pavement with 5% moisture in mineral aggregates.

3.4. Module A5—Construction (Paving)

The construction (A5) module includes paving with asphalt pavers and compaction with vibrating road rollers. The diesel consumption of asphalt pavers depends primarily (not linearly) on the layer thickness at a near-constant speed of 3 m per minute, with a thicker layer leading to a better ratio of consumption to material. For a typical section of asphalt pavement for a high traffic volume road in Austria with 27 cm total thickness (consisting of a 4 cm surface layer, 11 cm binder layer, and 12 cm base layer), we determined an average consumption of 0.26 L diesel per ton of asphalt pavement.

Vibrating road rollers are needed to ensure sufficient compaction of the asphalt pavements. Similar to asphalt pavers, their consumption per ton of asphalt pavement is a variable of the thickness of the layer being compacted. Calculation of the average consumption for a typical section of 27 cm thickness (compacted three times) results in usage of 0.19 L of diesel per ton. In addition, to prevent material from sticking to the roller, around 4 L of water (which has to be transported to the construction site) are used per ton of asphalt pavement.

A summary of the consumption amounts and rates along with their resulting GHG emissions is listed in Table 10. Note that due to the high water consumption, it was no longer possible to neglect its transportation cost; a transport distance of 10 km was assumed, even though the GHG emissions of water and its transport add up to only 0.004 kg CO_2e/t.

Nevertheless, the total emissions calculated here consist of diesel and water consumption, including transport.

Table 10. GHG—paving and compacting.

Type Unit	Diesel L/t	Water L/t	GHG kg CO_2e/t
Asphalt paver	0.26	-	0.81
Vibrating road roller	0.19	4.00	0.60 *
Paving & compacting	0.45	4.00	total 1.41 *

* incl. transport of water (10 km).

3.5. Module C1—Deconstruction

The deconstruction (C1) module is part of the end-of-life stage of asphalt production, and represents the removal/deconstruction of asphalt pavement, which is then called RAP. The process itself mainly contains asphalt milling, which consumes diesel and uses water for cooling the chisels and reducing dust emissions. RAP is then directly loaded onto a truck using a conveyor belt.

Energy consumption is highly dependent on the thickness of the milled layer. The average diesel and water consumption of different asphalt milling sites with layer thicknesses between 4 cm and 15 cm and their resulting GHG emissions of 2.09 kg CO_2e per ton of RAP can be found in Table 11. Transportation of water is included using a distance of 10 km, resulting in approximately 0.001 kg CO_2e/t of RAP.

Table 11. Materials and GWP—asphalt pavement milling.

Type Unit	Diesel L/t	Water L/t	Diesel kg CO_2e/t	Water kg CO_2e/t	Total kg CO_2e/t
Mean	0.59	1.52	1.87	0.23	2.09 *
SD	0.24	1.08	0.75	0.16	0.91 *

* incl. transport of water (10km)

3.6. Modules C3 and C4—Waste Processing and Disposal

Because RAP and reclaimed loose mineral aggregates represent valuable materials that can be substituted for virgin mineral aggregates and asphalt binder (bitumen), major waste treatment or disposal efforts are rarely necessary.

Waste processing is only needed if the RAP contains hazardous materials such as tar/pitch binders, which were used instead of asphalt binder before being proven to contain high amounts of carcinogenic PAHs. Care must be taken with such materials, as milling releases these pollutants and could harm the health of personnel or be washed into groundwater together with the water used to cool the milling machine's chisels.

Therefore, according to the Austrian Building Materials Recycling Regulation, limit values for the 16 EPA-PAHs of 12 to 300 mg/kg dry matter must be met, depending on the intended use. If the defined limit value for PAHs or other substances are exceeded, landfilling or thermal utilisation must be carried out.

Table A6 in the Appendix A shows the average annual RAP volume for Austria (2015–2019) [35], which amounts to 2 million tons, consisting of 0.6% hazardous RAP (mostly tar/pitch), 11% landfilled RAP, and 88.4% reused RAP in bound and unbound layers.

Because hazardous contamination of RAP is less than 1% and landfilling is permitted, it is assumed that all RAP that is not reused is disposed of in a landfill. This means that, on average, less than 11.6% is processed in a landfill; in this case, the primary activity is the use of a wheel loader, with a diesel consumption of 0.07 L/t (see Table 3), which results in GHG emissions of 0.21 kg CO_2e per ton of landfilled RAP. Subsequently, this means that, per ton of generated RAP, 11.6% produces 0.21 kg CO_2e/(t landfilled RAP), resulting in 0.024 kg CO_2e per ton of RAP.

According to the Federal Waste Management Plan [35], on average (2016: 0.830 Mt, 2017: 0.981 Mt) 45% of RAP reused is actually recycled, i.e., used in asphalt pavement and not in unbound layers as aggregate substitute. The latter is called down-cycling, and on average represents 55% of reused RAP.

3.7. Summary of Modules A1 to A5 and C1 to C4

Table 12 summarises the results of all modules from the production stage in dependence of the mineral aggregates' moisture content, the construction process stage, and the end-of-life stage. As previously indicated in Figure 3, the use stage, consisting of modules B1 to B7, is excluded in this study. Furthermore, module disposal (C4) is greatly rounded up from 0.024 to 0.1, which is indicated with an asterisk. In regard to the moisture content of the mineral aggregates, the total GHG emissions are between 44 and 55 kg CO_2e per ton of asphalt pavement. When only considering modules A1 to A3 (cradle-to-gate), the results are between 37 and 47 kg CO_2e/t, which seems plausible compared to findings in the literature (e.g., 35 to 38 kg CO_2e/t [1]).

Table 12. Summary of all considered modules (kg CO_2e/t).

Moist. Aggr.	Product St.			Constr.		Use	End of Life St.				GHG Total
	A1	A2	A3	A4	A5	B1–B7	C1	C2	C3	C4 *	
5%	20.6	2.2	24.3	1.9	1.4	-	2.1	1.9	0	0.1	54.5
4%	20.6	2.2	22.2	1.9	1.4	-	2.1	1.9	0	0.1	52.4
3%	20.6	2.2	20.1	1.9	1.4	-	2.1	1.9	0	0.1	50.3
2%	20.6	2.2	18.0	1.9	1.4	-	2.1	1.9	0	0.1	48.2
1%	20.6	2.2	15.9	1.9	1.4	-	2.1	1.9	0	0.1	46.1
0%	20.6	2.2	13.8	1.9	1.4	-	2.1	1.9	0	0.1	44.0

* Rounded up from 0.024 to 0.1.

3.8. Variation of the Footprint of Asphalt Binder and Mineral Aggregates

Although asphalt binder only accounts for 5% of the asphalt pavement, its footprint and variation of 365 ± 142 kg CO_2e (or ±39%) per ton of asphalt binder is quite high compared to other materials. Therefore, a variation is reasonable, and is shown in Table 13 for the given mix design with a water content of 5% in the mineral aggregate. The variations in the corresponding module A1 are quite high; however, they account for only 13% of the sum of all stages and modules (54.5 ± 7.1 kg CO_2e/t asphalt pavement).

In contrast, while the footprint and the variation of mineral aggregates is small (2.51 ± 0.49 kg CO_2e), the share by mass in asphalt pavements is high (95%). A variation of these parameters results in total GHG emissions of 54.5 ± 0.5 kg CO_2e (or ±1%), which is not significant, especially compared to asphalt binder (bitumen).

Table 13. Variation of asphalt binder footprint (kg CO_2e/t).

Asph. Bin.	Product St.			Constr.		Use	End of Life St.				GHG Total
	A1	A2	A3	A4	A5	B1–B7	C1	C2	C3	C4 *	
223	13.5	2.1	24.3	1.9	1.4	-	2.1	1.9	0	0.1	47.4
365	20.6	2.1	24.3	1.9	1.4	-	2.1	1.9	0	0.1	54.5
507	27.7	2.1	24.3	1.9	1.4	-	2.1	1.9	0	0.1	61.6

* Rounded up from 0.024 to 0.1.

3.9. Module D—Reuse, Recovery, and Recycling Potential

The reuse potential (D) module is the only module in the benefits and loads beyond system boundaries stage of asphalt production. It aims to provide information on possible advantages of reused and recycled materials in relation to the whole production process.

The main benefits of RAP are its substitution for virgin asphalt binder, avoiding high amounts of GHG emissions, and substitution for virgin mineral aggregates, which have low

emissions but represent the main component of asphalt pavements. Of course, the quality of RAP depends on the original road materials themselves; it can be difficult to obtain constant quality, as there are few records of the materials used in roads built before the 1980s. In addition, it is likely that maintenance, preservation, and improvement works will have been conducted on small sections of a given road in the meantime, which makes it difficult to detect inhomogeneities with only a limited number of drill cores.

The highest continuous quality is usually found in the high-level road network, where the quality of materials is well recorded and the asphalt pavement can be removed by milling layer by layer. In addition, the reclaimed materials are usually homogenised to ensure uniform quality. However, because each homogenised material has different specifications in terms of its grading curve and asphalt binder (bitumen) content, and every type of asphalt pavement has different specifications, it is difficult to provide a universal result for the benefits of RAP per se. Therefore, the composition of RAP is assumed to be as shown in the first row of Table 14. In addition, the table provides the substituted materials and substituted GHG emissions in the case of a 30% RAP quota.

Table 14. Assumed composition of RAP.

Unit	Filler	Mineral Aggr.	Asph. Bin.	RAP
%	9	88	3	100 (RAP)
kg	27	264	9	300 (RAP)
kg	291		9	300 (RAP)
kg CO_2e/t	2.51		365	0.37
kg CO_2e	0.73		3.29	0.11
kg CO_2e		$\sum$ 4.02		0.11
		total substituted GHG emission		total -3.90

In summary, 3.9 kg CO_2e per ton of asphalt pavement can be saved by adding 300 kg with a 30% quota of RAP to replace virgin material, with the main GHG emissions reduction being accounted for by the reuse of the binder in the RAP. Variation of the RAP content between 10 and 50% results in a reduction of 1.3–6.5 kg CO_2e per ton of asphalt pavement.

Although not taken into account, the energy required for drying the materials and evaporating the water in module A3 is reduced by 1.8 kWh/t, or 0.5 kg CO_2e per ton of asphalt pavement (using natural gas) when adding 30% RAP. This is due to the benefit of the lower moisture content in RAP (here, 3%) compared to virgin mineral aggregates (here, 5%).

3.10. Tool for Different Scenarios

As shown, there are a variety of different mix designs, especially the asphalt binder content, as well as a variety of different scenarios, including the moisture contents of the mineral aggregates and RAP and the transport distance, that lead to different GHG emissions. Therefore, a single study can only represent a certain combination of these characteristics, or preferably the possible effects in the form of variations.

Exactly these problems were decisive in the development of a calculation tool that enables evaluation of asphalt production for producers in terms of GHG emissions. A screenshot of the current version can be seen in Figure 4. As this tool is used by asphalt production companies to assess their energy demand and GHG emissions, as well as to obtain bonus points in the tendering process, only modules A1 to A4 (cradle-to-gate approach and transport to construction site) are included.

The user interface is vertically divided; the left side allow input from the user, while the right side displays the results in numerical form as well as graphically in absolute and relative terms compared to the final product. On the input side, the following characteristics can be chosen:

- Asphalt pavement mix design (final product)

- Share and composition of RAP
- Water content of materials
- Initial (storage) temperature
- Targeted temperature of each material, resulting in asphalt pavement total temperature
- Efficiency settings, allowing for adjustment to the conditions of different asphalt mixing plants
- Energy source used for heating and drying
- Transport distance to the mixing plant and construction site
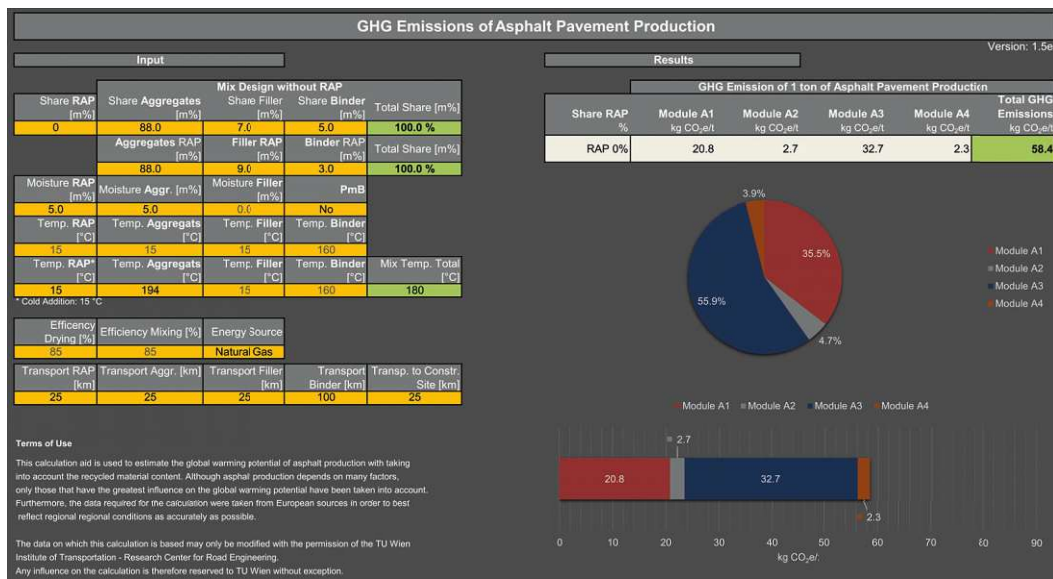
Figure 4. Screenshot of tool used to estimate GHG emissions (developed by author).

4. Comparison—Low Traffic Volume vs. High Traffic Volume Road Section

In order to be able to holistically review GHG emissions on a life-cycle level, two road section were investigated:

- A low traffic volume section with 1 million accumulated equivalent single axle loads (ESALs), leading to a construction type for 0.4 to 1.3 million ESALs, classified as LK 1.3 according to current Austrian guidelines and regulations [21].
- A high traffic volume section with 52.5 million ESALs, leading to a construction type for 42 to 82 million ESALs, classified as LK 82 [21].

These construction types can be seen in Figure 5. Both types consist of two unbound base layers on top of the subgrade: a 30 cm unbound lower base layer and 20 cm unbound upper base layer. Above that, the asphalt pavement starts, and is composed of an asphalt base, asphalt binder, and asphalt surface layer. In the case of LK 1.3, an asphalt binder layer is not necessary due to the low traffic volume. For the following calculation, all asphalt layers are the same type of asphalt as introduced before, with GHG emissions of 54.5 kg CO_2e/t (the worst scenario, that is, 5% moisture content and no RAP). For construction, the unbound layers are not further differentiated and are basically mineral aggregates. Accumulation of GHG emissions for unbound layers includes modules A1–A5 and C1–C4, producing 7.46 kg CO_2e/t, whereas for the transport modules, A4 and C2, a 25 km transport distance is assumed, resulting in a large share of 3.76 kg CO_2e/t (out of 7.46) in terms of total GHG emissions.

For the given section types, LK 82 and LK 1.3, calculations were conducted for 1 m² of asphalt pavement, including construction (LK 82: 47.35 kg CO_2e/m², LK 1.3: 29.63 kg CO_2e/m²) and two asphalt surface layer rehabilitations, i.e., removing the existing asphalt surface

layer (4 cm) and paving a new layer after 10 years of use (2×5.45 kg CO_2e/m²). The results of LK 82 and LK 1.3 coincide with findings in the literature for low traffic and high traffic volume pavements, with 46 kg CO_2e/m² and 27 kg CO_2e/m², respectively [2]. In addition, in order to place these results in relation to traffic, the total GHG emissions for construction and rehabilitation measures (LK 82: 58.25 kg CO_2e/m², LK 1.3: 40.53 kg CO_2e/m²) are then multiplied by the total width of a two-lane road section (2×3.5 m, not including road shoulders), leading to 408 kg CO_2e/m of road for LK 82 and 284 kg CO_2e/m of road for LK 1.3, respectively. Detailed information can be found in Table A7 in Appendix A.
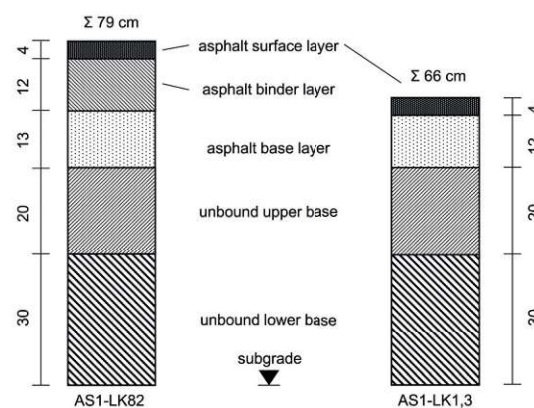
Figure 5. Sections of the two types of asphalt pavement [21].

In a scenario with 0% moisture in the mineral aggregate instead of 5%, GHG emissions for a road section including two asphalt layer rehabilitations decrease considerably (LK 82: 48.53 kg CO_2e/m², 340 kg CO_2e/m of road (−16.7%); for LK 1.3: 34.23 kg CO_2e/m²), 240 kg CO_2e/m of road (−15.5%)).

To estimate the GHG emissions caused by traffic, an increase of 2% p.a. of traffic is assumed. In addition, the share of electric vehicles (both cars and trucks) is expected to increase by two percentage points (pp) p.a., decreasing fossil fuel-based vehicle use by 2 pp p.a. For an assumed 30-year lifetime of pavement, this scenario is displayed in Appendix A in Table A9 for LK 82. In summary, the average annual daily traffic (AADT) increases from 30,686 in 2020 (27,366 light vehicles, 3320 heavy vehicles) to 54,494 vehicles (+78%: 48,598 light vehicles, 5896 heavy vehicles) in 2050. If no electric vehicles were used in this 30-year period, the GHG of all fossil-fueled vehicles would accumulate 135,296 kg CO_2e. Due to the assumed increase of electric mobility (pessimistically assuming no further technical improvements in the energy efficacy of electric vehicles will occur), the GHG emissions in this 30-year period amount to 108,918 kg CO_2e (−19% compared to 135,296 kg CO_2e). These figures are based on an assumed consumption of cars (7 L Diesel or 22 kWh electricity per 100 km) and trucks (30 L Diesel or 150 kWh electric energy per 100 km), whereas a 15% excess consumption due to charging losses of electric vehicles is included.

The traffic and GHG emissions analogous to LK 1.3 can be seen in Table A8 in Appendix A. As before, the AADT increases by 2% from 2650 in 2020 (2545 light vehicles, 105 heavy vehicles) to 4706 vehicles (+78%: 4520 light vehicles, 186 heavy vehicles) in 2050. If no electric vehicles were used in this 30-year period, the GHG of all fossil-fueled vehicles would accumulate 9742 kg CO_2e. Due to the assumed increase of electric mobility (+2 pp p.a. pessimistically assuming no further technical improvement of energy-efficacy of electric vehicles will occur), the GHG emissions in this 30-year period amount to 7778 kg CO_2e (−20% compared to 9742 kg CO_2e).

As seen in Figure 6, displaying the GHG emissions for a period of 30 years considering construction of the two-lane road (2×3.5 m), rehabilitation, and traffic reveals the enormous share of the latter. In this figure, the construction and rehabilitation category is

not visible due to its small proportion, which for LK 82 is 0.408 compared to 109 tons CO_2e and for LK 1.3 is 0.284 compared to 8 tons CO_2e.
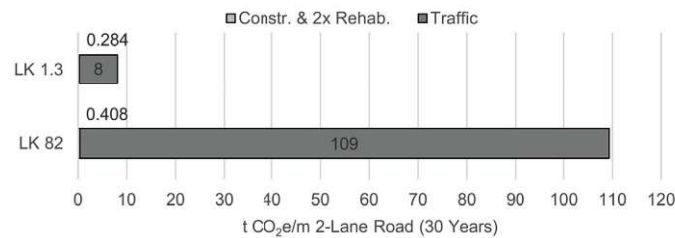
Figure 6. Comparison of GHG emissions for both pavement sections over 30 Years.

5. Conclusions

The aim of this work was to investigate the GHG emissions of asphalt pavement production and the extent of influencing factors during production, as well as to compare GHG emissions for a 30-year lifetime of asphalt pavement in low traffic and high traffic volume road sections (including rehabilitation measures, i.e., complete replacement of the asphalt surface layer every 10 years). In this scenario, ongoing operational measures such as winter maintenance, cleaning, etc., are not considered.

For the first part, the product one ton of asphalt pavement was divided into different stages according to EN 15804: the product stage (including modules A1–A3, representing raw material supply, transport, and manufacturing), construction process stage (modules A4–A5, representing transport and construction), end of life stage (modules C1–C4, representing deconstruction, transport, waste processing, and disposal), and benefits and loads beyond system boundary stage (module D, representing the potential for reuse, recovery, and recycling). For a clear overview, the main results are listed below.

5.1. Production Stage—Modules A1 to A3

- Mix design: 95% mineral aggregates (of which 7 pp are filler) and 5% asphalt binder.
- A1—Raw Material Supply: with average GHG emissions of 2.51 kg CO_2e/t of mineral aggregate and 365 kg CO_2e/t of asphalt binder (note: with high variation of 142 kg CO_2e/t), this module accumulates to 20.6 kg CO_2e/t of asphalt pavement.
- A2—Transport to Manufacturing: transportation of the raw materials to the batch asphalt mixing plant is assumed to involve 25 km from the quarry and 100 km from the asphalt binder supply, and totals 2.2 kg CO_2e/t of asphalt pavement.
- A3—Production: for the above mix design and asphalt pavement temperature of 180 °C, the total GHG emissions are 24.3 kg CO_2e/t when using natural gas as the energy source and accounting for high moisture content of 5% in mineral aggregates (0% moisture: 13.8 kg CO_2e/t). This result includes heating and electrical energy, which contribute as follows:
  - Energy demand, and consequently GHG emissions (using natural gas for heating and drying) increase massively, from 0% moisture (47.5 kWh/t, for natural gas: 12.4 kg CO_2e/t) to 5% moisture (88.1 kWh/t, 22.9 kg CO_2e/t).
  - The electrical energy required to operate the plant is highly dependent on the production volume, and averages 4 kWh/t (Austrian Energy Mix: 1.4 kg CO_2e/t).

Summarising modules A1 to A3 (cradle-to-gate approach) shows total GHG emissions of 47.1 kg CO_2e/t assuming 5% moisture in natural aggregates (0%: 36.6 kg CO_2e/t).

5.2. Construction Process Stage—Modules A4 to A5

In the construction process stage, a total of 3.3 kg CO_2e/t of GHG emissions are generated, consisting of the following modules:

- A4—Transport: 25 km transportation to the construction site, with 1.9 kg CO_2e/t.
- A5—Construction: paving and compacting on site, generating 1.4 kg CO_2e/t.

5.3. End of Life Stage—Modules C1 to C4

The GHG emissions of the end of life stage amount to 4.1 kg CO_2e/t.

- C1—Deconstruction: milling of asphalt pavement generates 2.09 kg CO_2e/t.
- C2—Transport: a 25 km transport distance to the processing site leads to 1.9 kg CO_2e/t.
- C3—Waste Processing: if hazardously contaminated, which is the case for less than 1% of RAP, landfilling is permitted; emissions are 0 kg CO_2e/t.
- C4—Disposal: on average, 12% of RAP is landfilled, which results in less than 0.1 kg CO_2e/t being generated.

Under these assumptions, the total GHG emissions of one ton of asphalt pavement, including all modules A1–A5 and C1–C4 and without including B1–B7 or D from the use stage, amount to 54.5 kg CO_2e/t with 5% moisture content in the mineral aggregate, and to 44.0 kg CO_2e/t with 0% moisture.

5.4. Variation of the Asphalt Binder Footprint and Mineral Aggregates

Although the asphalt binder typically accounts for about 5% of the mass of asphalt pavement and its footprint (module A1) and deviation are very high at 365 ± 142 kg CO_2e/t (or $\pm 39\%$), the variation of the footprint accounts for "only" a 13% change in total GHG emissions (54.5 ± 7.1 kg CO_2e/t). In contrast, the mineral aggregates have a small footprint (2.51 ± 0.49 kg CO_2e/t) and a high share of around 95% by mass, affecting only 1% of total GHG emissions (54.5 ± 0.5 kg CO_2e/t).

5.5. Benefits and Loads Beyond System Boundary

Finally, module D considers the loads and benefits of RAP by reducing the need for virgin materials. Assuming the addition of 300 kg of RAP (=30% recycling rate), consisting of 97% mineral aggregates (of which are 9 pp filler) and 3% asphalt binder, the GHG emissions to be reduced in module D recycling potential amount to -3.9 kg CO_2e/t asphalt pavement (with 30% RAP). Different shares of RAP show a reduction of 1.3 and 6.5 kg CO_2e/t asphalt pavement for 10% and 50% RAP, respectively.

These results are only valid for the assumed aspects; other scenarios may have different effects on GHG emissions. Therefore, a calculation tool was developed for asphalt production companies to asses their influence on climate change, as well as to be able to earn bonus points in the tendering process for high level network roads if certain emission limits are undershot.

5.6. Comparing Pavement Production (Including Rehabilitation) to Traffic

Furthermore, a portion of the use stage for a period of 30 years was calculated seperately for a high traffic road and a low traffic volume road, including rehabilitation measures (i.e., completely replacing the asphalt surface layer every 10 years). Because only parts of the use stage with modules B1 to B7 are considered (ongoing operational measures such as winter maintenance, cleaning, etc., are not considered), the results are not directly linked to the corresponding stage. Instead, they are presented to help estimate and contrast the orders of magnitude of the production of a two-lane asphalt road (7 m width) and the traffic passing over it.

- A high traffic volume two-lane road (AADT 30,000 with an 2% p.a. increase to 54,000 vehicles in 30 years) accumulates 135 t CO_2e per metre. If an increasing share of electric vehicles over 30 years is additionally assumed, this figure changes to 109 t CO_2e per metre.
- A low traffic volume two-lane road (AADT increase from 2600 to 4700 in 30 years) accumulates GHG emissions of 9.8 t CO_2e per metre in 30 years, or 8 t CO_2e/m with increasing share of electric vehicles.
- In this context, the GHG emissions due to the construction and rehabilitation processes are vanishingly small, with a total of 0.284 t CO_2e per metre of two-lane road for a low

traffic volume road (LK 1.3) and 0.408 t CO_2e per metre of two-lane road for a high traffic volume road (LK 82).

In conclusion, this study illustrates the benefits of a structured presentation of the results in order to create comparability and thereby fulfil the objective of EN 15804. As a next step, the theoretical approaches for calculating the energy consumption of drying and heating the material need to be verified or adapted using results from practice. Even though the production process results in relatively low GHG emissions compared to traffic, it nonetheless remains of the utmost importance to reduce those emissions that are within the sphere of the construction industry in order to meet climate goals.

Abbreviations

The following abbreviations are used in this manuscript:

MDPI	Multidisciplinary Digital Publishing Institute
GHG	Greenhouse Gas
ANFO	Ammonium Nitrate and Fuel Oil (a type of explosive)
ESALs	Equivalent Single-Axle Loads
pp	percentage points
p.a.	per annum (per year)
CO_2e	CO_2 equivalents
RAP	Reclaimed Asphalt Pavement
LCA	Life Cycle Assessment
EPD	Environmental Product Declaration
tkm	ton-kilometre

Appendix A

Appendix A.1. Module A1—Raw Materials

This section contains more detailed information on the calculation of the GHG emissions footprint of raw materials used for producing asphalt pavement. (ANFO = ammonium nitrate and fuel oil, which is a type of explosive)

Table A1 shows the energy and material sources needed to produce one ton of mineral aggregate.

Table A1. Materials—production of coarse mineral aggregate in quarry.

Type	ANFO	Elect.	Diesel	Heating Oil	Liq. Gas	Water
Unit	kg/t	kWh/t	L/t	L/t	L/t	L/t
n	7	10	10	4	4	2
Mean	0.06	3.09	0.51	0.021	0.003	0.001
SD	0.01	1.05	0.07	0.001	0.000	0.000

Tables A2 and A3 provide an overview of the GHG emissions per ton of coarse and fine mineral aggregates found in the literature, databases, and EPDs.

Table A2. GHG—production of coarse mineral aggregate in quarry.

Type	Source	URL (accessed on 1 March 2023)	kg CO_2e/t
Gravel 2/32	Oekobaudat (CSV)	https://tinyurl.com/yc5vazr9	2.48
Crushed Natural Aggregates 4/X	EPD Switzerland	https://tinyurl.com/3vkrbz4n	2.38
Gravel (in Bulk)	EPD Italy	https://tinyurl.com/2p9d344r	2.67
Aggregates 8/11, 11/16, 8/16	EPD Sweden	https://tinyurl.com/4yz3w87p	2.26
Crushed Sand and Gravel	EPD Norway	https://tinyurl.com/2dp37wvz	3.13
Crushed Aggregates	EPD Romania	https://tinyurl.com/y3sjrwd5	3.20
Crushed Gravel Production	Ecoinvent 3.5	https://ecoinvent.org/	3.51
		Mean (n = 7)	2.79
		SD	0.43

The data found in the literature were used to verify the data calculated from Austrian quarries. The latter were used for all further calculations.

Table A3. GHG—production of fine mineral aggregate in quarry.

Type	Source	URL (accessed on 1 March 2023)	kg CO_2e/t
Sand 0/2	Oekobaudat (CSV)	https://tinyurl.com/yc5vazr9	2.48
Sand	ProBas	https://tinyurl.com/4dar5yrp	1.61
Rounded Natural Aggregates 0/4	EPD Switzerland	https://tinyurl.com/4n6ucsn2	1.71
Crushed Natural Aggregates 0/4	EPD Switzerland	https://tinyurl.com/4n6ucsn2	1.81
Wet Sand (in Bulk)	EPD Italy	https://tinyurl.com/2p9d344r	2.67
		Mean (n = 5)	2.06
		SD	0.43

Appendix A.2. Module A3—Production of Asphalt Pavement

For calculating the energy demand of heating and drying the mineral aggregate in the drying drum, the specific heat capacities of materials shown in Table A4 were used. To calculate the amount of GHG emissions, the corresponding values for different energy sources are listed in Table A5.

Table A4. Specific heat capacity of different materials.

Filler kJ/kgK	Min. Aggr. kJ/kgK	Asph. Bin. kJ/kgK	RAP kJ/kgK	Water kJ/kgK	Water Vapor. kJ/kg
0.85	0.85	1.7	0.89	4.183	2257

Table A5. GHG emissions of different energy sources [33].

Type	GHG Emissions kg CO$_2$e/kWh	Energy kWh	Total GHG kg CO$_2$e
Natural Gas	0.26	88.1	22.9
Fuel Oil	0.33	88.1	29.1
Hard Coal	0.38	88.1	33.5
Lignite	0.41	88.1	36.1

Appendix A.3. Modules C3 and C4—Waste Processing and Disposal

Table A6 shows the average annual reclaimed asphalt pavement volume for Austria (2015–2019), which amounts to 2 million tons, consisting of 0.6% hazardous RAP (mostly tar/pitch), 11% landfilled RAP, and 88.4% RAP reused in bound and unbound layers [35].

Table A6. Annual RAP volume for Austria [35].

Type	2015	2016	2017	2018	2019	Average
RAP prod.	1.881 Mt	2.006 Mt	2.186 Mt	2.003 Mt	2.220 Mt	2.068 Mt
RAP hazard.	1.1%	0.6%	0.6%	0.6%	0.3%	0.6%
RAP landfill	10.9%	4.0%	2.3%	19.4%	18.4%	11.0%
RAP reused	88.0%	95.4%	97.1%	80.0%	81.3%	88.40%
RAP recycled	88.0%	95.4%	97.1%	80.0%	81.3%	88.40%

Appendix A.4. Comparison of Road Sections

The following Table A7 provides the base data used to calculate the GHG emissions for the road sections shown in Figure 5.

Table A7. Construction of 1 m² of road section.

Type	Unit	LK 82 1 m²		LK 1.3 1 m²
Asphalt Pavement	cm	29		16
Unbound Upper Base	cm	20		20
Unbound Lower Base	cm	30		30
Asphalt Pavement	t	0.73		0.40
Asphalt Pavement	kg CO$_2$e/m²	39.51		21.80
Unbound Base - Aggregates	t		1.05	
Asphalt Pavement	kg CO$_2$e/m²		7.83	
Total GHG Emissions	kg CO$_2$e/m²	47.35		29.63
Rehabilitation of Surface Layer	t		0.10	
Asphalt Pavement	kg CO$_2$e/m²		5.45	
Total Constr. & 2 × Rehab.	kg CO$_2$e/m²	58.25		40.53
Two-Lane Road Section (2 × 3.5 m)	kg CO$_2$e/m	408		284

In Section 4, the AADT of both two-lane road sections (2 × 3.5 m width) and their corresponding GHG emissions are presented. Table A8 shows the AADT divided into cars and trucks along with an annual increase of 2% from 2020 to 2050 (30 years) for the low traffic volume road segment. In addition, the GHG emissions with assumed decreasing share (2 pp p.a.) of fossil fuel-based vehicles and increasing share (2 pp p.a.) of electric vehicles is included. In summary, after 30 years, 39.2 million vehicles pass over the one-meter road section, emitting 7778 kg of CO$_2$e.

Analogous to the previous Table, Table A9 shows the results for a high traffic volume road segment. With 454.4 million vehicles driving over the one-meter segment of two-lane road, 108,918 kg CO_2 are emitted over 30 years.

Table A8. Traffic for road type LK 1.3.

Year	Cars/24h +2%p.a.	Trucks/24h +2%p.a.	Cars Fossil −2 pp p.a.	Cars Elect. +2 pp p.a.	Trucks Fossil −2 pp p.a.	Trucks Elect. +2 pp p.a.
	Vehicles		kg CO_2e/Year			
2020	2545	105	204	0	36	0
2021	2596	107	204	1	36	0
...	...	...	...	...	...	...
2049	4431	183	202	34	36	9
2050	4520	186	202	35	36	10
Sum	37.7 Mill.	1.6 Mill.	6086	481	1076	135
Total	39.2 Mill.		7778 kg CO_2e in 30 years			

Table A9. Traffic for road type LK 82.

Year	Cars/24h +2%p.a.	Trucks/24h +2%p.a.	Cars Fossil −2 pp p.a.	Cars Elect. +2 pp p.a.	Trucks Fossil −2 pp p.a.	Trucks Elect. +2 pp p.a.
	Vehicles		kg CO_2e/Year			
2020	27,366	3320	2194	0	1141	0
2021	27,913	3386	2193	10	1440	8
...	...	...	...	...	...	...
2049	47,645	5780	2170	362	1128	299
2050	48,598	5896	2169	379	1128	313
Sum	405.2 Mill.	49.2 Mill.	65,446	5169	34,027	4276
Total	454.4 Mill.		108,918 kg CO_2e in 30 years			

References

1. Moretti, L.; Mandrone, V.; D'Andrea, A.; Caro, S. Comparative "from Cradle to Gate" Life Cycle Assessments of Hot Mix Asphalt (HMA) Materials. *Sustainability* **2017**, *9*, 400. https://doi.org/10.3390/su9030400.
2. White, P.; Golden, J.S.; Biligiri, K.P.; Kaloush, K. Modeling climate change impacts of pavement production and construction. *Resour. Conserv. Recycl.* **2010**, *54*, 776–782. https://doi.org/10.1016/j.resconrec.2009.12.007.
3. Milad, A.; Babalghaith, A.M.; Al-Sabaeei, A.M.; Dulaimi, A.; Ali, A.; Reddy, S.S.; Bilema, M.; Yusoff, N.I.M. A Comparative Review of Hot and Warm Mix Asphalt Technologies from Environmental and Economic Perspectives: Towards a Sustainable Asphalt Pavement. *Int. J. Environ. Res. Public Health* **2022**, *19*, 14863. https://doi.org/10.3390/ijerph192214863.
4. Bonoli, A.; Degli Esposti, A.; Magrini, C. A Case Study of Industrial Symbiosis to Reduce GHG Emissions: Performance Analysis and LCA of Asphalt Concretes Made With RAP Aggregates and Steel Slags. *Front. Mater.* **2020**, *7*, 572955. https://doi.org/10.3389/fmats.2020.572955.
5. Sollazzo, G.; Longo, S.; Cellura, M.; Celauro, C. Impact Analysis Using Life Cycle Assessment of Asphalt Production from Primary Data. *Sustainability* **2020**, *12*, 10171. https://doi.org/10.3390/su122410171.
6. Farina, A.; Zanetti, M.C.; Santagata, E.; Blengini, G.A. Life cycle assessment applied to bituminous mixtures containing recycled materials: Crumb rubber and reclaimed asphalt pavement. *Resour. Conserv. Recycl.* **2017**, *117*, 204–212. https://doi.org/10.1016/j.resconrec.2016.10.015.
7. Anthonissen, J.; Braet, J.; Van den bergh, W. Life cycle assessment of bituminous pavements produced at various temperatures in the Belgium context. *Transp. Res. Part D: Transp. Environ.* **2015**, *41*, 306–317. https://doi.org/10.1016/j.trd.2015.10.011.
8. Almeida-Costa, A.; Benta, A. Economic and environmental impact study of warm mix asphalt compared to hot mix asphalt. *J. Clean. Prod.* **2016**, *112*, 2308–2317. https://doi.org/10.1016/j.jclepro.2015.10.077.
9. Androjić, I.; Alduk, Z.D.; Dimter, S.; Rukavina, T. Analysis of impact of aggregate moisture content on energy demand during the production of hot mix asphalt (HMA). *J. Clean. Prod.* **2020**, *244*, 118868. https://doi.org/10.1016/j.jclepro.2019.118868.
10. Peinado, D.; de Vega, M.; García-Hernando, N.; Marugán-Cruz, C. Energy and exergy analysis in an asphalt plant's rotary dryer. *Appl. Therm. Eng.* **2011**, *31*, 1039–1049. https://doi.org/10.1016/j.applthermaleng.2010.11.029.
11. del Carmen Rubio, M.; Moreno, F.; Martínez-Echevarría, M.J.; Martínez, G.; Vázquez, J.M. Comparative analysis of emissions from the manufacture and use of hot and half-warm mix asphalt. *J. Clean. Prod.* **2013**, *41*, 1–6. https://doi.org/10.1016/j.jclepro.2012.09.036.

12.   Vidal, R.; Moliner, E.; Martínez, G.; Rubio, M.C. Life cycle assessment of hot mix asphalt and zeolite-based warm mix asphalt with reclaimed asphalt pavement. *Resour. Conserv. Recycl.* **2013**, *74*, 101–114. https://doi.org/10.1016/j.resconrec.2013.02.018.

13.   Giani, M.I.; Dotelli, G.; Brandini, N.; Zampori, L. Comparative life cycle assessment of asphalt pavements using re-claimed asphalt, warm mix technology and cold in-place recycling. *Resour. Conserv. Recycl.* **2015**, *104*, 224–238. https://doi.org/10.1016/j.resconrec.2015.08.006.

14.   Araújo, J.P.C.; Oliveira, J.R.; Silva, H.M. The importance of the use phase on the LCA of environmentally friendly solutions for asphalt road pavements. *Transp. Res. Part D Transp. Environ.* **2014**, *32*, 97–110. https://doi.org/10.1016/j.trd.2014.07.006.

15.   Hossain, M.U.; Poon, C.S.; Lo, I.M.; Cheng, J.C. Comparative environmental evaluation of aggregate production from recycled waste materials and virgin sources by LCA. *Resour. Conserv. Recycl.* **2016**, *109*, 67–77. https://doi.org/10.1016/j.resconrec.2016.02.009.

16.   Santero, N.J.; Masanet, E.; Horvath, A. Life-cycle assessment of pavements. Part I: Critical review. *Resour. Conserv. Recycl.* **2011**, *55*, 801–809. https://doi.org/10.1016/j.resconrec.2011.03.010.

17.   Samieadel, A.; Schimmel, K.; Fini, E.H. Comparative life cycle assessment (LCA) of bio-modified binder and conventional asphalt binder. *Clean Technol. Environ. Policy* **2018**, *20*, 191–200. https://doi.org/10.1007/s10098-017-1467-1.

18.   Chen, X.; Wang, H.; Horton, R.; DeFlorio, J. Life-cycle assessment of climate change impact on time-dependent carbon-footprint of asphalt pavement. *Transp. Res. Part D Transp. Environ.* **2021**, *91*, 102697. https://doi.org/10.1016/j.trd.2021.102697.

19.   Jullien, A.; Gaudefroy, V.; Ventura, A.; de la Roche, C.; Paranhos, R.; Monéron, P. Airborne Emissions Assessment of Hot Asphalt Mixing. *Road Mater. Pavement Des.* **2010**, *11*, 149–169. https://doi.org/10.1080/14680629.2010.9690264.

20.   *EN 15804+A2:2019*; Sustainability of Construction Works—Environmental Product Declarations—Core Rules for the Product Category of Construction Products . CEN-CENELEC: Bruxelles, Belgium, 2019.

21.   *RVS 03.08.63*; Pavement Design (German: Oberbaubemessung). FSV—Oesterreichische Forschungsgesellschaft Strasse—Schiene—Verkehr. FSV: Wien, Austria, 2021.

22.   *ISO 14040:2006:amd:2020*; Environmental management—Life Cycle Assessment—Principles and Framework. International Organization for Standardization: Geneva, Switzerland, 2020.

23.   Brunner P.H.; Rechberger, H. *Handbook of Material Flow Analysis: For Environmental, Resource, and Waste Engineers,* 2nd ed.; CRC Press: Boca Raton, FL, USA, 2016. https://doi.org/10.1201/9781315313450.

24.   Southern, M. *The Eurobitume Life-Cycle Inventory for Bitumen v3.1*; European Bitumen Association: Prague, Czech Republic, 2020.

25.   Butt, A.A. Life Cycle Assessment of Asphalt Roads. Ph.D. Thesis, KTH Roayal Institute of Technology: Stockholm, Sweden, 2014.

26.   Stripple, H. *Life Cycle Assessment of Road*; Report; IVL Swedish Environmental Research Institute: Stockholm, Sweden, 2001.

27.   Yang, R.; Ozer, H.; Kang, S.; Al-Qadi, I.L. Environmental impacts of producing asphalt mixtures with varying degrees of recycled asphalt materials. In Proceedings of the International Symposium on Pavement LCA, Davis, CA, USA, 14–16 October 2014; pp. 14–16.

28.   Hakkinen, T.; Makela, K. *Environmental Adaption of Concrete: Environmental Impact of Concrete and Asphalt Pavements*; VTT Technical Research Centre of Finland: Tampere, Finland, 1996.

29.   Mukherjee, A. *Life Cycle Assessment of Asphalt Mixtures in Support of an Environmental Product Declaration*; National Asphalt Pavement Institute: Lanham, MD, USA, 2016.

30.   Meil, J. *A Life Cycle Perspective on Concrete and Asphalt Roadways: Embodied Primary Energy and Global Warming Potential*; Athena Research Institute: Chester Springs, PA, USA, 2006.

31.   Wildnauer, M.; Mulholland, E.; Liddie, J. *Life Cycle Assessment of Asphalt Binder*; Asphalt Institute and Thinkstep AG: Lexington, KY, USA, 2019.

32.   Jungbluth, N.; Meili, C.; Wenzel, P. *Life Cycle Inventories of Oil Refinery Processing and Products*; ESU-services Ltd. (Commissioned by BFE, BAFU, Erdoel-Vereinigung): Schaffhausen, Switzerland, 2018.

33.   *Austria's National Inventory Report 2022*; Environment Agency Austria: Seibersdorf, Austria, 2022.

34.   *RVS 11.03.22—Decision-Making Aid in the Use of Granulated Asphalt in the Production of Asphalt Mixtures*; FSV—Oesterreichische Forschungsgesellschaft Strasse—Schiene—Verkehr: Wien, Austria, 2012.

35.   *Annual Federal Waste Management Plan*; Federal Ministry for Climate Action: Berlin, Germany, 2021.

Paper II

Deicing performance of common deicing agents for winter maintenance with and without corrosion-inhibiting substances

Michael R. Gruber [a,*], Bernhard Hofko [a], Markus Hoffmann [b], David Stinglmayr [c], Teresa M. Seifried [c], Hinrich Grothe [c]

[a] *TU Wien, Institute of Transportation, Karlsplatz 13/E230-3, 1040 Vienna, Austria*
[b] *Hoffmann Consult e. U. & TU Wien, Institute of Transportation, Fürst-Liechtenstein-Str. 13, 1230 Vienna, Austria*
[c] *TU Wien, Institute of Materials Chemistry, Getreidemarkt 9/E165-01-5, 1060 Vienna, Austria*

ARTICLE INFO

ABSTRACT

Sodium chloride (SC) is by far the most cost-effective deicing agent in winter road maintenance and therefore is used by road authorities worldwide. However, chloride ions foster high corrosivity, which significantly reduces the service lifetime of metals and reinforced concrete of transport infrastructures. Hence, a holistic evaluation with the main criteria of deicing performance and corrosion is demanded and, if possible, alternatives should be considered.

This paper focuses on the deicing performance of sodium chloride and other common acetate-, carbonate-, chloride- and formate-based deicing agents. A newly developed test method is presented, enabling high volume testing at good repeatability. From its results a nonlinear model is derived to predict deicing performance up to five hours after application. Subsequently, this model is compared with both existing empirical and theoretical approaches for evaluating the deicing performance. In addition, the impact of added corrosion-inhibiting substances like sugars on deicing performance is investigated. Finally, a comparison of all tested substances in terms of corrosivity and deicing performance is presented, with corrosion being investigated in detail in another paper.

1. Introduction

The availability and safety of transport infrastructures during the winter season is the main objective of winter maintenance, with the economic benefits far exceeding the costs. These objectives are primarily achieved through snow removal and the spreading of gritting materials or deicing agents during hoar frost, snowfall or freezing rain. As an efficient use of gritting materials is limited to sidewalks and roads with low traffic, the application of deicing agents has become a de facto standard in winter maintenance on all kinds of transport infrastructure (Hanke and Nutz, 2019).

Sodium chloride (SC; non-technical abbreviation to improve readability, especially for other substances, as will be shown later) is by far the most cost-effective deicing agent based on the criteria of availability, cost and deicing performance, and therefore the most commonly used deicing agent in industrialized countries with regular winter maintenance (PIARC, n.d.). However, since common deicing agents are highly corrosive and this being one of the main factors for reduced service life

of metal-based and reinforced transportation infrastructures (Shi et al., 2013; Shi et al., 2014; Koch et al., 2008; Shi et al., 2009), a significant reduction in corrosivity would lead to an increase in service life and substantial savings in infrastructure investment needs. In order to find alternatives to SC with lower corrosivity, a holistic evaluation of other deicing agents is needed, being based on the criteria deicing performance, application rates, costs, corrosion, impact on environment, and life cycle costs (Hoffmann et al., 2022).

This paper focuses on assessing the deicing performance of common deicing agents and, furthermore, on the influence of sugar-based corrosion-inhibiting substances added to SC. In the first part, an overview of the different theoretical and empirical approaches to evaluate deicing performance is presented, including a newly developed test method, allowing a more cost- and time efficient testing. For this method, a nonlinear regression model is derived, with confidence and prediction bands being calculated for SC and other common acetate-, carbonate-, chloride-, and formate-based deicing agents. The second part of the paper compares results obtained from the different models for

---

* Corresponding author.
   E-mail addresses: michael.gruber@tuwien.ac.at (M.R. Gruber), bernhard.hofko@tuwien.ac.at (B. Hofko).

the maximum deicing performance of SC at $-5\ ^{\circ}$C and finally, a relation is established between all tested substances in terms of their corrosivity and deicing performance.

2. Deicing performance

All known deicing agents lower the thermodynamic freezing point of water, i.e. preventing the formation of snow and ice, according to their eutectic properties based on the phase diagram. In contrast, deicing performance determines the amount of ice or snow that can be thawed at a given temperature and in a given time and is largely based on the freezing curve. As the possible theoretical limit of deicing performance diminishes at lower temperatures, the deicing performance also decreases. For efficient winter maintenance, it is therefore crucial to determine the deicing performance of the respective deicing agents or products consisting of primary deicing agents, additives and impurities for the respective temperature range.

Basically, there are two approaches for the determination of freezing curves and deicing performance, i.e. empirical testing and calculation through freezing point depression (FPD). The latter is based on Raoult's idealized law (Albright, 2008), which can be seen in Eq. (1) and states that the partial pressure p_i of each component i of an ideal mixture of liquids (with mole fraction x_i) is equal to the vapor pressure of the pure component $p_i{}^*$.

$$p_i = p_i{}^* \times x_i \tag{1}$$

Since the decrease in vapor pressure is associated with a decrease in freezing point, the latter can be calculated and results only from the molar mass of the solution (colligative properties) and the Van't Hoff factor (Tro, 2020) (dissociative properties of the solute) as shown in Eq. (2).

$$\Delta T_f = K_f \times i \times b \qquad K_f \dots cryoscopic\ constant\ of\ water = -1.86 \left[\frac{kg\ K}{mol}\right]$$

$$\Delta T_f \dots freezing\ point\ depression\ (FPD)\ [K]$$

$$i \dots Van't\ Hoff\ factor\ [-]$$

$$b \dots molality \left[\frac{mol}{kg}\right] \tag{2}$$

The definition of molality can be seen in Eq. (3).

$$b = \frac{n_{solute}}{m_{solvent}} \qquad n_{solute} \dots mole\ of\ solute\ [mol]$$

$$m_{solvent} \dots mass\ of\ solvent\ [kg] \tag{3}$$

Using Eq. (4), molality b can alternately be expressed by Eq. (5)

$$for\ 1\ g: n_{solute} = \frac{1}{M} \qquad M \dots molar\ mass \left[\frac{g}{mol}\right] \tag{4}$$

$$b = \frac{\frac{1}{M}}{m_{solvent}} = \frac{1}{M \times m_{solvent}} \tag{5}$$

With this expression, the freezing point depression in Eq. (6) is now in dependence of the molar mass instead of the molality.

$$\Delta T_f = (K_f \times 1000) \times i \times \frac{1}{M \times m_{solvent}} \tag{6}$$

Eq. (7) converts Eq. (6) to $m_{sovlent}$ as result, which is identical to the deicing performance seen in Eq. (8).

$$m_{solvent} = \frac{K_f \times i \times 1000}{M \times \Delta T_f} \tag{7}$$

$$deicing\ performance \left[\frac{g}{g}\right] = \frac{K_f \times i \times 1000}{M \times \Delta T_f} \tag{8}$$

Thus, it is possible to determine the maximum deicing performance (= deicing capacity) at a certain temperature by converting the FPD for a certain concentration. For example: A FPD of 5 K with a mass concentration of 10m% SC (10m% SC, 90m% water) corresponds to SC thawing 9 times its own mass, which results to 9 g/g deicing capacity at infinite time. In contrast, a representation of deicing performance as a function of time is allowed by empirical test methods, such as the commonly used SHRP H-205.1 and H-205.2 (Chappelow et al., 1992) methods.

In the following section, a new empirical method is presented and compared to also empirically determined results (SHRP test as well as from other literature (Melinder, 2007)), and to the maximum deicing performance derived from Raoult's law.

2.1. Standard SHRP test method

In the standard method for empirical testing SHRP H-205.1 (Chappelow et al., 1992) for solid and SHRP H-205.2 (Chappelow et al., 1992) for liquid deicing agents, deicing agents (4.17 g solid or 3.8 ml liquid) are applied onto an ice slab (130 ml of frozen water in a 223 × 3.2 mm circular plastic dish) at a specific temperature. After a specific time period (10, 20, 30, 45 and 60 min) the melted ice and residual deicing agent are removed, the mass difference is weighed and divided by the mass of the initially applied deicing agent to obtain the deicing performance. Producing ice slabs, applying deicing agents, and measuring the weight loss is time-consuming. Additionally, the number of tests is limited by the size of the climate chamber and ice slabs. Furthermore, it is reported that the SHRP methods have low reproducibility and underestimate the deicing performance (Nilssen et al., 2016; Akin and Shi, 2012; Fay and Shi, 2011; Koefod et al., 2012). Therefore, a modified ice melting test evolved, using smaller circular petri dishes (100 × 15 mm), only applying 1 g solid or 0.9 ml liquid deicer (Akin and Shi, 2012).

Based on this idea, the authors tested deicing performance in a climate chamber, with extended time periods to account for typical deicer application cycles, according to national standards (FSV, 2010) (3 h for highways and 5 h for regional roads).

Therefore, measuring intervals are set to 5, 10, 30, 60, 120 and 240 min to plot a time-dependent deicing performance for a common winter reference temperature of $-5 \pm 1\ ^{\circ}$C.

The complete setup is shown in Fig. 1 and includes 8 specimens (250 g of frozen water in 205 × 15 mm circular stainless-steel containers, 8 deicing agents (prepared samples of 10 ± 1 g), a scale and a bucket for melted water. For temperature control, a dynamic climate chamber (Binder MKF-720) with arm inlets to allow handling the specimens from outside was used. Since temperature mapping shows a certain inhomogeneity of temperature inside the chamber, specific areas were assigned with weighting factors to normalize the results and produce comparable results. The weighting factors were chosen so that the deicing performance for the same time is equal for every position inside the climate chamber.

After all prepared specimens are frozen at $-5\ ^{\circ}$C overnight, the mass of the specimen and its container is weighed, 10 ± 1 g of deicing agent is applied, weighed again and time of application is noted. After 5, 10, 30, 60, 120 and 240 min the specimen is weighed again (to identify possible sublimation or handling error), the brine and melted water is poured out, and the remaining specimen is weighed. The difference between deicing agent applied and melted ice divided by the amount of deicing agent applied is the deicing performance in dependency of time per gram of deicer.

To compare this SHRP-based test method with the newly developed test method, the deicing performance of SC was determined in the climate chamber at $-5\ ^{\circ}$C by conducting 20 tests.

2.2. Cryostat-based test method (CEDA)

To mitigate the problem of SHRP-based methods, which underestimate the deicing performance (Nilssen et al., 2016; Akin and Shi, 2012;

Fig. 1. Climate chamber for testing deicing performance according to SHRP H-205.1/2.

Fay and Shi, 2011; Koefod et al., 2012), a new test method (CEDA: Cryostat-based Evaluation of Deicing Agents) was developed at the Institute of Materials Chemistry, TU Wien. It accelerates the process and increases testing efficiency by using reaction plates (Bio Plas 80 Well Micro Tube Rack) instead of ice slabs and a cryostat (Huber ministat 240) instead of a climate chamber to maintain the desired temperature, allowing more tests in less time compared to the SHRP method (see Fig. 2).

Each well in the reaction plate is filled with 400 μl (399.28 μg at 20 °C) of purified water using a micropipette, then covered to prevent evaporation/sublimation, and frozen at −20 °C overnight. Subsequently to the entire freezing, the reaction plate is placed inside the cryostat, and after reaching the target temperature of −5 °C, different masses of a deicing agent (30 to 500 μg) are put onto the frozen sample. The maximum amount of deicing agent was chosen to achieve results for exposure times of up to 300 min.

To determine how much time has passed until the ice is fully melted, a digital camera (Canon EOS 2000d) is used to take a picture every minute. Once all samples have been deiced, the images are manually reviewed, and as soon as a sample is visually classified as fully melted, the time is noted. The optical difference between a deiced and partly frozen state is displayed in Fig. 3, where, in contrast to the right wells (which are fully melted), in the left wells small formations of ice can still be detected by non-centered or multiple reflection of the light source above. The deicing performance at a specific time (here, the period from adding the deicing agent until the ice is fully melted) is then calculated by dividing the mass of the ice (which is constant) by the exact amount of deicing agent on each sample.

The size of the employed cryostat allows the number of samples to be 40 per test (compared to a maximum of 8 samples in the climate chamber when using the SHRP method). A manual visual classification of the sample's aggregate conditions may be slightly inaccurate. However, in comparison with the standard test method according to SHRP H-205.1/2 in a climate chamber, both the necessary effort and the deviation of this new method are significantly lower, as will be shown later.

2.3. Testing schedule

The deicing performance was tested for SC and other common acetate-, carbonate-, chloride- and formate-based deicing agents according to Table 1, which states the chemical formula and introduces a non-technical abbreviation (e.g., PA = Potassium acetate = CH_3COOK) for improved readability, especially in figures. The other substances were tested as anhydrates except for calcium chloride (CC) and magnesium chloride (MC), which were only available as di- or hexahydrate. Inhibitory substances were added with 8m% of the mass of SC (e.g., 100 μg SC + 8 μg Glucose).

2.4. Calculated freezing point depression

As mentioned before, Raoult's idealized law (Albright, 2008) can be used to calculate the freezing point depression. It links the concentration of dissolved solute in an ideal solution (increased entropy, decreased chemical potential) to the changes in its vapor pressure. Since the decrease in vapor pressure is accompanied by an increase in boiling point and decrease in freezing point, the latter can be calculated and
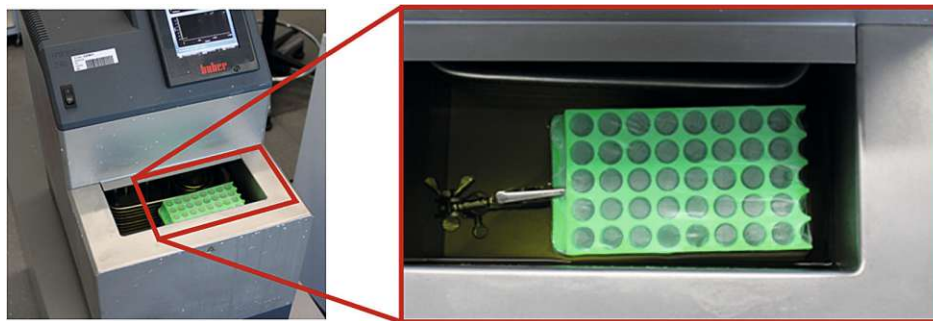
Fig. 2. CEDA: Cryostat (left) and reaction plate (right).
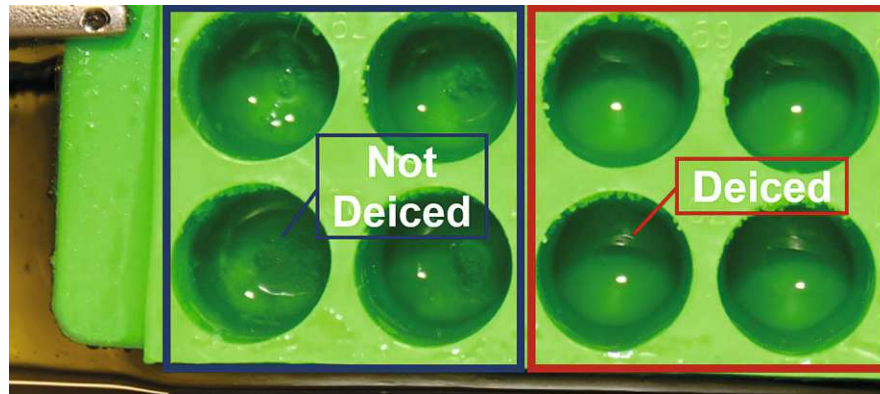
Fig. 3. Distinction of deiced state: Partly frozen (left) and deiced (right).

Table 1

Overview of the tested deicing agents including their abbreviations, formulas and number of studied samples.

Agent	Abbr.	Formula	Samples
Sodium chloride	SC	NaCl	25
Potassium carbonate	PC	K_2CO_3	14
Calcium chloride dihydrate	CC	$CaCl_2 \cdot 2H_2O$	14
Magnesium chloride hexahydrate	MC	$MgCl_2 \cdot 6H_2O$	14
Sodium acetate	SA	CH_3COONa	20
Sodium formate	SF	HCOONa	24
Potassium acetate	PA	CH_3COOK	26
Potassium formate	PF	HCOOK	14
Sodium chloride +8m% Arabinose	SC + Ara	$NaCl + C_5H_{10}O_5$	28
Sodium chloride +8m% Glucose	SC + Glu	$NaCl + C_6H_{12}O_6$	30
Sodium chloride +8m% Maltose monohydrate	SC + Mal	$NaCl + C_{12}H_{22}O_{11} \cdot H_2O$	28
Sodium chloride +8m% Mannose	SC + Man	$NaCl + C_6H_{12}O_6$	25

results only from the amount of substance of the solute (colligative characteristics) and its Van't Hoff factor (Tro, 2020) (dissociative characteristics).

For example, the molar mass of SC (58.44 g/mol) is only a third of glucose (180.16 g/mol), so three times the mass of glucose is needed to achieve the same freezing point depression compared to SC. Furthermore, SC dissociates into Na^+ and Cl^-, hence its Van't Hoff factor is twice the factor of the non-dissociating glucose ($C_6H_{12}O_6$). Summarizing both characteristics results in only 1/6 of SC needed to achieve the same FPD as glucose. Table 2 shows the molar mass and Van't Hoff factor for every tested substance.

3. Results and comparison

3.1. Calculated maximum deicing performance (Raoult's law)

As described in the previous section, the maximum deicing performance of all tested deicing agents was calculated according to Eq. (8) for −5 °C and are given in Table 3.

3.2. Measured maximum deicing performance according to Melinder

Melinder (Melinder, 2007) empirically investigated the freezing point of different aqueous solutions as a function of concentration. His findings are shown in Table 4 and are displayed in Fig. 8 as the "Melinder Model". Based on his results, the maximum deicing performance (= deicing capacity) can be derived from the known

Table 2

Molar mass (M) and Van't Hoff factor (i) for all tested substances.

Substance	Abbr.	Formula	M g/mol	i
Sodium chloride	SC	NaCl	58.44	2
Magnesium chloride	MC	$MgCl_2$	95.01	3
Magnesium chl. Hexahydr.	MC	$MgCl_2 \cdot 6H_2O$	203.01	3
Calcium chloride	CC	$CaCl_2$	110.78	3
Calcium chloride dihydrate	CC	$CaCl_2 \cdot 2H_2O$	146.78	3
Potassium carbonate	PC	K_2CO_3	138.21	3
Glucose	Glu	$C_6H_{12}O_6$	180.06	1
Arabinose	Ara	$C_5H_{10}O_5$	150.05	1
Mannose	Man	$C_6H_{12}O_6$	180.06	1
Maltose	Mal	$C_{12}H_{22}O_{11}$	342.12	1
Maltose monohydrate	Mal	$C_{12}H_{22}O_{11} \cdot H_2O$	360.31	1
Sodium acetate	SA	CH_3COONa	82.01	2
Potassium formate	PF	HCOOK	84.11	2
Sodium formate	SF	HCOONa	68.00	2
Potassium acetate	PA	CH_3COOK	98.12	2
NaCl+8m%Glu	SC + Glu	$NaCl + C_6H_{12}O_6$	58.44/180.06	2/1
NaCl+8m%Ara	SC + Ara	$NaCl + C_5H_{10}O_5$	58.44/150.05	2/1
NaCl+8m%Man	SC + Man	$NaCl + C_6H_{12}O6$	58.44/180.06	2/1
NaCl+8m%Mal.H_2O	SC + Mal	$NaCl + C_{12}H_{22}O_{11} \cdot H_2O$	58.44/360.31	2/1

To calculate the deicing performance or the factor of ice that can be melted at −5 °C (which is a freezing point depression of 5 K), Eq. (8) can be used.

Table 3

Calculated deicing performance of the tested substances for $-5\ ^\circ$C.

Substance	Abbr.	Formula	Calculated max. deicing perf. [g/g]
Sodium chloride	SC	NaCl	12.73
Magnesium chloride	MC	$MgCl_2$	11.75
Calcium chloride	CC	$CaCl_2$	10.07
Potassium carbonate	PC	K_2CO_3	8.07
Glucose	Glu	$C_6H_{12}O_6$	2.07
Arabinose	Ara	$C_5H_{10}O_5$	2.48
Mannose	Man	$C_6H_{12}O_6$	2.07
Maltose	Mal	$C_{12}H_{22}O_{11}$	1.09
Sodium acetate	SA	CH_3COONa	9.07
Potassium formate	PF	HCOOK	8.85
Sodium formate	SF	HCOONa	10.94
Potassium acetate	PA	CH_3COOK	7.58
NaCl+8m%Glu	SC + Glu	$NaCl+C_6H_{12}O_6$	11.88
NaCl+8m%Ara	SC + Ara	$NaCl+C_5H_{10}O_5$	11.91
NaCl+8m%Man	SC + Man	$NaCl+C_6H_{12}O6$	11.88
NaCl+8m%Mal. H2O	SC + Mal	$NaCl+C_{12}H_{22}O_{11}\cdot H_2O$	11.80
Magnesium chl. Hexahydr.	MC	$MgCl_2\cdot 6H_2O$	5.50
Calcium chloride dihydrate	CC	$CaCl_2\cdot 2H_2O$	7.60
Maltose monohydrate	Mal	$C_{12}H_{22}O_{11}\cdot H_2O$	1.03

Table 4

Concentration for FPD obtained from Melinder (Melinder, 2007) and derived deicing performance.

Agent	Formula	Abbr.	Concentration for FPD 5 K [m%]	Deicing Capacity [g/g]
Sodium chloride	NaCl	SC	7.89	11.67
Potassium carbonate	K_2CO_3	PC	13.66	6.32
Sodium formate	HCOONa	SF	10.12	8.88
Potassium formate	HCOOK	PF	16.67	6.32

concentration for an FPD and is calculated in the last column of Table 4. For example, a 7.89m% concentration consists of 7.89 g SC and 92.11 g water. The deicing capacity is then calculated dividing 92.11 by 7.89 = 11.67 g/g.

Table 5

Parameters of nonlinear regression model.

Agent	Abbr.	b_0	b_1
Sodium chloride	SC	12.74952	0.01806
Potassium carbonate	PC	6.73984	0.01927
Calcium chloride dihydrate	CC	8.28207	0.01341
Magnesium chloride hexahydrate	MC	6.82678	0.01708
Sodium acetate	SA	8.15554	0.00988
Sodium formate	SF	11.40702	0.01924
Potassium acetate	PA	10.59200	0.01800
Potassium formate	PF	6.38179	0.03885
Sodium chloride +8m% Arabinose	SC + Ara	11.63396	0.01679
Sodium chloride +8m% Glucose	SC + Glu	11.62069	0.02083
Sodium chloride +8m% Maltose monohydrate	SC + Mal	11.74680	0.01645
Sodium chloride +8m% Mannose	SC + Man	10.37474	0.02430

3.3. Measured deicing performance (CEDA)

The deicing performance is the amount of ice melted per mass of the deicing agent as a variable of time and temperature. The results were obtained from the CEDA test method as described in 2.2.

Statistical analysis was conducted using the programming language R; for determination of the nonlinear least-squares estimates of the parameter of a nonlinear regression model for the deicing performance, the nls-function was used with the formula provided in Eq. (9).

$$y(x) = b_0 \times \left(1 - e^{-b_1 \times x}\right) \tag{9}$$

For the calculation of the 95% confidence interval and the 95% prediction interval, the samples were bootstrapped (nlsBoot-function with 999 resamples) and calculated with the help of nlsBootPredict-function. The computed parameters b_0 and b_1 of the nonlinear regression model for each deicing agent are listed in Table 5. The entire program code is listed in the supplementary data section.

Fig. 4 shows the results and the regression model (incl. 95% confidence interval in red and 95% prediction interval in grey) of the time-dependent deicing performance at $-5\ ^\circ$C for sodium chloride (SC), potassium carbonate (PC), magnesium chloride hexahydrate (MC), and calcium chloride dihydrate (CC). It can be seen that SC shows the best deicing performance after 300 min with 12.7 g/g. The low ability to deice of MC with 6.8 g/g as well as of CC with 8.1 g/g is due to their hydrated form: with increasing amounts of water being solved or chemically bound, the deicing performance will decrease until an equilibrium with no further deicing capacity is reached. This equilibrium is determined by the concentration of the freezing curve for the given temperature.

As shown in Fig. 5, sodium formate (SF), and potassium acetate (PA) exhibit a similar deicing performance compared to SC, with 11.4 g/g and 10.5 g/g, respectively. Potassium formate (PF) and sodium acetate (SA) show significantly lower deicing performance with 6.4 g/g and 7.7 g/g respectively.

Since SC has the best deicing performance of the tested primary deicing agents with 12.7 g/g, another set of tests was conducted to examine the influence of a sugar-based inhibitors on the deicing performance of SC. Since sugars do not dissociate like SC (NaCl; into Na$^+$ and Cl$^-$), a lower amount of melted ice can be expected. The results of the tests in Fig. 6 confirm this expectation. Except for Mannose, all added sugars show a reduced performance at around 11.6 g/g (which is 92% of SC's performance). Mannose-doped SC only deices 10.4 g/g.

3.4. Comparison of deicing performance CEDA and SHRP

Since it is reported that the SHRP test method underestimates the deicing performance (Nilssen et al., 2016; Akin and Shi, 2012; Fay and Shi, 2011; Koefod et al., 2012), a comparison between SHRP and the newly developed CEDA test method was conducted. For the results obtained from SHRP, a nonlinear regression model was derived from the data with the formula provided in Eq. (9), analogous to the previous section. The parameters for the nonlinear regression models are listed in Table 6.

Fig. 7 displays the results and the regression model (incl. 95% confidence interval in red and 95% prediction interval in grey) of the time-dependent deicing performance at $-5\ ^\circ$C for SC, clearly showing the underestimation of the deicing performance derived from the SHRP-based test method: At 300 min, only 9.5 g/g are deiced, which is 25% less than the result of the cryostat-based model (CEDA). Furthermore, the maximum deicing performance (= deicing capacity) of CEDA at 300 min is closer to the theoretical deicing capacity of 11.67 g/g (dashed line in Fig. 7) calculated from the FPD (Melinder, 2007).
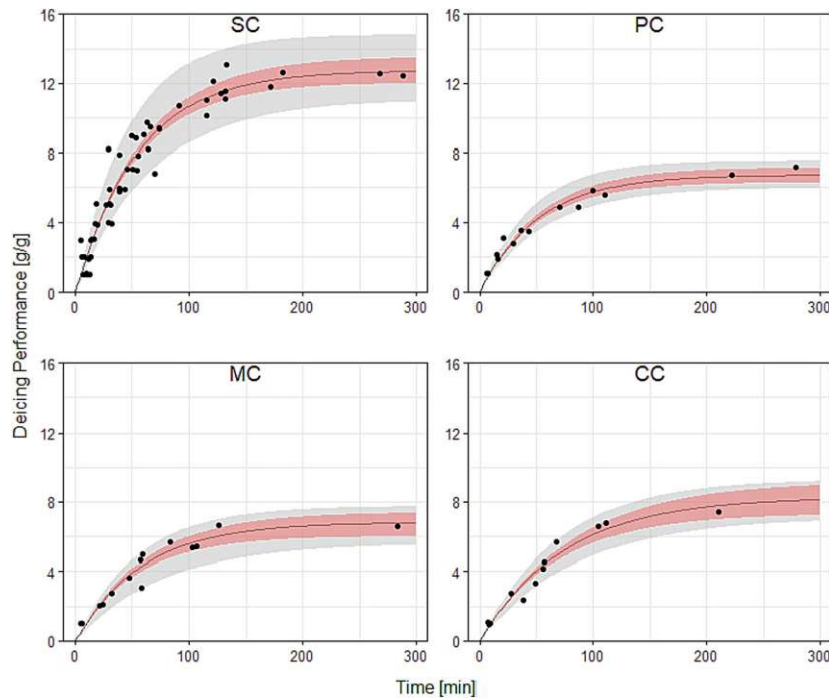
Fig. 4. Deicing performance of sodium chloride (SC), potassium carbonate (PC), magnesium chloride hexahydrate (MC) and calcium chloride dihydrate (CC).
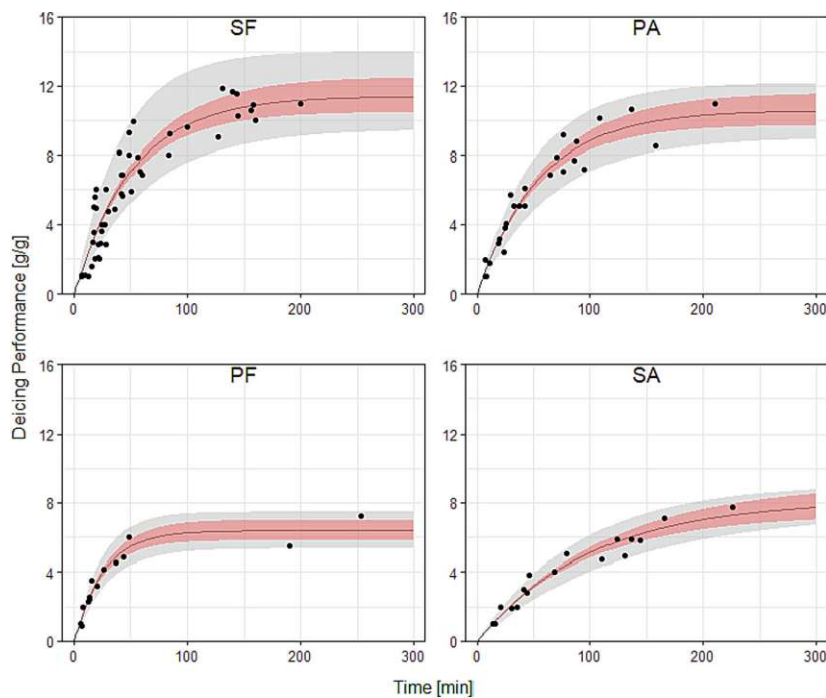
Fig. 5. Deicing performance of sodium formate (SF), potassium acetate (PA), potassium formate (PF) and sodium acetate (SA).

3.5. Comparison calculated and measured FPD

Fig. 8 compares the calculated (Raoult's law - 3.1) and measured (Melinder - 3.2) FPD with the solution's concentration. Additionally, the

95% confidence interval of the concentration needed for achieving an FPD of 5 K (to −5 °C) is displayed, which was converted (deicing performance at 300 min converted back to get the concentration) from the deicing performance tests (CEDA) at −5 °C presented in 3.3. Thus, the

6
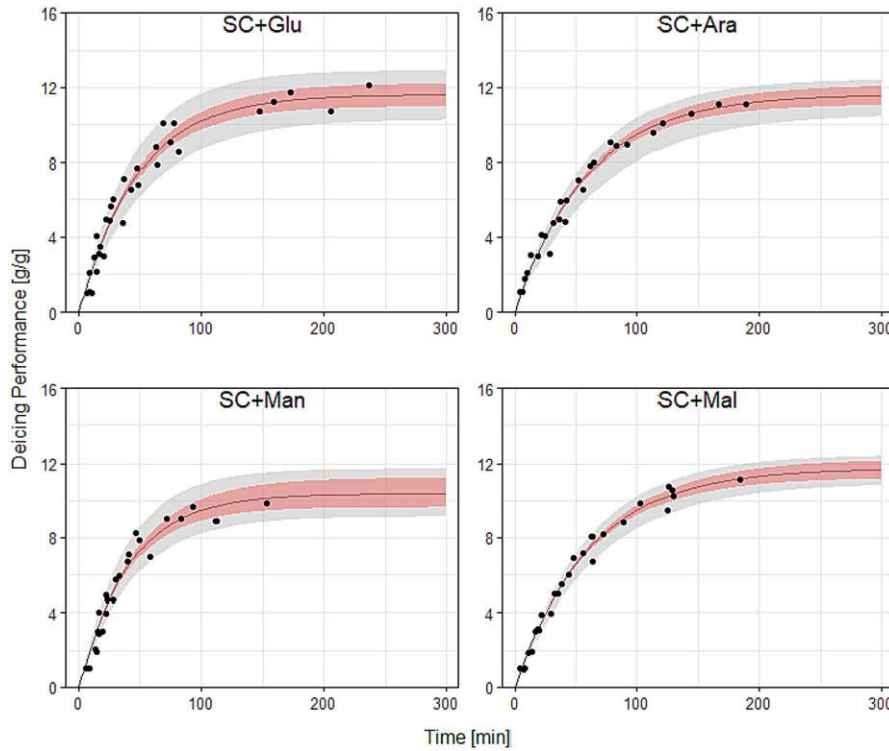
Fig. 6. Deicing performance of sodium chloride (SC) with 8% Glucose (Glu), 8% Arabinose (Ara), 8% Mannose (Man), and 8% Maltose Monohydrate (Mal).

Table 6
Parameters of the nonlinear regression model for CEDA and SHRP.

Agent	Test Method	Abbr.	b_0	b_1
Sodium chloride	CEDA	SC - CEDA	12.74952	0.01806
Sodium chloride	SHRP	SC - SHRP	9.48086	0.01506

data given in Fig. 8 allow for comparison of all investigated methods.

For SC, a comparison of the Raoult's and Melinder's model shows accordance until a FPD of 15 K (to $-15\,°C$) and concentrations up to 20 m %. At higher concentrations, the FPD diverges. The measured model (converted from the deicing performance of the cryostat-based method CEDA) matches both calculated and Melinder's model at a temperature of $-5\,°C$. For all other compared deicing agents (SF, PC, and PF), the cryostat-based FPD is more likely to line up with the measured results

obtained from Melinder, while the calculated (Raoult's law) FPD model indicates a better deicing performance. As the measured results exhibit some deviations, but a high repeatability and are independently acquired, there is a high probability that Raoult's law is of limited use for accurate calculations and predictions on the behavior of other substances.

4. Comparison deicing performance and corrosion

The primary purpose of deicing in winter maintenance is to provide a sufficient level of skid resistance by avoiding freezing due to preventive spreading or by removing residual snow and ice after plowing by applying necessary amounts of deicing agent. With a focus beyond winter maintenance and highly expensive transport infrastructure consisting of metals and reinforced concrete (e.g. train stations, bridges,
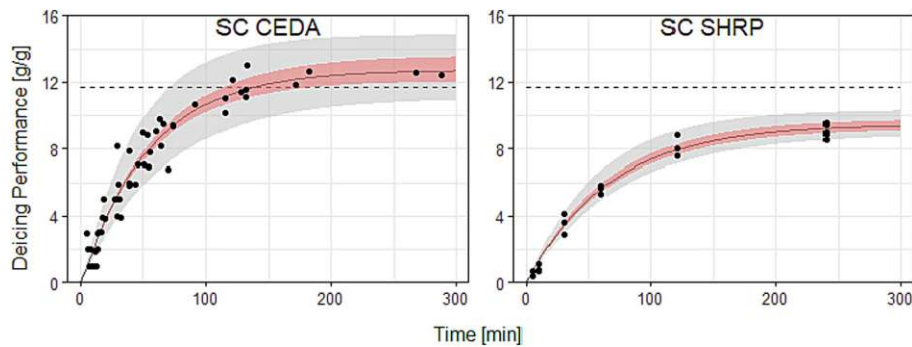
Fig. 7. Deicing performance of sodium chloride (SC) obtained with the CEDA (left) and with SHRP H-205.1 (right) – dashed line represents the theoretical deicing capacity (11.67 g/g).

7
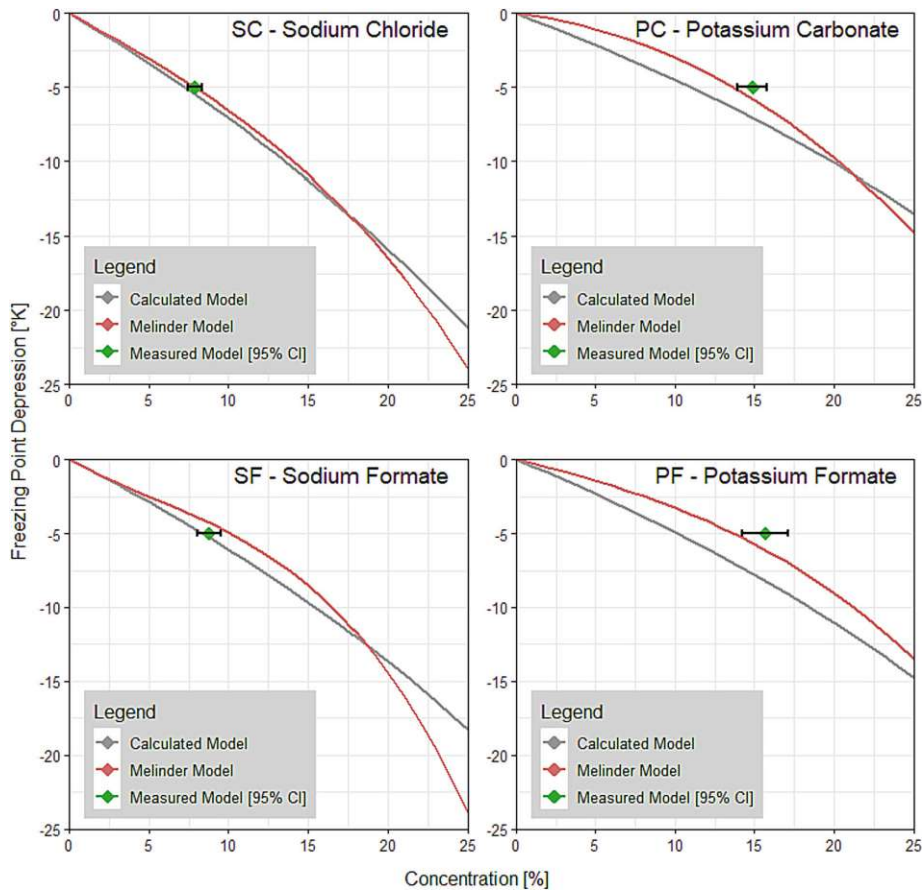
Fig. 8. Comparison of the FPD in dependence of the concentration [m%] of all models.
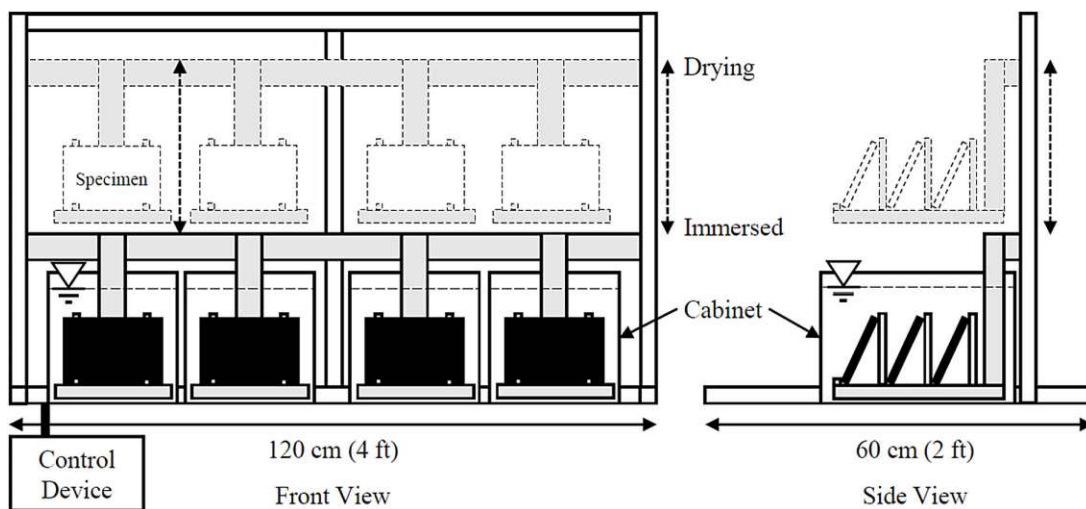
Fig. 9. Testing device for alternate immersion (AI) test (Gruber et al., 2023).

airports), corrosion will be an additional and decisive factor from a life cycle perspective for any infrastructure operator or owner.

Data for mass loss due to corrosion are extracted from (Gruber et al., 2023). In this paper, corrosion was produced with help of the alternate immersion test method based on the standard ISO 11130 (ISO, 2017): At a surrounding temperature of 35 °C, metal plates (unalloyed steel EN 10025 S235JR (Austrian Standards, 2004), dimensions $150 \times 100 \times 1$ mm) are submerged into a 5m% solution of the deicing agent for 10 min,

Table 7
Median of relative mass loss due to corrosion at 35 °C (Gruber et al., 2023).

Agent	Abbr.	Specimens	Median relative mass loss [m%]
Sodium chloride	SC	38	14.16
Potassium carbonate	PC	6	0.96
Calcium chloride	CC	6	5.21
Magnesium chloride	MC	6	3.63
Sodium acetate	SA	6	4.97
Sodium formate	SF	6	5.93
Potassium acetate	PA	6	4.87
Potassium formate	PF	6	10.18
Sodium chloride +8m% Arabinose	SC + Ara	6	7.17
Sodium chloride +8m% Glucose	SC + Glu	6	7.23
Sodium chloride +8m% Maltose	SC + Mal	6	9.45
Sodium chloride +8m% Mannose	SC + Man	6	5.23
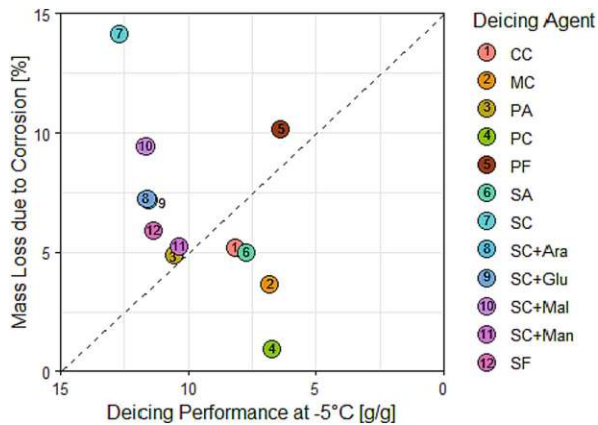
Fig. 10. Comparison of mass loss due to corrosion (Gruber et al., 2023) and deicing performance.

then dried for 50 min. This cycle is repeated, and after 21 days, the metal plates are cleaned until mass constancy (ISO 8407 – Corrosion of metals and alloys – Removal of corrosion products) (ISO, 2021) in an ultrasonic bath with a 20m% diammonium hydrogen citrate solution. Relative mass loss is then calculated by dividing the total mass loss by the initial mass before the test. A scheme of the testing device for alternate immersion can be seen in Fig. 9.

The median of relative mass loss due to corrosion produced by alternate immersion is presented in Table 7. All agents were tested as 5m % solution, except SC with an added inhibitory substance, which was tested as 5m% solution plus 8m% inhibitor (8m% based on dry mass of deicing agent). That means to a 1000 g of 5m% sodium chloride solution, consisting of 50 g SC and 950 g water, 8 m% inhibitor (8m% of 50 g = 4 g) was added. Results show that SC has the highest (14.2m%) and PC (1m%) the lowest mass loss due to corrosion. In addition, the inhibitory substances are proven to be able to reduce corrosion by up to 60% compared to SC.

Fig. 10 provides a comparison of all tested deicing agents with and without inhibitory substances regarding relative mass loss due to corrosion (vertical axis) and deicing performance at −5 °C (horizontal axis) derived from the measured CEDA model in 3.3. The figure is structured in a way that the best performing deicing agents are at the bottom left. Potassium carbonate (PC, color: green, No: 4) has the same deicing performance as potassium formate (PF, color: burgundy, No: 5), but has only one-tenth of the corrosion.

5. Conclusions and outlook

Deicing agents in winter road maintenance are critical in providing safe roads at all times by guaranteeing an adequate level of skid resistance. Even though sodium chloride (SC) is the most cost-effective deicing agent, it is highly corrosive and significantly shortens the service life of transport infrastructures. Therefore, efficient alternatives or ways to reduce corrosion effects without diminishing the road safety are key to saving billions of transport infrastructure investments every year on a world-wide scale. This paper presents the results of extensive research and analysis of the essential criterion of deicing agents: deicing performance. Additionally, a possible reduction due to corrosion-inhibiting additives is presented. Finally, a comparison of deicing performance and corrosion is provided.

A new method (CEDA) for an efficient and repeatable evaluation of deicing performance with increased testing capacity compared to standard procedures was introduced. The test schedule based on this procedure included SC as well as other common acetate-, carbonate-, chloride- and formate-based deicing agents. Furthermore, the addition of sugar-based corrosion-inhibiting substances to SC was investigated, exhibiting minimal decrease in deicing performance (11.6 g/g) to SC (12.7 g/g). Based on the obtained results, a nonlinear model was derived clearly showing the time and temperature dependency of the deicing performance allowing for reliable predictions of the necessary amounts of deicers for any given situation. The comparison with other empirical models in the literature are consistent for different deicing agents in contrast to theoretical approaches (e.g. Raoult's law). Utilizing the colligative characteristics of the solution and the dissociative characteristics of the solute to calculate the freezing point depression and in further consequence the deicing performance, exhibits a much lower predictive accuracy compared to the empiric results with high repeatability.

Additionally, the relative mass loss of unalloyed steel due to corrosion is compared to deicing performance for different deicing agents. This allows a purposive decision for different areas of application, especially when the service life of metal-based transport infrastructure needs to be considered. It is shown that with minimal sacrifice in deicing performance, a significant reduction of up to 60% in corrosion on unalloyed steel can be achieved by the addition of inhibitors such as sugar. Less corrosion at the expense of lower deicing performance can be achieved with other deicing agents. For instance, potassium carbonate (PC) produces only 1m% of relative mass loss compared to 14m% mass loss of SC, but has only half of the deicing performance at −5 °C.

In summary, the research has shown that the developed cryostat-based test method CEDA is not only suitable, but highly efficient for determining deicing performance, helping to decide which deicing agent to prefer in areas with costly transport infrastructure. Although literature (Klein-Paste and Wåhlin, 2013) indicates a much lower amount of deicing agents needed due to the ability of traffic to weaken ice or to prevent its formation altogether, this study is based on the freezing point depression theory and suggests amounts of deicing agents without considering these effects. There are also ongoing efforts (Klein-Paste and Wåhlin, 2017) to represent the deicing process by deicing rate (g/h), rather than by deicing capacity (g/g), as it should give more detailed results, especially for the initial deicing process. However, this study focuses on the most used method, displaying the deicing performance respectively deicing capacity. Nevertheless, the next step is to identify and test additional inhibitors with respect to corrosion and deicing performance (also at lower temperatures).

Overall, the methods and results in this paper provide concise answers and a clear path for future research towards cost-effective deicing agents with significantly lower corrosion compared to SC. Thus, extending the service life of transport infrastructures at reasonable additional costs has become a feasible option.

CRediT authorship contribution statement

Michael R. Gruber: Conceptualization, Methodology, Software, Validation, Formal analysis, Investigation, Resources, Data curation, Writing – original draft, Writing – review & editing, Visualization. **Bernhard Hofko:** Conceptualization, Methodology, Formal analysis, Resources, Writing – review & editing, Supervision, Project administration, Funding acquisition. **Markus Hoffmann:** Conceptualization, Methodology, Validation, Formal analysis, Resources, Writing – review & editing, Supervision, Funding acquisition. **David Stinglmayr:** Investigation, Resources, Data curation, Writing – review & editing. **Teresa M. Seifried:** Methodology, Validation, Formal analysis, Investigation, Resources, Data curation, Writing – review & editing. **Hinrich Grothe:** Conceptualization, Methodology, Formal analysis, Resources, Writing – review & editing, Supervision, Project administration, Funding acquisition.

Declaration of Competing Interest

The authors declare the following financial interests/personal relationships which may be considered as potential competing interests:

Michael R. Gruber reports article publishing charges was provided by TU Wien. Markus Hoffmann reports financial support was provided by Austrian Research Promotion Agency.

Data availability

Data will be made available on request.

Acknowledgement

References

Akin, M., Shi, X., 2012. Development of standard laboratory testing procedures to evaluate the performance of deicers. J. Test. Eval. 40 (6), 1015–1026. https://doi.org/10.1520/JTE103615.

Albright, L., 2008. Albright's Chemical Engineering Handbook, 325. CRC Press. ISBN 978-0-8247-5362-7.

Austrian Standards, 2004. OENORM EN 10025–1:2004. Hot Rolled Products of Structural Steels - Part 1: General Technical Delivery Conditions. Wien. www.austrian-standards.at.

Chappelow, C.C., McElroy, A.D., Darwin, D., et al., 1992. Handbook of Test Methods for Evaluating Chemical Deicers. National Academy of Sciences: Strategic Highway Research Program. Volume SHRP-H-332. Washington DC.

Fay, L., Shi, X., 2011. Laboratory Investigation of Performance and Impacts of Snow and Ice Control Chemicals for Winter Road Service. https://doi.org/10.1061/(ASCE)CR.1943-5495.0000025.

FSV, 2010. RVS 12.04.12: Winter Maintenance – Organization and Performance.Wien www.fsv.at.

Gruber, M.R., Hofko, B., Hoffmann, M., Stinglmayr, D., Grothe, H., 2023. Cost-Efficient and Low-Corrosion Deicing Agents for Winter Maintenance. Corrosion Engineering, Science and Technology.

Hanke, H., Nutz, P., 2019. International Development of Application Methods of De-Icing Chemicals-State of the Art and Best Practice, pp. 4–9. ISBN: 978-2-84060-514-0.

Hoffmann, M., Gruber, M.R., Hofko, B., 2022. Winterlife: effective, sustainable and non-corrosive deicing agents in winter maintenance. In: PIARC - XVI World Winter Service and Road Resilience Congress, 2022.

ISO, 2017. ISO 11130:2017. Corrosion of metals and alloys — Alternate immersion test in salt solution. International Organization for Standardization. www.iso.org.

ISO, 2021. ISO 8407:2021. Corrosion of Metals and Alloys — Removal of Corrosion Products from Corrosion Test Specimens. International Organization for Standardization. www.iso.org.

Klein-Paste, A., Wåhlin, J., 2013. Wet Pavement Anti-icing — A Physical Mechanism, Cold Regions Science and Technology, 96, pp. 1–7. S. https://doi.org/10.1016/j.coldregions.2013.09.002.

Klein-Paste, A., Wåhlin, J., 2017. The effect of mass diffusion on the rate of chemical ice melting using aqueous solutions. In: Cold Regions Science and Technology, vol. 139, pp. 11–21. ISSN 0165-232X. https://doi.org/10.1016/j.coldregions.2017.04.001.

Koch, G.H., Brongers, M., Thompson, N.G., et al., 2008. Handbook of Environmental Degradation of Materials. https://doi.org/10.1016/B978-081551500-5.50003-3.

Koefod, S., Adkins, J., Akin, M., 2012. Alternative Approaches to Measuring Deicer Ice-Melting Capacity, Transportation Research Circular E-C162, pp. 432–442. ISSN 0097-8515.

Melinder, A., 2007. Thermophysical Properties of Aqueous Solutions Used as Secondary Working Fluids. Doctoral dissertation.. Royal Institute of Technology KTH. Stockholm.

Nilssen, K., Klein-Paste, A., Wåhlin, J., 2016. Accuracy of ice melting capacity tests: review of melting data for sodium chloride. Transp. Res. Rec. 2551 (1), 1–9. https://doi.org/10.3141/2551-01.

PIARC; Snow and Ice Databook 2018 - SIDB 2018EN. PIARC Technical Committee B.2 Winter Service, La Défense. www.piarc.org.

Shi, X., Fay, L., Yang, Z., et al., 2009. Corrosion of deicers to metals in transportation infrastructure: introduction and recent developments. Corros. Rev. 27 (1–2), 23–52. https://doi.org/10.1515/CORRREV.2009.27.1-2.23.

Shi, X., Veneziano, D., Xie, N., Gong, J., 2013. Use of chloride-based ice control products for sustainable winter maintenance: a balanced perspective. Cold Reg. Sci. Technol. 86, 104–112. ISSN 0165-232. https://doi.org/10.1016/j.coldregions.2012.11.001.

Shi, X., Jungwirth, S., Akin, M., et al., 2014. Evaluating snow and ice control chemicals for environmentally sustainable highway maintenance operations. J. Transp. Eng. 140 (11) https://doi.org/10.1061/(ASCE)TE.1943-5436.0000709, 5014005.

Tro, Nivaldo J., 2020. Chemistry: A Molecular Approach, Fifth ed. Person Education, Hoboken. NJ. ISBN 978-0-1349-8889-4.

Paper III

I·M3
Institute of Materials, Minerals & Mining

Taylor & Francis
Taylor & Francis Group

RESEARCH ARTICLE

OPEN ACCESS   Check for updates

Analysis of metal corrosion methods and identification of cost-efficient and low corrosion deicing agents

Michael R. Gruber [a], Bernhard Hofko [a], Markus Hoffmann [a,b], David Stinglmayr[c] and Hinrich Grothe [c]

[a]Institute of Transportation, TU Wien, Vienna, Austria; [b]Hoffmann Consult e.U., Vienna, Austria; [c]Institute of Materials Chemistry, TU Wien, Vienna, Austria

ABSTRACT
Deicing agents in winter maintenance are critical in providing safe roads at all times. Sodium chloride (SC) is the most common, efficient and favourable agent but has a drawback of high corrosiveness, thus substantially shortening the service life of metal-based transport infrastructures. This work focuses on corrosion and addresses approaches for the following corrosion test methods that quantify the mass loss of metals for different deicing agents: standardised neutral salt spray test (ISO 9227), salt solution immersion test (ASTM G31-72) and alternate immersion test (ISO 11130). A wide range of different deicing agents with and without corrosion inhibitors are tested on unalloyed steel, and an analytical and visual comparison is made. Results reveal a substantially reduced corrosion effect at reasonable costs by selecting the appropriate deicing agent with or without corrosion inhibitors. For the final selection of deicers, deicing performance and cost-effectiveness are compared.

Introduction

The main goal of winter maintenance is to guarantee the full accessibility and safety of transport infrastructure during winter periods by providing an adequate level of skid resistance. This goal is achieved mainly by snow plowing and spreading of gritting materials or deicing agents in case of hoarfrost, snowfall events, or freezing rain. With gritting as the main method for low-volume roads and pedestrian walkways with limited lasting effects, the usage of deicing agents is the current standard in most areas of transport infrastructure [1]. According to the criteria of availability, costs and deicing performance, sodium chloride (nontechnical abbreviation is SC, for other abbr. see Table 9) is by far the most cost-effective deicer and is the most used deicing agent in developed countries with regular winter maintenance [2]. However, corrosion is one of the main factors in the reduced service life of transport infrastructure consisting of metals (mostly painted steel and weathering steel) and reinforced concrete [3–6]. Since deicing agents, such as SC, are highly corrosive, a significant reduction in corrosivity would lead to significant savings in investments and energy.

To find alternative deicing agents, a holistic evaluation is required [7]. However, this work focuses on cost effectiveness and corrosion by comparing the deicing performance and mass loss due to corrosion of different deicing agents. In addition to SC and other common acetate-, carbonate-, chloride- and formate-based deicing agents, sugars are tested as inhibitory substances to SC mainly because of their nonhazardous characteristics. The first part of this paper compares the repeatability of three corrosion test methods that are based on, but do not strictly follow, the corresponding standard: (i) standardised neutral salt spray test (ISO 9227) [8], (ii) salt solution immersion test (ASTM G31-72) [9] and (iii) alternate

immersion test (ISO 11130) [10]. In the second part, optical results and mass loss due to corrosion on unalloyed steel are investigated for all known principal deicers and selected inhibitors. Finally, the paper concludes with a comparison of corrosivity and cost effectiveness among all tested substances. Effectiveness is determined by deicing performance, which was evaluated using a newly developed method introduced in a separate paper (see section 5) [11].

Quantitative assessment of corrosivity is crucial to judge the influence of different deicing agents on corrosion and resulting service life. In general, corrosion in atmospheric environment is controlled by the diffusion rate of oxygen through each barrier present on the reactive steel surface. Thus, corrosion strongly depends on oxygen exposure and temperature. The latter dependence is non-linear since on one hand corrosion multiplies with increasing temperature due to the overcome of the Arrhenius activation barrier, but on the other hand, corrosion also increases with decreasing temperature due to the greater dissolved oxygen content in the aqueous phase at low temperatures (14 mg O_2 per L H_2O at 0°C, 7 mg/L at 35°C) [12–20]. Interestingly, oxygen is essential for depassivation but corrosion progression can also proceed without further oxygen supply [21]. For SC solutions between 2 and 6 wt-% concentrations and exposure time of 10–16 days, it was found that oxygen solubility is higher in lowly concentrated SC solutions than in highly concentrated ones [13]. Another important parameter is conductivity of the environment resulting from the mobile ions: Higher conductance implies higher corrosion rates. Carbon steel is passive at pH higher than approximately 10 but will start to corrode where the chloride-to-hydroxide ration exceeds certain values and when the concrete is carbonated so that the pH is lower than approximately 9 [14,21].

Some studies have already assessed different corrosion tests with SC. For the full immersion test (FI) a mass loss of 0.6 wt-% due to corrosion was achieved after a total exposure time of 127 days [22], revealing the unsatisfactory performance of this method due to the lack of oxygen [22,23]. A 72-hour alternate immersion test (AI) showed high corrosion rates with 5 wt-% mass loss [19] with SC solutions between 3 and 5 wt-%. At the same time, these high corrosion rates mean that the results cannot be directly applied to real-life applications [24].

Repeatable results in corrosion testing are of particular importance to provide a stable testing environment. For the reliable assessment of different deicers and the effects of inhibitors, significant corrosion effects are necessary to avoid high data scatter related to measurement and handling inaccuracies. Thus, the three corrosion test methods are analysed by comparing the corrosion rates of 5 wt-% SC solutions on unalloyed steel (according to EN 10025 S235JR) [25] specimens ($150 \times 100 \times 1$ mm, 235 ± 2.4 g).

Corrosion methods and identification

In the next sections, the following three test methods that quantify the mass loss due to corrosion on unalloyed steel for different solutions are introduced and compared: (i) standardised neutral salt spray test (ISO 9227) [8], (ii) salt solution immersion test (ASTM G31-72) [9] and (iii) alternate immersion test (ISO 11130) [10].

Neutral salt spray tests – NSS*

The ISO 9227 standard (corrosion test in artificial atmospheres – salt spray tests) [8] specifies three procedures to assess corrosion resistance. Among them, the standardised neutral salt spray (NSS), in which metal specimens ($150 \times 70 \times 1$ mm) are wetted by continuous misting (indirect spraying) 5 wt-% SC solution at a temperature of $35 \pm 2°C$ between 2 and 1008 h.

For simplification, the reproduced test method (Figure 1) is altered as stated in Table 1 with the main modifications being non-continuous spraying to achieve higher oxygen

exposure and direct spraying of the specimens to increase surface wetting. The modified test method is referred to as NSS*, where the asterisk (*) indicates that it is based on but does not strictly comply to the standardised NSS method in ISO 9227.

Salt solution full immersion tests – FI

In accordance with ASTM G31-72 standard (laboratory immersion corrosion testing of metals) [9], specimens are immersed into a test solution for 48–168 h. Owing to the simplicity of the test method (see scheme in Figure 2), almost no alterations are made for the test as seen in Table 2.

Alternate salt solution immersion tests – AI

The ISO 11130 standard (corrosion of metals and alloys – alternate immersion test in a salt solution) [10] specifies another procedure to assess corrosion resistance. In this method, specimens are repeatedly immersed in a testing solution and dried for specific periods. For standard testing, 3.38 wt-% SC solution is filled into a specimen cabinet. The specimens should be completely immersed at least 10 mm below the solution's surface. The concentration is retained by adding deionised water to counteract evaporation. Every 168 h, the solution is entirely replaced. The specimens are immersed for 10 min and dried for 50 min,

Table 1. Modification of the test method used to ISO 9227.

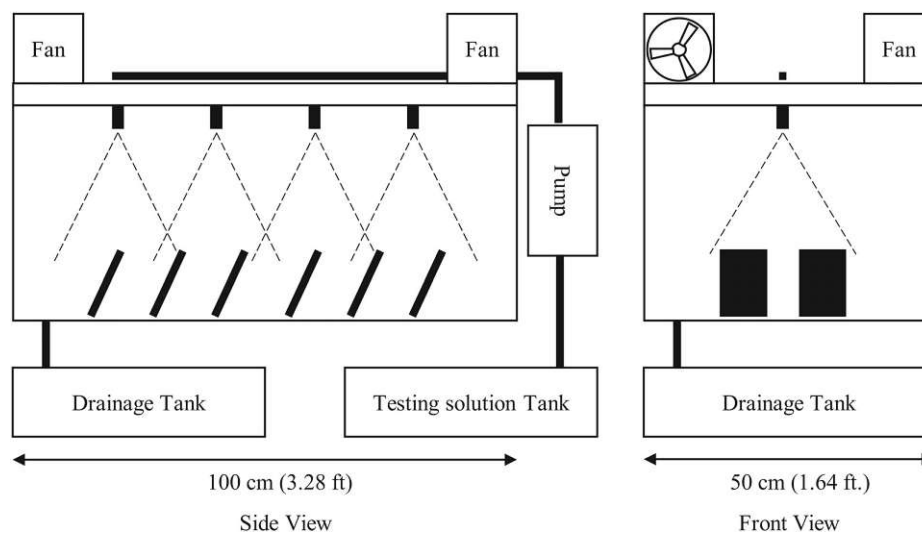|	Test according to ISO 9227 [8]	Modified test [Figure 1]
Spraying method	Specimen indirectly sprayed on	Specimen directly sprayed on
Spraying duration	Continuous spraying	Non-continuous spraying: 115–117 min spraying 3–5 min drying
Test solution	5% SC, must not be reused	5% SC, reused
Temperature	$35 \pm 2°C$	$19 \pm 1°C$
Specimen dimension	$150 \times 70 \times 1$ mm –	$150 \times 100 \times 1$ mm 235 ± 2.4 g
Number of specimens	≥ 4	12
Test duration	2–1008 h	504 h (21 days)

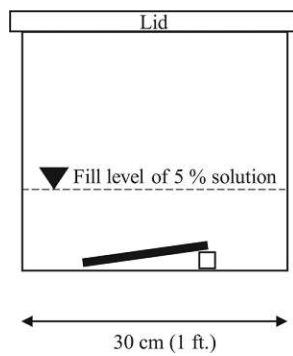**Figure 1.** Testing device for neutral spray test (NSS*).

Figure 2. Testing device for full immersion (FI) test.

Table 2. Modification of the test method used to ASTM G31-72.

	Test according to ASTM G31-72 [9]	Reproduced test [Figure 2]
Test solution	–, 0.5–5 L	5% SC, 3 L
Temperature	–	22 ± 1°C
Specimen dimension	circular 38 × 3 mm –	150 × 100 × 1 mm 235 ± 2.4 g
Number of specimens	–	1
Test duration	48–168 h (2–7 days)	504 h (21 days)

altogether being exposed from 20 to 90 days. After

Table 3. Modification of the test method used to ISO 11130.

	Test according to ISO 11130 [10]	Reproduced test [Figure 3]
Specimen immersion	10 min immersed 50 min drying	10 min immersed 50 min drying
Test solution exchange	Every 7 days	Every 7 days
Test solution	3.38% SC	5% SC, 8 L
Temperature solution	25 ± 2°C	–
Temperature / RH air	70 ± 2°C, ≤50%	RT: 19 ± 1°C, 32 ± 5% CC: 34 ± 1°C, >70% CT: 34 ± 1°C, ≤80 ± 10%
Specimen dimension	120 × 90 × 1 mm –	150 × 100 × 1 mm 235 ± 2.4 g
Number of specimens	≥3	12 (3 in 4 cabinets)
Test duration	20–90 days	504 h (21 days)

thoroughly cleaning and drying, the mass loss is determined at the end of the test. For overall cleaning and handling of specimens, it is referred to ISO 8407 [26]. Differences in the reproduced test method used in this paper compared to ISO 11130 are shown in Table 3 and include testing at different temperatures: Room temperature (RT) and elevated temperature in a climate chamber (CC) and temperature-controlled container (CT). A scheme of the apparatus is provided in Figure 3.

Procedure for the determination of corrosion mass loss

The correct determination of mass loss due to corrosion is crucial for comparing different test methods, especially when low rates of corrosion are produced. Therefore, the ISO 8407 standard (corrosion of metals and alloys – removal of corrosion products) [26] is followed. Light mechanical treatment by brushing is recommended. For further cleaning, chemical, electrolytic and vigorous mechanical treatments are applied until mass consistency is achieved. The use of 20 wt-% diammonium hydrogen citrate solution in an ultrasonic bath has shown the best repeatability for cleaning the samples of corrosion products. Mechanical procedures, such as scaping, scrubbing, brushing and grit blasting, have low costs but may lead to biased results because the removal of corrosion products may not be performed uniformly.

In this work, the suggested combination of (light) mechanical and chemical cleaning with the help of an ultrasonic bath is used. After the end of each test period, all specimens are cleaned with tap water, and adherent corrosion products are removed by gently dabbing with a paper towel. Up to 9 specimens are thoroughly cleaned in an ultrasonic bath (see Figure 4) with a 20 wt-% diammonium hydrogen citrate solution at 50°C for 30 min and then dabbed dry with a paper towel and weighed. This step is repeated (time in the ultrasonic bath is reduced to 10 min after an initial run with 30 min) until mass consistency is achieved. Relative mass loss is calculated by dividing the total mass loss by the initial mass of the specimen (150 × 100 × 1 mm, 235 ± 2.4 g) before the test using Equation (1). On the basis of the results of this procedure, a high level of repeatability is achieved compared
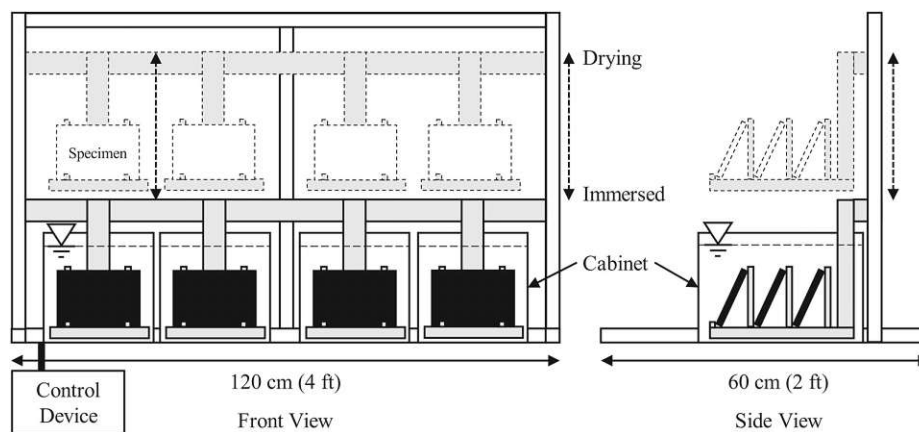
Figure 3. Testing device for alternate immersion (AI) test.
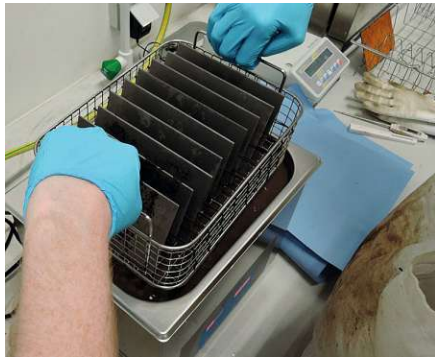
Figure 4. Ultrasonic bath with 20 wt-% diammonium hydrogen citrate.

with that in the other methods.

$$\text{relative mass loss [wt\%]} = \frac{m_{\text{before}} - m_{\text{after}}}{m_{\text{before}}} \times 100 \quad (1)$$

Test schedule for the comparison of corrosion methods

As stated in ISO 11130 [10], corrosion is influenced by many factors and can vary significantly under different conditions. Consequently, the AI, FI and NSS* tests are not directly applicable to real-life situations. Tests conducted under real-life conditions (e.g. temperatures below freezing, long

Table 4. Testing conditions for 5 wt-% SC solution of all corrosion methods.

Category	Test method	Test environment	Temperature	Relative humidity	Cycle period	Specimens
AI@CC	Alternate immersion	Climate chamber	34.25°C ± 0.68°C	est. >70%	1 h: 10 min immersed, 50 min drying	12
AI@CT	Alternate immersion	Container temp.-contr.	34.24°C ± 0.72°C	79.47% ± 8.61%	1 h: 10 min immersed, 50 min drying	23
AI@RT	Alternate immersion	Room temperature	18.72°C ± 0.72°C	32.12% ± 4.67%	1 h: 10 min immersed, 50 min drying	12
FI@RT	Full immersion	Room temperature	21.87°C ± 0.95°C	NA	21 days immersed	5
NSS*@RT	Neutral salt spray	Room temperature	19.15°C ± 0.79°C	33.73% ± 7.69%	2 h: 3 min spraying, 117 min drying	15
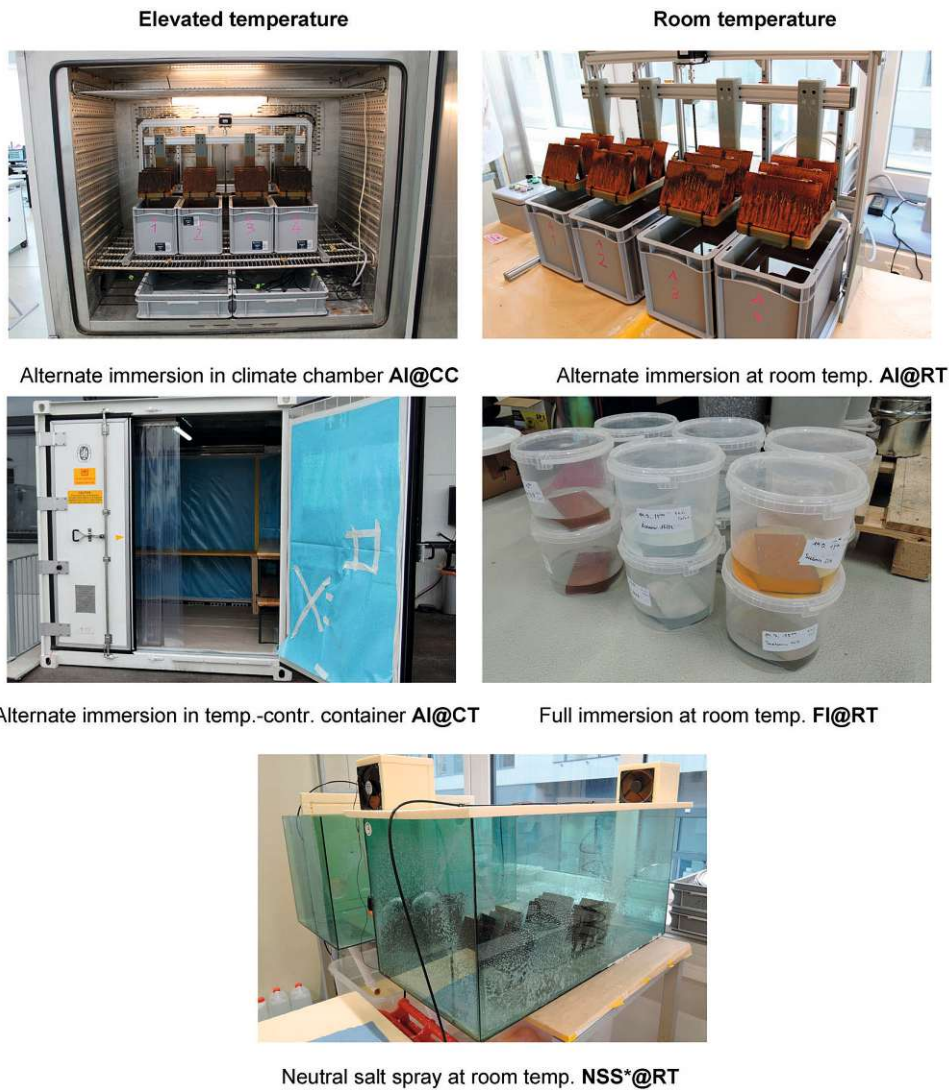
Figure 5. Pictures of test methods and surroundings (left: elevated temp./right: room temp.).

immersion and drying periods) would lead to a substantial increase in test duration, rendering any test programme inefficient and expensive.

Table 4 provides an overview of the test methods and their surrounding conditions. All tests are conducted with a 5 wt-% SC solution on unalloyed steel (EN 10025 S235JR [25]).

For the AI test, two different ambient temperatures, namely, room temperature (AI@RT) and elevated temperature $34 \pm 1°$ C, are investigated in a climate chamber (AI@CC). A large number of specimens are simultaneously tested in a 10-feet temperature-controlled container (AI@CT). For these tests, the immersion cycle is 1 h, with 10 min of fully immersing the specimens in 5 wt-% SC solution and 50 min of drying.

For the FI test, the specimens are immersed for 21 days at room temperature (FI@RT). The ambient temperature is slightly higher ($22 \pm 1°C$) than that in other tests at room temperature ($19 \pm 1°C$) because the system allows only minimal air exchange with the surrounding environment.

For the NSS* test, three cabinets are built in which the specimens are exposed to a 2-hour cycle consisting of 3 min of spraying 5 wt-% SC solution, followed by 117 min of drying at room temperature (NSS*@RT). This cycle is chosen to maintain a throughput of 30 L of solution daily. An overview of the methods stated in Table 4 can be found in Figure 5.

Analytical comparison of corrosion test methods and applicability

A comparison of the results from different methods as box-plots with marked outliers outside of the maximum whisker length of 1.5-times the interquartile range (IQR) can be found in Figure 6. The FI test method exhibits minimal effect on corrosion presumably due to low aeration [12–14,21,22]. The total mass loss is 0.2 wt-% (0.5 g) after 21

days; handling errors and cleaning procedure might have significantly biased the results. All other test methods produce a higher level of mass loss at room temperature but low corrosion effects to avoid the significant impacts of handling and cleaning errors. The NSS* test method showed problems with clogged spraying nozzles, possibly caused by reusing the solution and precipitation of salt inside the nozzles caused by not sufficiently humifying incoming air (both alterations to the standard NSS test according to ISO 9227). In addition to these problems, the NSS* test spreads aerosols containing SC, which might cause corrosion of the surrounding materials. Consequently, testing at high temperatures in a climate chamber or temperature-controlled container is not a feasible option due to the expected damages. Thus, the AI test remained as the only feasible method for testing inside the climate chamber.

Tests inside the climate chamber reveal significant variance (interquartile range IQR of 4.7 wt-% at a median of 11.7 wt-% or 27.4 g mass loss) probably induced by the irregular strong air flow generated by the air conditioning unit to maintain the temperature level. The size of the climate chamber accommodates just one testing device (containing 12 specimens), limiting the number of tests in a given time.

Therefore, a 10-feet temperature-controlled container is used to hold three devices, allowing for the simultaneous testing of 36 specimens (test setup shown in Figure 8). The results for 23 specimens (obtained at three different series of 21 days) show smaller variance compared to those in the climate chamber (IQR of 0.8 wt-% at a median of 14.2 wt-% or 33.2 g mass loss).

Optical comparison of corrosion tests

A visual comparison of the specimens before testing (5 wt-% SC solution on unalloyed steel), after 21 days testing, and
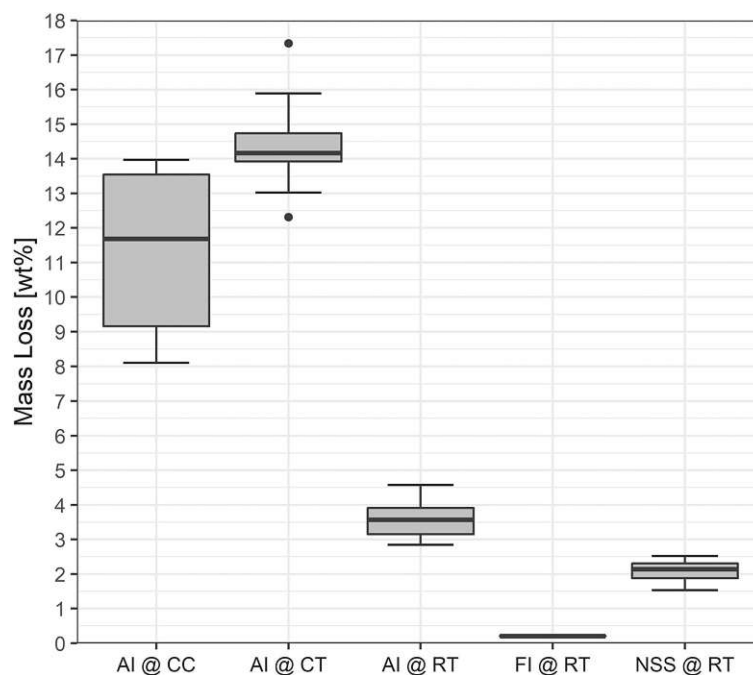
Figure 6. Results of all test methods with 5 wt-% SC solution.
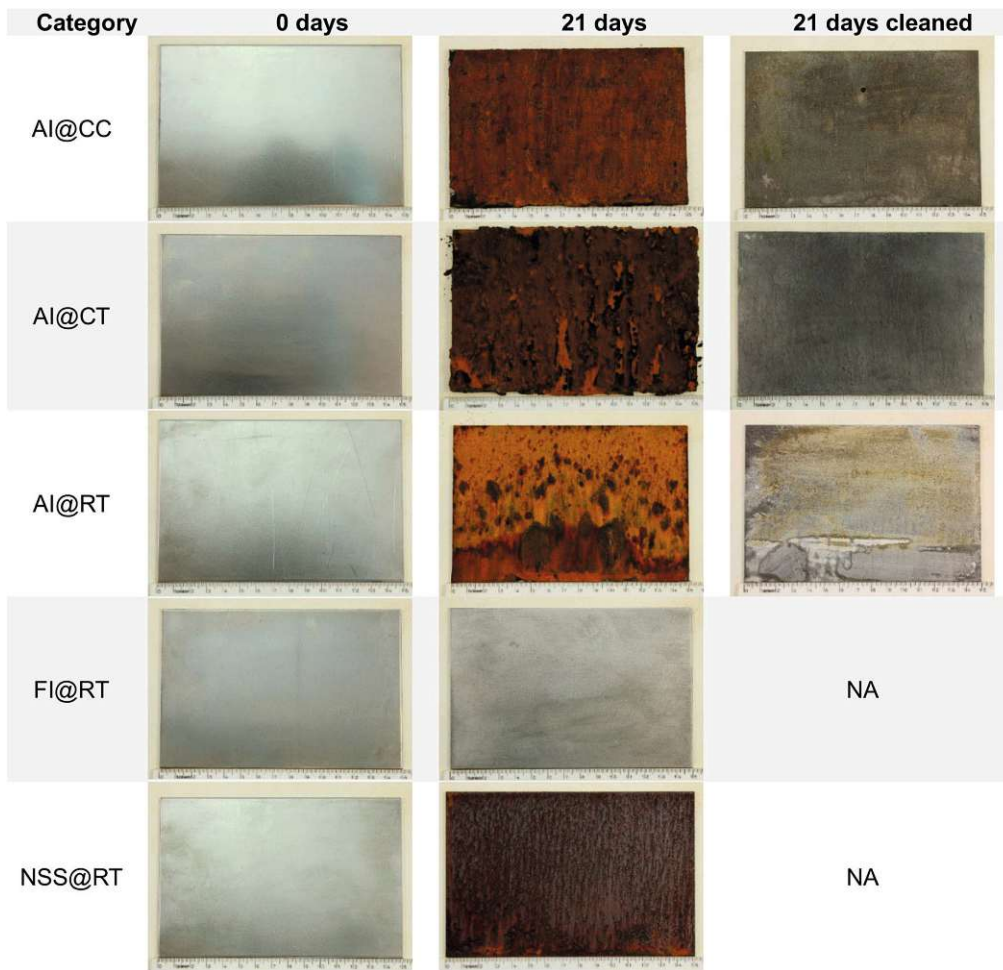
Figure 7. Optical comparison of the specimens before and after testing with 5 wt-% SC solution.

Figure 8. Test setup inside the temperature-controlled container (AI@CT).

after cleaning for all test methods can be seen in Figure 7. Similar to the results in Figure 6, differences among the high corrosion effects of the AI test at high temperature, the medium effects of the AI test at room temperature and the low effects of all other test methods can be observed. The high corrosion effects for AI test in the container compared with that in the climate chamber can be explained by the high relative humidity inside the container and the irregular strong airflow inside the climate chamber.

Table 5. Tested deicing agents without added inhibitory substances.

Agent	Abbr.	Sol. [wt-%]	Formula	Specimens
Sodium chloride	SC	5	NaCl	38
Potassium carbonate	PC	5	K_2CO_3	6
Calcium chloride	CC	5	$CaCl_2$	6
Magnesium chloride	MC	5	$MgCl_2$	6
Sodium acetate	SA	5	CH_3COONa	6
Sodium formate	SF	5	HCOONa	6
Potassium acetate	PA	5	CH_3COOK	6
Potassium formate	PF	5	HCOOK	6

Table 6. Test schedule of SC with different concentrations of glucose.

Agent	Inhibitor	Abbrev.	Formula	Specim.
SC 5 wt-%	Glucose 2 wt-%	SC + 2%Glu	$NaCl + C_6H_{12}O_6$	6
SC 5 wt-%	Glucose 4 wt-%	SC + 4%Glu	$NaCl + C_6H_{12}O_6$	6
SC 5 wt-%	Glucose 6 wt-%	SC + 6%Glu	$NaCl + C_6H_{12}O_6$	6
SC 5 wt-%	Glucose 8 wt-%	SC + 8%Glu	$NaCl + C_6H_{12}O_6$	6

Table 7. Test schedule of SC with different sugars.

Agent	Inhibitor	Abbrev.	Formula	Specim.
SC 5 wt-%	Arabinose 8 wt-%	SC + 8%Ara	$NaCl + C_5H_{10}O_5$	6
SC 5 wt-%	Glucose 8 wt-%	SC + 8%Glu	$NaCl + C_6H_{12}O_6$	6
SC 5 wt-%	Maltose 8 wt-%	SC + 8%Mal	$NaCl + C_{12}H_{22}O_{11}$	6
SC 5 wt-%	Mannose 8 wt-%	SC + 8%Man	$NaCl + C_6H_{12}O_6$	6

Corrosion of deicing agents and inhibitors

Given that the AI test inside the temperature-controlled container (AI@CT) shows the highest corrosion products and good repeatability, this setup is used to classify the corrosion effects of other deicing agents (as anhydrate) on unalloyed steel (EN 10025 S235JR) [25]. Figure 8 shows the test setup inside the container. Table 5 shows the testing schedule for the deicing agents in a 5 wt-% solution and introduces non-technical abbreviations (e.g. PA = Potassium acetate = CH_3-COOK) for improved readability, especially in figures.

Given that most alternative deicing agents are quite expensive compared with SC, another option is to add a small amount of (possibly expensive) corrosion inhibitor to (rather inexpensive) SC. Therfore, glucose is tested with different concentrations of 2 wt%, 4 wt-%, 6 wt-% and 8 wt-% to identify the effect of different concentrations on corrosion (Table 6). The concentration of the inhibitor is based on the dry mass of SC, that is, 1000 g of 5 wt-% SC solution (50 g of SC and 950 g of water) 2 wt-% of the inhibitor (2 wt-% of 50 g = 1 g) are added.

Other sugars such as arabinose, maltose and mannose are also tested as corrosion inhibitors with a dosage of 8 wt-% of the mass of SC. The corresponding test schedule can be seen in Table 7.

Analytical comparison

After 21 days of exposure to the AI test inside the temperature-controlled container (AI@CT) and cleaning until mass consistency is achieved, the resulting relative mass loss is displayed as boxplots in Figure 9. SC has the highest mass loss due to corrosion on unalloyed steel of around 14.2 wt-% (33.2 g). The mass loss of other deicing agents ranges from 3 wt-% (7.0 g) to 6 wt-% (14.1 g), except
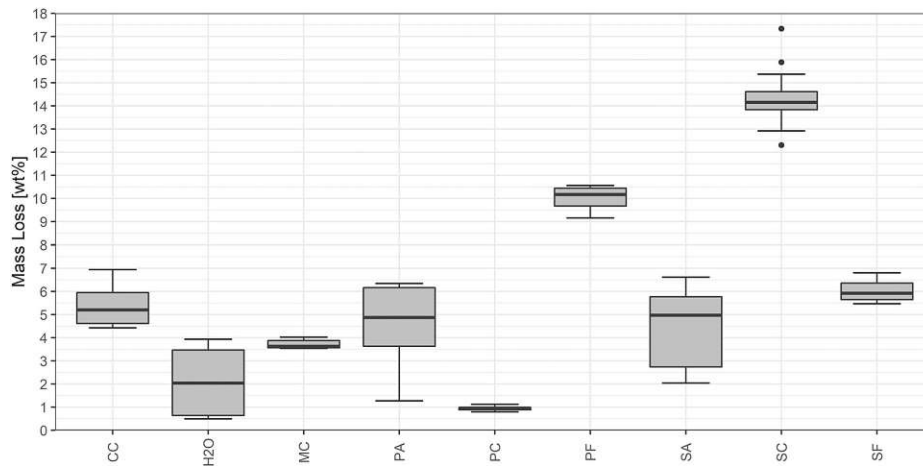
Figure 9. Results of all tested main deicing agents.
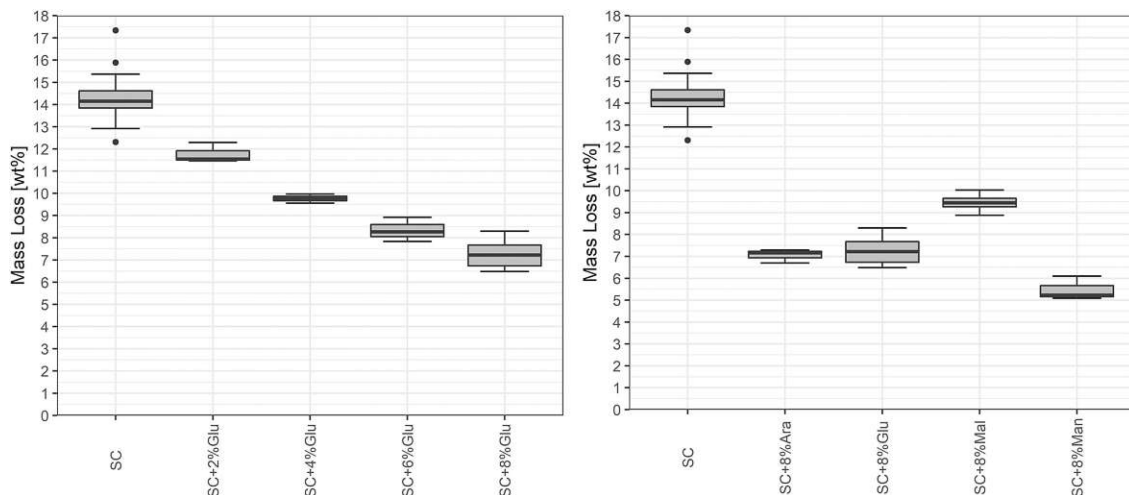
Figure 10. Results of different dosages of glucose (left) and of different sugars (right).

Category	0 days	21 days	21 days cleaned
$CaCl_2$ CC			
H_2O			
$MgCl_2$ MC			
CH_3CO_2K PA			
K_2CO_3 PC			
HCO_2K PF			
CH_3CO_2Na SA			
NaCl SC			
HCO_2Na SF			

Figure 11. Optical comparison of the specimen before and after testing (deicing agents).

potassium formate (PF) (10.2 wt-% or 24.0 g) and potassium carbonate (PC) (0.9 wt-% or 2.1 g). PC provides better protection compared to water (H_2O: with 2.1 wt-% or 4.9 g), as it forms an alkaline solution leading to a passivation of the steel surface and consequently to reduced corrosion.
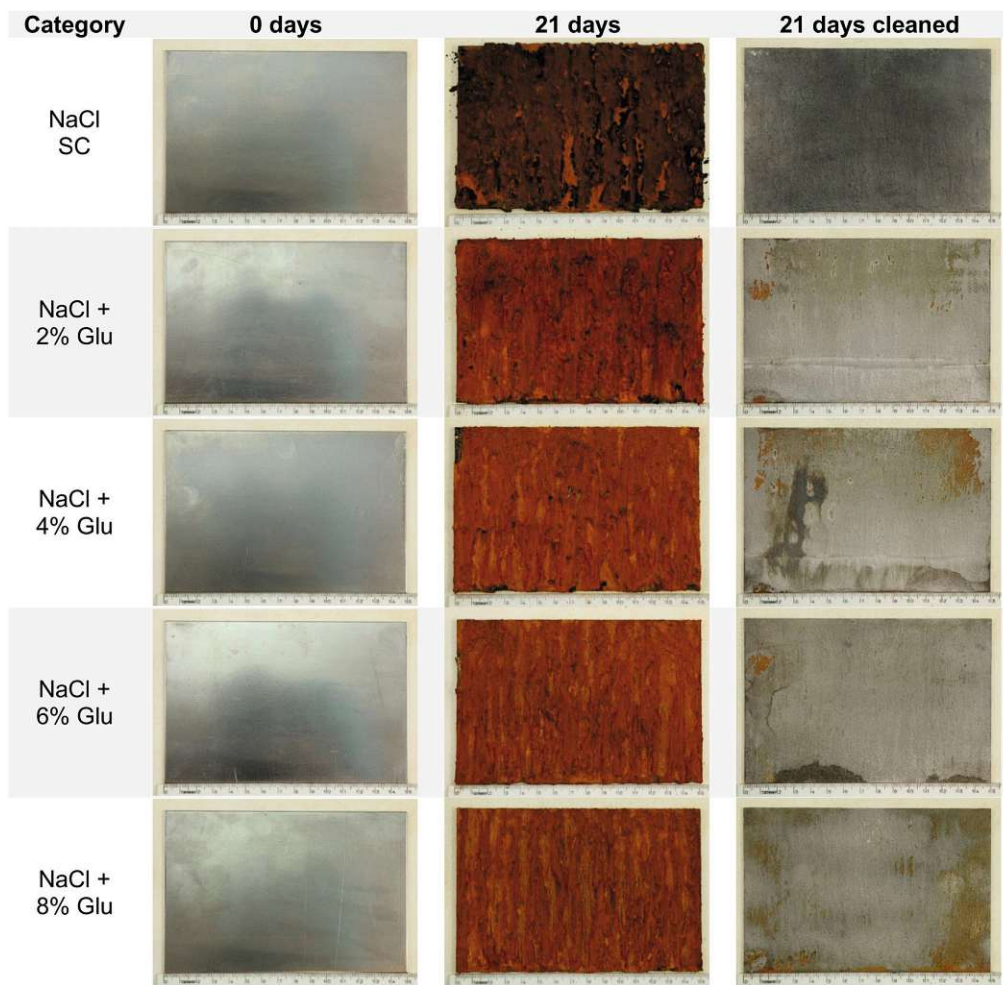
Figure 12. Optical comparison of the specimen before and after testing (glucose).

The left part of Figure 10 shows the results of the testing schedule according to Table 6. As expected, an increase in the amount of glucose added to SC leads to a decrease in corrosion. This positive effect starts to flatten with an 8 wt-% dosage, indicating an optimal dosage from an economic point of view. Therefore, 8 wt-% dosage is chosen as a reference to test other sugars as stated in Table 7. The right part of Figure 10 shows that arabinose and glucose reduce the corrosion products by around 50%, and mannose performs better with 60% reduction compared with SC. By contrast, maltose only allows for a 30% reduction in corrosion.

Optical comparison

In addition to the analytical comparison, Figure 11 shows the specimens before and after testing in a 5 wt-% solution. SC has the most corrosive effect on the unalloyed steel, and PC has the least. All other deicing agents are somewhere in between. A difference in corrosion pattern is observed between magnesium chloride (MC) and potassium acetate (PA).

The set of tests comparing the corrosion of SC (as a 5 wt-% solution) with an inhibitor added (percentage related to the amount of SC) in Table 6 are shown in Figure 12. Glucose is tested at 2, 4, 6 and 8 wt-% to identify the increase in inhibitory effect with the amount of the substance added. This effect can be seen but at high amounts, only minimal difference can be spotted.

All other tested sugars in Table 7 can be seen in Figure 13. A reliable optical differentiation is not possible, since corrosion reduction is in a narrow range between 40% and 60% compared to SC.

Acquisition costs

Given that cost-effectiveness is the main factor for choosing deicing agents, the market prices for all main agents are surveyed. Apart from principal availability in consider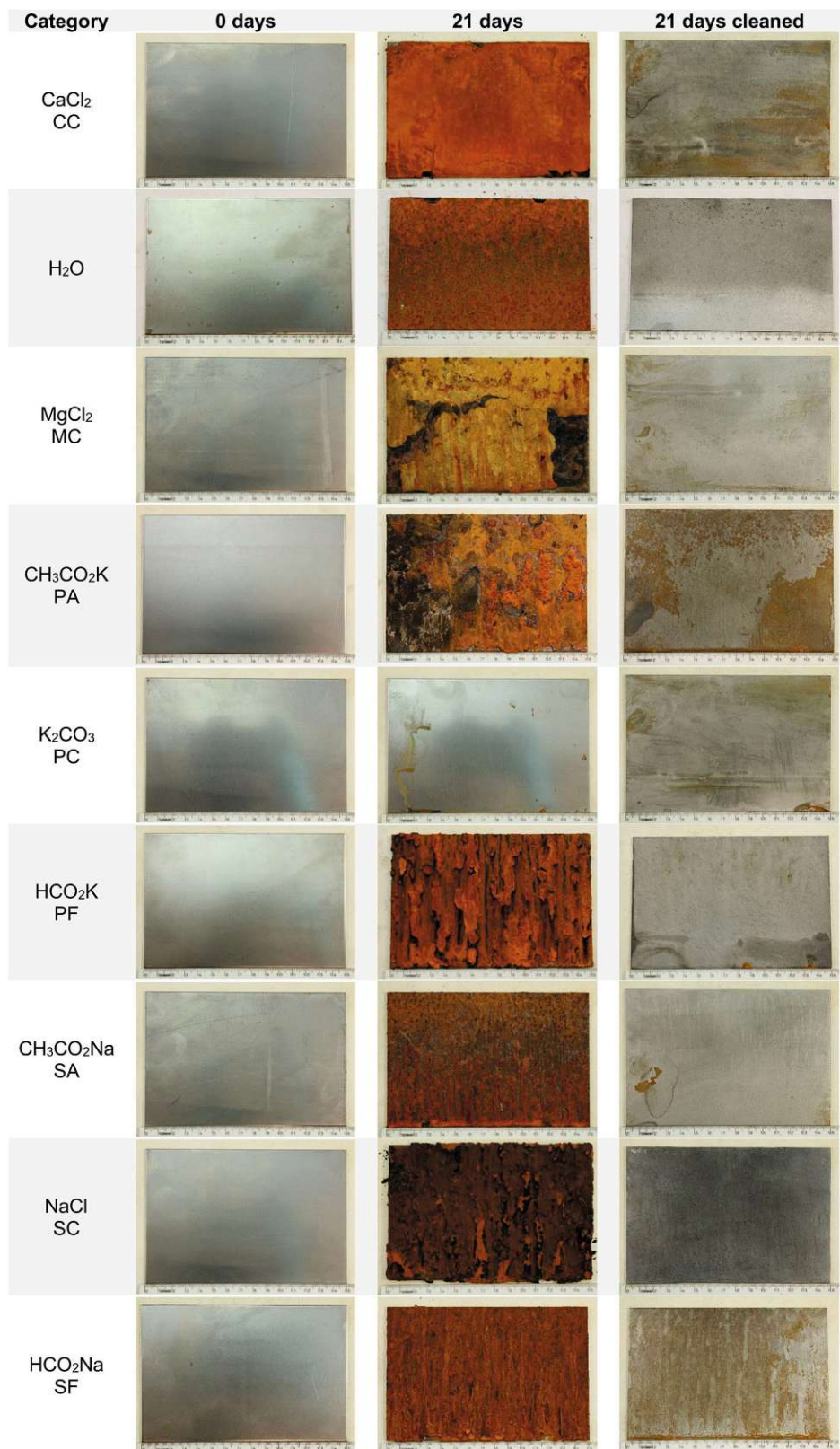able quantities, the unit prices decrease sharply with the increasing amounts [7]. This phenomenon is called economy of scales, an example for SC can be seen in Figure 14. In addition, the provided data from the market analysis may vary because of considerable seasonal and regional fluctuations regarding prices and availability. Table 8 lists the prices in Euro (Central Europe 2021) of the main deicing agents per metric ton when buying large quantities (≫10 tons). The last column shows the relative price to SC (=100%). This image is a snapshot and probably no longer accurate due to the strong fluctuations in prices and currency exchange rates caused by the COVID pandemic and the war in Europe.
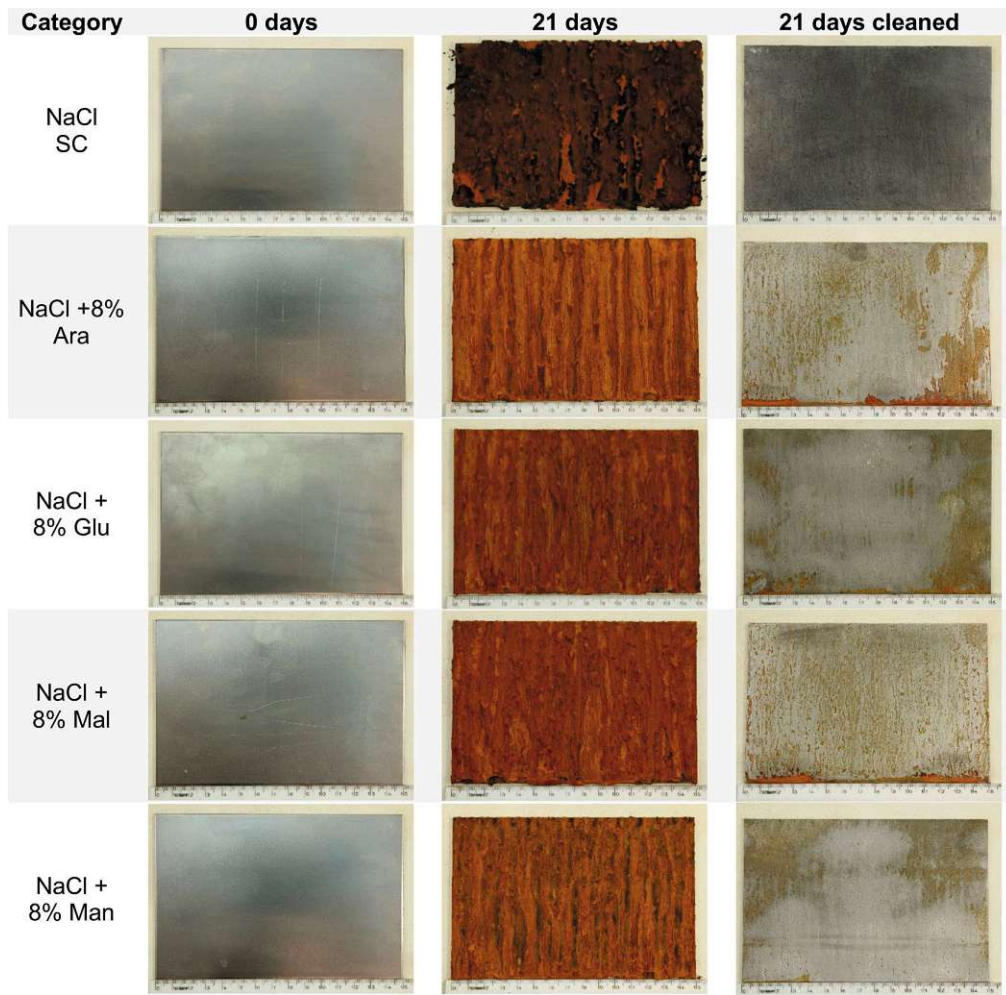
Figure 13. Optical comparison of the specimen before and after testing (all sugars).

Comparison of corrosion and cost efficiency

The primary purpose of deicing in winter maintenance is to provide a sufficient level of skid resistance by avoiding freezing due to preventive spreading or to remove residual snow and ice by applying deicing agents. The necessary amount for the latter is determined by the deicing performance, which states the amount of ice or snow that can be deiced (in grams ice per gram deicing agent, g/g) at a given temperature. Given that deicing performance is largely based on the freezing curve, it decreases for all deicers at low temperatures.

For cost-efficient winter maintenance, the deicing performance and costs of relevant deicing agents or products consisting of primary deicers, additives and impurities must be determined. The deicing performance was investigated in a separate paper [11], in which a non-linear model was derived from the results of a newly developed
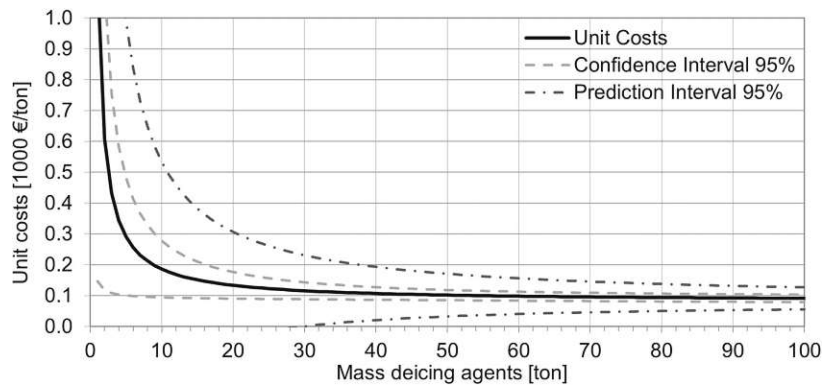
Figure 14. Unit costs of SC by quantity [7].

Table 8. Prices (≫10 t) of deicing agents and inhibitors (Central Europe 2021).

Agent	Formula	Abbrev.	Price [€/ton]	Relat. costs to SC [%]
Calcium chloride (dih.)	$CaCl_2 \cdot 2H_2O$	CC	170	142
Potassium carbonate	K_2CO_3	PC	900	750
Potassium acetate	CH_3COOK	PA	600	500
Potassium formate	$HCOOK$	PF	700	583
Magnesium chloride (hexah.)	$MgCl_2 \cdot 6H_2O$	MC	250	208
Sodium acetate	CH_3COONa	SA	250	208
Sodium chloride	$NaCl$	SC	120	Base = 100
Sodium chloride + 8 wt-% arabinose	$NaCl + C_5H_{10}O_5$	SC + 8% Ara	155	129
Sodium chloride + 8 wt-% glucose	$NaCl + C_6H_{12}O_6$	SC + 8% Glu	155	129
Sodium chloride + 8 wt-% maltose	$NaCl + C_{12}H_{22}O_{11}$	SC + 8% Mal	155	129
Sodium chloride + 8 wt-% mannose	$NaCl + C_6H_{12}O_6$	SC + 8% Man	155	129
Sodium formate	$HCOONa$	SF	250	208

Table 9. Deicing performance obtained from CEDA after 300 Min at −5°C [11].

| Agent	Abbr.	Deicing perf. [g/g]
Sodium chloride	SC	12.75
Potassium carbonate	PC	6.74
Calcium chloride dihydrate	CC	8.28
Magnesium chloride hexahydrate	MC	6.83
Sodium acetate	SA	8.16
Sodium formate	SF	11.41
Potassium acetate	PA	10.59
Potassium formate	PF	6.38
Sodium chloride + 8 wt-% arabinose	SC + Ara	11.63
Sodium chloride + 8 wt-% glucose	SC + Glu	11.62
Sodium chloride + 8 wt-% maltose monohydr.	SC + Mal	11.75
Sodium chloride + 8 wt-% mannose	SC + Man	10.37

method for testing deicing performance (called CEDA). CEDA shows the time-temperature dependency of the deicing performance, allowing for reliable predictions of the necessary amounts of deicers for any given situation. Table 9 gives an overview of the deicing performance of different deicing agents after 300 min exposure at −5°C.

In addition to the deicing performance, the market price is a key factor in the decision-making process. However, with focus beyond winter maintenance on highly expensive transport infrastructure consisting of metals and reinforced concrete (e.g. train stations, bridges, airports), corrosion also becomes a decisive factor from a life cycle perspective.

Thus, the left part of Figure 15 shows a comparison of relative mass loss due to corrosion and costs per ton of ice melted among all tested deicing agents with and without inhibitory substances (at −5°C).

For example, SC (colour: aquamarine) is highly corrosive but a cost-effective deicing agent and thus is placed on the top left of the diagram. By contrast, PC (colour: green) produces minor corrosion but is rather expensive and is therefore placed on the bottom right. A comparison of corrosion and deicing performance (at −5°C) without considering costs is provided in the right part of Figure 15. The figure shows that PC (colour: green) has the same deicing performance as PF (colour: burgundy) but produces only one-fifth of its corrosion. In general, both figures are structured in a way that the best performing deicing agents are at the bottom left of the diagram, the *y*-axis displays relative mass loss [wt-%], and the *x*-axis shows costs per ton of ice melted (Figure 15 left) or deicing performance at 300 min of exposure (Figure 15 right).

Conclusions and outlook

Deicing agents in winter road maintenance are critical in providing safe roads at all times. Beyond winter maintenance, SC as main deicer is highly corrosive and substantially shortens the service life of transport infrastructures. Therefore, cost-efficient alternatives or ways to reduce corrosion effects without diminishing the road safety are the key to saving billions of transport infrastructure investments every year on a worldwide scale. This paper presents the results of extensive research and analysis of the essential criteria of deicing agents: deicing performance, corrosion on metals and costs.

A comparative analysis of the three commonly used test methods to reproduce corrosion effects is conducted to quantify the mass loss of unalloyed steel exposed to deicing agents. All test methods are generally based on the corresponding standard but have been modified to reduce the testing effort. FI test has led to barely measurable mass loss, and NSS* test is unreliable due to the clogging of spraying nozzles (presumably due to modifications to the standard ISO 9227). AI test produces the highest quantity of corrosive products at an elevated temperature of +34 ± 1°C with a high level of repeatability. With this method, all relevant main deicing agents can be tested. In addition, corrosion inhibitors such
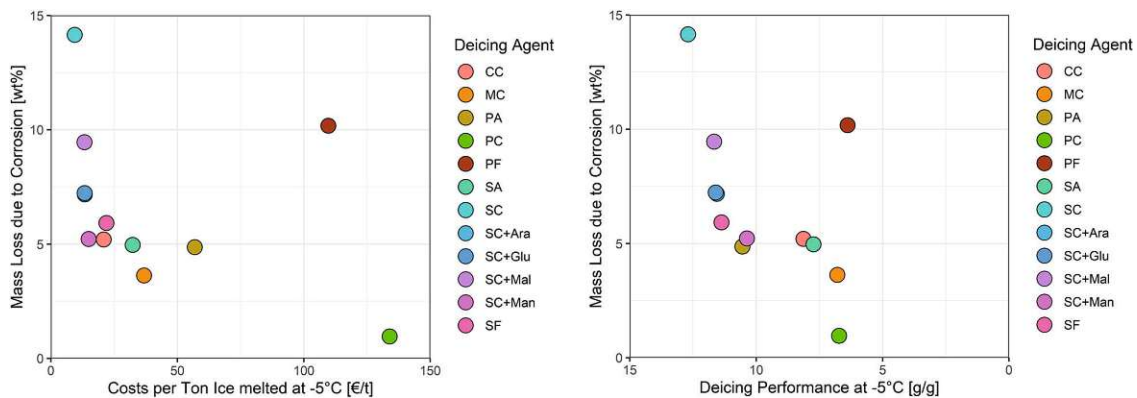

Figure 15. Comparison of corrosion (ordinate) and costs (left) or deicing performance (right) [11].

as sugars are added to SC to identify their impact on reducing corrosion at different dosages.

Since the procedure of determining mass loss is significant for comparable results, a gentle mechanical cleaning in combination with chemical cleaning in an ultrasonic bath until mass consistency using a 20 wt-% solution of diammonium citrate (ISO 8407) was used and led to accurate results. According to the comparison of the relative mass loss of different deicing agents, PC causes the passivation of steel and has therefore the least corrosive effect on unalloyed steel (specimens $150 \times 100 \times 1$ mm, 235 g) with 0.9 wt-% (2.1 g) mass loss compared with 14.2 wt-% (33.4 g) of SC. For a mixture of (inexpensive) SC with only a minor (8 wt-% based on the mass of SC) corrosion inhibitor, the monosaccharide glucose has a significant effect and reduces mass loss by half from 14 wt-% to nearly 7 wt-%. Other monosaccharides (arabinose, maltose and mannose) show similar results.

In summary, sufficient reduction in corrosion rates can be achieved either by choosing a different deicing agent or by adding an inhibitory substance such as a monosaccharide. An answer to which primary deicing agent or combination of deicing agents and corrosion inhibitors can provide the best overall performance is illustrated in this research. For limited areas of application with high unit costs, such as train stations, using alternative deicers or corrosion inhibitors is usually cost-effective. In general, the selection of the most suitable deicing agent or inhibitors, or both, depends largely on whether the additional costs for the deicing agent producing similar deicing performance are outweighed by the savings due to increased service life. The next stepsare the identification and testing of additional inhibitors and materials. Nevertheless, the methods and results in the current work provide concise answers and a clear path for future research toward cost-effective deicing agents with significantly lower corrosion than SC.

Disclosure statement

No potential conflict of interest was reported by the author(s).

Funding

ORCID

Michael R. Gruber ⬤ http://orcid.org/0000-0002-6179-7565
Bernhard Hofko ⬤ http://orcid.org/0000-0002-8329-8687
Markus Hoffmann ⬤ http://orcid.org/0000-0003-2690-1192
Hinrich Grothe ⬤ http://orcid.org/0000-0002-2715-1429

References

[1] Hanke H, Nutz P. International development of application methods of deicing chemicals-state of the art and best practice. France: La Defense; 2019. p. 4–9. ISBN: 978-2-84060-514-0

[2] PIARC. Snow and Ice Databook 2018-SIDB 2018EN. PIARC Technical Committee B.2 Winter Service; 2019, 25–33.

[3] Shi X, Veneziano D, Xie N, et al. Use of chloride-based ice control products for sustainable winter maintenance: a balanced perspective. Cold Reg Sci Technol. 2013;86:104–112. doi:10.1016/j.coldregions.2012.11.001.

[4] Shi X, Jungwirth S, Akin M, et al. Evaluating snow and Ice control chemicals for environmentally sustainable highway maintenance operations. J Transport Eng. 2014;140(11):5014005. doi:10.1061/(ASCE)TE.1943-5436.0000709.

[5] Koch GH, Brongers M, Thompson NG et al. Handbook of environmental degradation of materials. Norwich, NY; 2005. doi:10.1016/B978-081551500-5.50003-3.

[6] Van der Wegen G, Polder RB, Van Breugel K. Guideline for service life design of structural concrete – a performance based approach with regard to chloride induced corrosion. Heron. 2012;57(3):153–168.

[7] Hoffmann M, Gruber MR, Hofko B, et al. Winterlife: effective, sustainable and non-corrosive deicing agents in winter maintenance. PIARC-XVI World Winter Service and Road Resilience Congress; 2022, Calgary.

[8] ISO 9227:2017: Corrosion tests in artificial atmospheres-salt spray tests. International Organization for Standardization; 2017. Available from: www.iso.org.

[9] Astm G31-72(2004): Standard practice for laboratory immersion corrosion testing of metals, West Conshohocken, PA, ASTM International; 2004. Available from: www.astm.org.

[10] ISO 11130:2017: Corrosion of metals and alloys-alternate immersion test in salt solution. International Organization for Standardization; 2017. Available from: www.iso.org.

[11] Gruber MR, Hofko B, Hoffmann M, et al. Deicing performance of common deicing agents for winter maintenance with and without corrosion-inhibiting substances. Cold Reg Sci Technol. 2023;208. doi:10.1016/j.coldregions.2023.103795.

[12] Ismail A, Adan NH. Effect of oxygen concentration on corrosion rate of carbon steel in seawater. Am J Eng Res. 2014;3(1):64–67.

[13] Boies DB, Bortz S. Economical and effective deicing agents for use on highway structures. Chicago, IL: National Cooperative Highway Research Report (NCHRP); 1965. p. 19.

[14] Yuan Y, Ji Y, Jiang J. Effect of corrosion layer of steel bar in concrete on time-variant corrosion rate. Mater Struct. 2009;42:1443–1450. doi:10.1617/s11527-008-9464-9.

[15] Wang J, Wang J, Ming H, et al. Effect of temperature on corrosion behavior of alloy 690 in high temperature hydrogenated water. J Mater Sci Technol. 2018;34(8):1419–1427.

[16] Skaperdas GT, Uhlig HH. Corrosion of steel by dissolved carbon dioxide and oxygen. Indus Eng Chem. 1942;34(6):748–754.

[17] Mercer AD, Lumbard EA. Corrosion of mild steel in water. Br Corros J. 1995;30(1):43–55. doi:10.1179/bcj.1995.30.1.43.

[18] Tromans D. Modeling oxygen-controlled corrosion of steels in hot waters. Corrosion. 1999;55(10):942–947.

[19] Speller N. Corrosion, causes, and prevention. 3rd ed. New York: McGraw-Hill; 1951, p. 168.

[20] Paul S. Estimation of corrosion rate of mild steel in seawater and application of genetic algorithms. Can Metall Q. 2010;45:99–106.

[21] Andrade C. Correction to: propagation of reinforcement corrosion: principles, testing and modelling. Mater Struct. 2020;53. doi:10.1617/s11527-019-1420-3.

[22] Callahan M. Deicing salt corrosion with and without inhibitors. Washington, DC: Highway Division, Iowa Department of Transportation; 1988.

[23] Tempest B, Whelan M, Prah-Enin PK et al. Quantifying corrosive potential of de-icing and anti-icing solutions on bridge components – Final Report, North Carolina Department of Transportation Research Project FHWA/NC/2012-08; 2013.

[24] Shi X, Fay L, Yang Z, et al. Corrosion of deicers to metals in transportation infrastructure: introduction and recent developments. Corros Rev. 2009;27(1–2):23–52. doi:10.1515/CORRREV.2009.27.1-2.23.

[25] Austrian Standards. OENORM EN 10025-1:2004: Hot rolled products of structural steels – Part 1: General technical delivery conditions; 2004. Available from: www.austrian-standards.at.

[26] ISO 8407:2021: Corrosion of metals and alloys-removal of corrosion products from corrosion test specimens. International Organization for Standardization; 2021. Available from: www.iso.org.

Paper IV

Optimierungspotenziale im betrieblichen Winterdienst

Angesichts der Tatsache, dass geräumter Schnee nicht getaut werden muss, ist ein gutes Räumbild für einen wirtschaftlichen Winterdienst von wesentlicher Bedeutung. Die Entwicklung von geeigneten Verfahren für den Vergleich der Schneeräumungseffizienz und Dauerhaftigkeit unterschiedlicher Pflugsysteme war daher einer der Schwerpunkte eines Forschungsprojektes im Auftrag von ASFINAG, BMVIT und den Bundesländern in Österreich. Ausgehend von umfangreichen Vorversuchen zur Ermittlung der Restschneemengen wurde eine Vorgehensweise für groß angelegte Feldversuche entwickelt. Weiters wurden Versuche zur Abnutzung von Räumleisten durchgeführt, deren Ergebnisse verlässliche Aussagen zur Dauerhaftigkeit und Wirtschaftlichkeit von Stahl- und Kombiräumleisten ermöglichen. Ein zukünftiger Langzeitversuch in Kooperation mit Straßen- und Autobahnmeistereien könnte zudem einen Vergleich nach Hersteller ermöglichen. Die Einhaltung der ÖNORM EN 16811-1:2016-11 zu einem (Mindest-)Feuchtigkeitsgehalt von NaCl beeinträchtigt gemäß Beobachtungen die Rieselfähigkeit und hat in der Praxis schon zu Verstopfungen in Salzsilos geführt. Anhand der gut bewährten Versuchsmethode zur Rieselfähigkeit mit der Auslaufbox nach Sonntag wurde daher ein breites Spektrum an Auftaumitteln geprüft. Die Auslaufrate und der Auslaufwinkel haben die Beobachtungen bestätigt und sind gemäß den Ergebnissen geeignet, den Einfluss von Antibackmittel- und Feuchtegehalt praxisnah zu belegen.

Based on the fact that cleared snow does not have to be thawed, a good clearing pattern is essential for an economic winter maintenance. The development of suitable procedures for comparing the snow removal efficiency and durability of different plough systems was therefore one of the focal points of a research project on behalf of ASFINAG, BMVIT and the federal states in Austria. Based on extensive preliminary tests to determine the amount of remaining snow, a procedure for large-scale field tests was developed. In addition, tests were carried out on the wear and tear of snow plough blades, the results of which enable reliable conclusions to be drawn about the durability and economy of steel and combiblades. A future long-term trial in cooperation with road and highway maintenance departments will also enable a comparison by manufacturer. The recommendations of ÖNORM EN 16811-1: 2016-11 regarding a (minimum) moisture content of NaCl may impair the pourability leading to observed blockages in salt silos. A wide range of de-icing agents were therefore tested using the well-tried test method for pourability with the outlet box after Sonntag. The discharge rate and the discharge angle have confirmed the observations and, according to the results, are suitable for demonstrating the influence of the anti-caking agent and moisture content in a practical manner.

■ Verfasser

Dipl.-Ing. Michael Ronald Gruber
michael.gruber@tuwien.ac.at

**Assoc. Prof. Dipl.-Ing. Dr. techn.
Bernhard Hofko**
bernhard.hofko@tuwien.ac.at

TU Wien – Institut für Verkehrswissenschaften –
Forschungsbereich Straßenwesen
Gußhausstraße 28/230-03
A-1040 Wien

**Priv.-Doz. Dipl.-Ing. Dr. techn.
Markus Hoffmann**
markus.hoffmann@tuwien.ac.at

Hoffmann-Consulting
Fürst-Liechtenstein-Straße 13
A-1230 Wien

Hofrat Dipl.-Ing. Josef Neuhold
josef.neuhold@noel.gv.at

Amt der NÖ Landesregierung
Abteilung ST2 Straßenbetrieb
Landhausplatz 1
A-3109 St. Pölten

1 Einleitung

In Zeiten der Klimaerwärmung klingt es vielleicht widersprüchlich, Forschung im Bereich Winterdienst voranzutreiben, jedoch bedingt die Erwärmung auch eine Häufung von regionalen Wetterextrema. Plötzliche Wintereinbrüche mit massiven Schneefällen in kurzer Zeit, rasche Temperaturwechsel und anhaltende gefrierende Niederschläge können demgemäß öfter auftreten und in weiterer Folge zu unerwartet starken Verkehrsbehinderungen führen. Gerade in diesen Zeiten ist ein optimierter und damit effizienter Winterdienst erforderlich.

Betrachtet man die gesamte Kette der Planung und Durchführung des betrieblichen Winterdienstes, so erkennt man die Abhängigkeit von vielen Faktoren: Die Zuverlässigkeit der Wettervorhersage, das Zusammenspiel und die Verlässlichkeit der stationären und mobilen Sensorik, die Verfügbarkeit von Personal, technischer Ausrüstung und der eingesetzten Mittel. Doch unabhängig vom Fortschritt der Technik sind die

wesentlichen Punkte des Winterdienstes immer noch dieselben: das Räumen von Schnee und Eis und das Verhindern von Glätte bzw. das Beseitigen von Glätte durch Auftaumittel.

Daher wurde ein Forschungsprojekt der Technischen Universität Wien (TU Wien), Hoffmann-Consulting, der österreichischen Bundesländer unter Federführung von Hofrat Dipl.-Ing. Josef Neuhold, dem Bundesministerium für Verkehr, Innovation und Technologie (BMVIT) und der ASFINAG ins Leben gerufen. Ein Ziel dabei war es, den Einfluss der Feuchtigkeit und des Anteils von Antibackmitteln auf die Rieselfähigkeit von Natriumchlorid zu untersuchen. Die Ergebnisse sind sowohl für die Ausschreibung als auch die Lagerung in Hallen und Salzsilos wesentlich, um eine Klumpenbildung und Verstopfungen in Salzsilos sowie eine erschwerte Beladung der Streufahrzeuge zu vermeiden.

Doch auch die effektivste Streumethode und das beste Auftaumittel sind nur begrenzt wirksam, wenn die nach der Räumung verbleibende Restschneemenge zu groß ist.

Hauptverantwortlich für eine schlechte Räumleistung sind Spurrinnen oder Unebenheiten in der Straßenoberfläche, wo Schneepflüge mit langen, starren Räumleisten nur begrenzt wirksam sind. Bereits am Markt befindliche Lösungen ermöglichen eine deutliche Verbesserung des Räumbildes durch sich sektoral an die Fahrbahnoberfläche anpassende Räumschilder (Klavierpflug) oder durch Verwendung einer zusätzlichen elastischen Nachräumleiste. Ein wesentliches Ziel des Forschungsprojektes ist daher die Entwicklung einer Methodik für den Vergleich der Pflugsysteme und Räumleisten in Bezug auf das Räumergebnis und die Lebensdauer. In einem weiteren Schritt sind diese den Kosten gegenüberzustellen, um den Betreibern einen effizienten wirtschaftlichen Einsatz der Ressourcen zu ermöglichen.

2 Räumqualität – Restschneebestimmung

2.1 Einleitung

Wie einleitend dargestellt, sind das Räumbild und die Restschneemenge in Abhängigkeit von Pflugtyp und Straßenzustand wesentliche Aspekte eines effizienten Winterdienstes. Da geräumter Schnee nicht getaut werden muss, ist ein gutes Räumbild für einen wirtschaftlichen Winterdienst von wesentlicher Bedeutung [1]. Hersteller geben fallweise eine Räumleistung (m^3/h) ihrer Pflugsysteme an, jedoch ohne Angaben zum Räumbild, das mit Straßenzustand, Schneekonsistenz und Pflugtyp von einer Vielzahl an Faktoren abhängig ist. Vor allem auf Straßen mit schlechter Längsebenheit oder Spurrinnen gibt es jedoch erhebliche Unterschiede in den verbleibenden Schneemengen. Die Kenntnis der Restschneemenge zusammen mit der Temperatur erlaubt zudem Rückschlüsse auf die zu streuende Salzmenge während und nach Niederschlagsereignissen sowie auf die Entwicklung des Straßenzustandes.

2.2 Methodik

Zur Bewertung des Räumbildes wurden mehrere Vorversuche mit Schnee bzw. mit Schneeersatzmaterial durchgeführt. Neben einer entsprechenden Recherche wurden u. a. Löschschaum, Wärmedämmschüttung, Trockenschüttung und Feinsand als Ersatzmaterial näher untersucht. Ausgehend von theoretischen Überlegungen sowie praktischen Vorversuchen hat sich gezeigt, dass

1. **Auswahl der Versuchsstrecke:**
   Die Versuchsstrecke sollte für die Dauer der Versuche gesperrt werden können und einen möglichst einheitlichen Deckenbelag mit mehr oder weniger ausgeprägten Spurrinnen sowie Asphalttextur aufweisen.

2. **Voruntersuchung der Versuchsstrecke:**
   Zur Ermittlung der Ausgangsbedingungen an der Versuchsstrecke ist die Spurrinnentiefe mindestens alle 10 bis 25 m mittels 4-Meter-Latte aufzunehmen und in einem Übersichtsplan zu dokumentieren (z. B. nach DIN EN 13036-3:2003-06). Wie in Bild 1 dargestellt, hat die Querebenheit bzw. haben Spurrinnen einen wesentlichen Einfluss auf die Restschneemenge.

   Im selben Abstand (alle 10 bis 25 m) ist jeweils in der Fahrbahnmitte und in der Spurrinne die Fahrbahntextur mittels geeigneter Verfahren, z. B. gemäß DIN EN ISO 13473-1:2004-07 (Sandfleckverfahren), zu erfassen. Beim Sandfleckverfahren kann die Oberflächentextur bzw. das Texturvolumen ermittelt werden [2], wodurch ein Tauen des Restschnees für die Erfassung nach einem manuellen Abziehen der Oberfläche mittels Spachtel entfallen kann. Die Restschneemenge ist dann für alle Versuche gleich und kann über Texturvolumen und Schneedichte rückgerechnet werden.

3. **Räumung der Versuchsstrecke:**
   Für die Räumdurchgänge ist es wesentlich, die einzelnen Einflüsse unter möglichst gleichen Bedingungen zu untersuchen. So wird es sinnvoll sein, die Räumversuche mit demselben Räumfahrzeug durchzuführen. Auf diesem werden verschiedene Räumschilder montiert, unterschiedliche hydraulische Pflugentlastungsstufen aktiviert und anderes Zubehör wie Nachräumleisten eingesetzt. Für ausreichend stabile Ergebnisse ist eine entsprechende Anzahl an Versuchen bzw. Messungen je Konfiguration erforderlich (3 bis 5 Messungen je Versuch).

4. **Räumleistung und Restschneemessung:**
   Zur Bestimmung der Restschneemengen ist es sinnvoll, den zu untersuchenden Bereich durch eine Anzahl von 3 bis 5 flexiblen Messrahmen mit Dichtung an der Unterseite abzugrenzen (Bild 2). Dadurch wird gewährleistet, dass die Fläche zur Aufnahme des Restschnees konstant bleibt und es im Fall eines Auftauens des Restschnees zu keinen größeren Abweichungen kommt. Für die Aufnahme des Restschnees innerhalb des Rahmens stehen mehrere Verfahren zur Verfügung, die sich in ihrer Genauigkeit und Anwendbarkeit sowie im Aufwand unterscheiden:

   a) **Abziehen mit Spachtel & Rückrechnung:**
   Am einfachsten ist ein Abziehen der Restschneemengen im Messrahmen mit einer breiten Spachtel und getrennten Wägung dieser Restschneemengen. Die verbleibende Restschneemenge kann dann aus dem Texturvolumen und der Schneedichte rückgerechnet werden.

   b) **Abziehen mit Spachtel, Tauen & Aufnehmen:**
   Wie zuvor wird die Restschneemenge im Messrahmen mittels Spachtel aufgenommen. Der in der Textur verbleibende Schnee kann mittels einer definierten Menge Salz getaut und mit einem Nassstaubsauger aufgesaugt oder einem Schwamm aufgenommen werden. Eine Erhitzung zur Einleitung des Tauvorgangs ist ebenfalls möglich, es sollte aber auf eine mögliche Verdunstung geachtet werden.

   c) **Laserscanning vor und nach Räumung:**
   Durch den Laserscan (z. B. terrestrisch oder mit Messbalken) vor der Beschneiung und nach der Räumung entfällt die Notwendigkeit einer Erfassung von Spurrinnentiefe und Textur. Das Restschneevolumen ergibt sich aus der Differenz der beiden Scans im definierten Auswertebereich. Die Restschneemenge kann aus der stichprobenartig erhobenen Dichte rückgerechnet werden. Entscheidend für die Genauigkeit dieses rein messtechnischen Verfahrens ist die Auflösung bzw. Punktdichte im Aufnahmebereich.

Tabelle 1: Entwickelter Versuchsaufbau zur Beurteilung der Räumqualität

der Straßenzustand bzw. insbesondere die Querebenheit (Spurrinnen) und die Straßentextur der Asphalt- bzw. Betonoberfläche einen wesentlichen Einfluss auf das Räumbild haben. Weitere wesentliche Faktoren sind der Zustand der Schneedecke (frisch gefallen oder festgefahren) sowie die Umgebungstemperatur, da sie die Konsistenz und Dichte des Schnees beeinflussen.

Die Wiederholbarkeit der Versuche auf Basis natürlicher Schneefälle unter sich ändernden Rahmenbedingungen wird daher selbst unter optimalen Bedingungen nur begrenzt erreichbar sein. Praktisch ergibt sich daraus eine hohe erforderliche Anzahl an Wiederholungen, um den Einfluss dieser Faktoren statistisch abzusichern. Weiters sind ausgedehnte Versuche während bzw. unmittelbar nach Schneefallereignissen aufgrund der begrenzten personellen Kapazitäten in den Meistereien nicht einfach durchführbar. Der Einsatz von ausgewählten und geprüften Schneeersatz-Materialien kann dagegen zu einem beliebigen Zeitpunkt durchgeführt werden, sofern eine Eignung und Übertragbarkeit gegeben sind. Die Ergebnisse mit den gewählten Ersatzmaterialien haben zwar die grundsätzlich erwarteten Zusammenhänge bestätigt, sind aber nur begrenzt übertragbar und könnten im Zweifelsfall z. B. bei Auswahlentscheidungen hinterfragt werden.

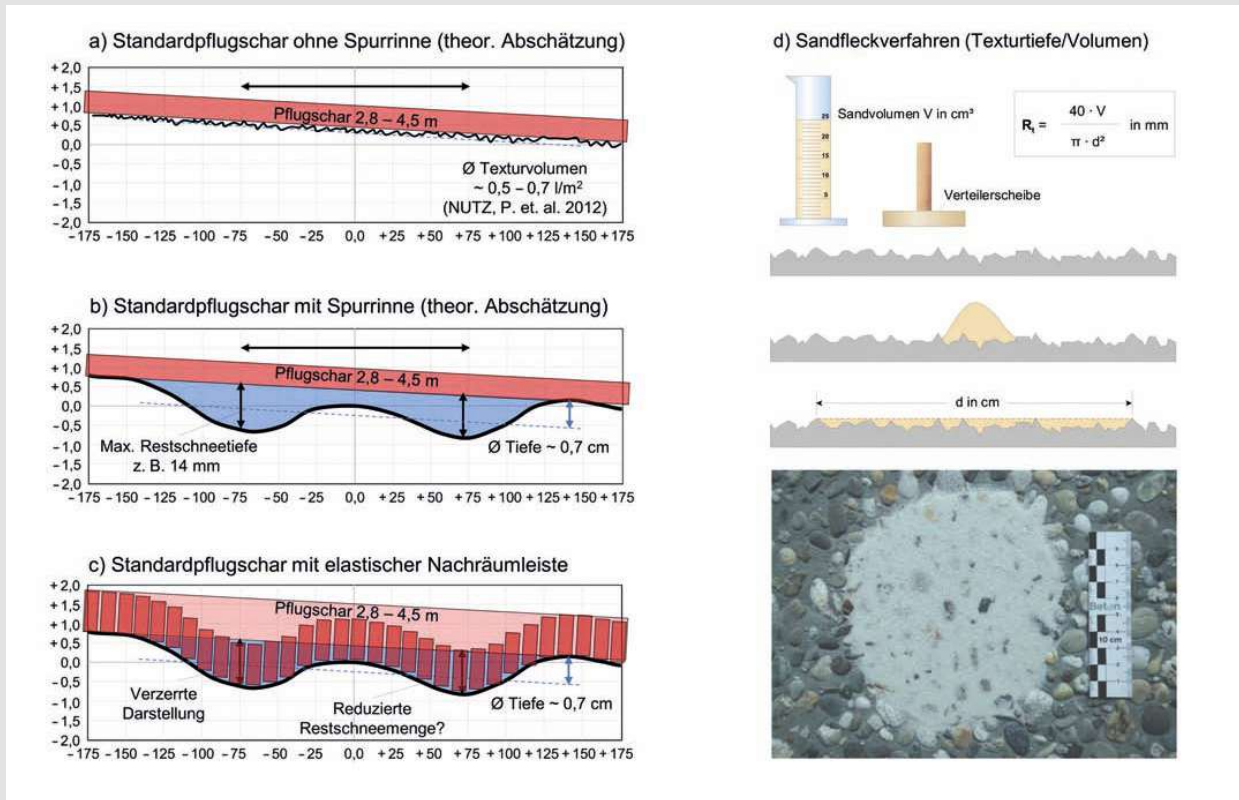Als besondere Herausforderung bei den

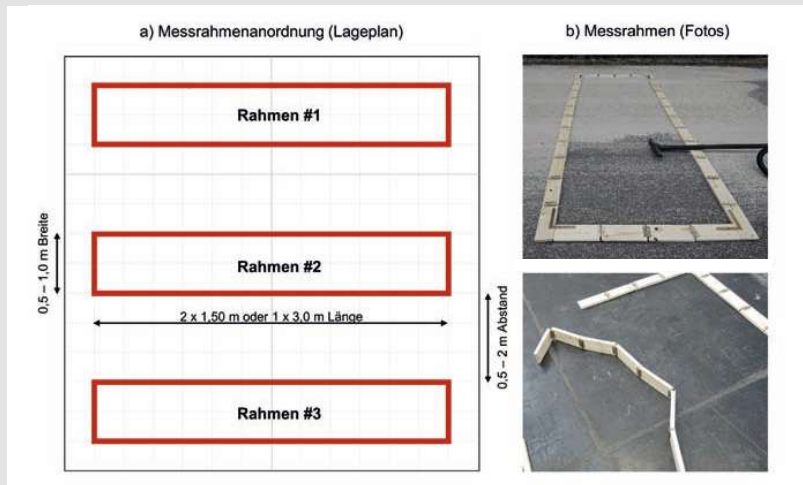Bild 1: Voruntersuchung von Querebenheit und Oberflächentextur [2]

Bild 2: Rahmen zur Ermittlung der Restschneemengen

3 Räumqualität – Räumleistenverschleiß

3.1 Einleitung

Einen weiteren wesentlichen Aspekt zur Optimierung des Winterdienstes stellt die Kenntnis der möglichen Einsatzdauer von Räumleisten bzw. ihrem Tauschintervall dar. Durch Gegenüberstellung der Räumleistenabnutzung in Millimetern zu den dabei zurückgelegten Kilometern können verschiedene Leisten klassifiziert werden. Dazu wurde in einem ersten Schritt eine Umfrage bei den österreichischen Straßen- und Autobahnmeistereien durchgeführt. Das Ziel der Umfrage war, die Identifikation der am häufigsten eingesetzten Pflugsysteme und Räumleisten sowie die typischen Tauschintervalle zu identifizieren. Auf Basis der Umfrageergebnisse wurde ein Prüfprogramm aufgestellt, in dem die ausgewählten Leisten einer Verschleißsimulation unterzogen wurden.

3.2 Methodik

Für die Verschleißsimulation wurde von einem Pflughersteller ein für diesen Zweck

Ersatzmaterialien, aber insbesondere bei Schnee hat sich die wiederholbare, möglichst genaue Aufnahme der Rest(schnee)menge erwiesen. Gerade für eine statistisch signifikante Untersuchung der Unterschiede zwischen Pflugtypen, Anstellwinkeln, Anpressdruck sowie Nachräumleisten ist eine hohe Wiederholbarkeit und Genauigkeit bei

vertretbarem Aufwand entscheidend für belastbare Aussagen. In Tabelle 1 wird daher ein Versuchsaufbau präsentiert, von dem zu erwarten ist, dass die angestrebten Ziele bei entsprechender Optimierung erreichbar sind. Ein groß angelegter Versuch dazu wird voraussichtlich im Winter 2020/21 stattfinden.

Bild 3: Feldversuch Verschleiß der Räumleistensegmente

Bild 4: Erste Charge des Verschleißversuchs

entwickelter Prototyp zur Verfügung gestellt. Auf diesem sind bis zu 14 Räumleistensegmente parallel in einen Träger eingespannt und werden individuell belastet, um die Flächenpressung für alle Segmente gleich zu halten. Zur Simulation einer Räumfahrt wird der Träger anschließend auf ein Fahrzeug montiert, bei winterlichen Bedingungen einige Kilometer über Asphalt bzw. die Schneedecke gezogen und anschließend der Abrieb der einzelnen Leisten gemessen (Bild 3). Der Einfluss auf den Abrieb durch Spurrinnen und Unebenheiten auf der Teststrecke wird durch Positionswechsel der Räumleistensegmente untereinander minimiert.

3.3 Prüfprogramm

In Summe wurden 28 unterschiedliche Räumleisten aus Stahl und Kombi-Räumleisten aus Stahl-Korund-Gummi in zwei Chargen zu je 14 Leisten geprüft (Bild 4). Nach einer Fahrt auf der Prüfstrecke (13,1 km Länge) wurde die Höhe der Leiste und somit der kilometerbezogene Verschleiß gemessen und die Position der Leisten von außen nach innen um einen Platz verschoben. Die Gesamtkilometerleistung je Räumleiste lag bei ungefähr 90 Kilometern mit durchschnittlich 30 % Schneefahrbahnanteil. Gegenüber einem praktischen Einsatz ist dieser Anteil vergleichsweise gering, ein höherer Anteil hätte jedoch eine weitaus größere Kilometerleistung erfordert. Zudem waren die Bedingungen für alle eingesetzten Räumleisten gleich. Eine statistisch signifikante Auswertung der Abnutzung nach Hersteller hätte ein wesentlich umfassenderes Prüfprogramm erfordert, weshalb die Ergebnisse kumulativ wiedergegeben werden.
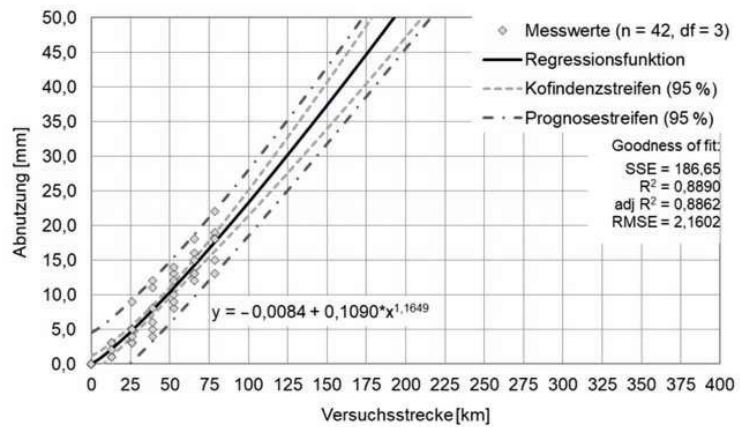
Bild 5: Abnutzung und Zustandsprognose Stahlleisten (ohne Ausreißer)
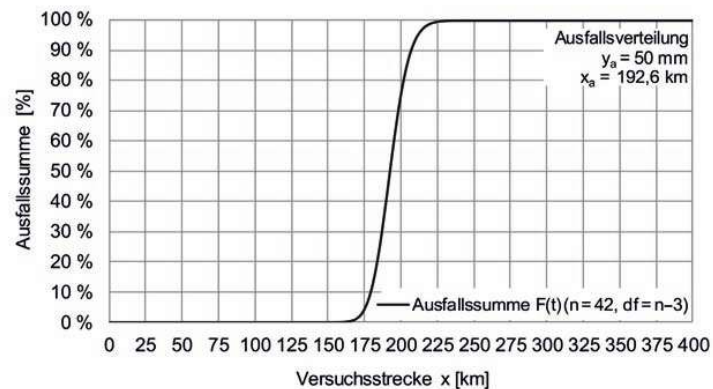
Bild 6: Laufleistung und Ausfallverteilung ohne Ausreißer (Ausfall = 50 mm)

3.4 Ergebnisse

Mittels Regressionsrechnung lässt sich ein Zustandsmodell anpassen und daraus die Laufleistung bis zu einer Abnutzungsgrenze prognostizieren [3]. Da die Versuchswerte der unterschiedlichen Stahlräumleisten eine gewisse Schwankungsbreite aufweisen, ergibt sich an der Ausfallsgrenze y_a = 50 mm eine mittlere Laufleistung von 162,3 km bei einer entsprechend breiten Ausfallverteilung. Da die Messwerte einer Stahlräumleiste auffallend schlecht waren, wurde diese in der

Bild 7: Auslaufbox nach Sonntag
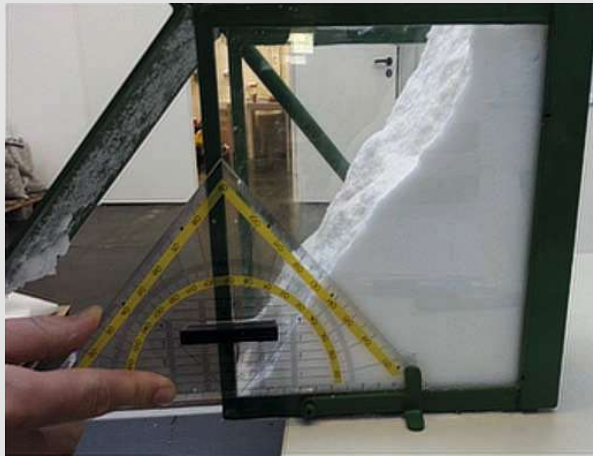
Auftausalz	Korngröße [mm]	Antibackmittel	Antibackmittelgehalt [mg/kg]
	fein	Natriumferrocyanid	70–80
	0/2	Natriumferrocyanid	70–100
	0/2	ohne	0
	0/3	Natriumferrocyanid	70–100
	0/3	ohne	0
Steinsalz/ Rock Salt/ RS	0/3	Natriumferrocyanid	70–80
	0/3	Natriumhexacyanoferrat	80–120
	0/3	ohne	0
	0/5	Natriumferrocyanid	70–80
	0/5	Natriumferrocyanid	70–100
	0/5	ohne	0
	0/6	Natriumhexacyanoferrat	80–120
	fein	Natriumhexacyanoferrat	8
	fein	Natriumhexacyanoferrat	0
	fein	Natriumferrocyanid	8
Siedesalz/ Vacuum Salt/ VS	fein	ohne	0
	fein	Natriumferrocyanid	20
	fein	biologisch	12
	fein	Natriumhexacyanoferrat	80–100
	fein	ohne	0
	0/1	Natriumferrocyanid	60
Meersalz	0/1	ohne	0
	0,5/2	Natriumferrocyanid	60

Tabelle 2: Verfügbare Auftausalze (NaCl) und Antibackmittel sowie -gehalte für Österreich

zu einer extremen Abnutzung von Stahlräumleisten führt und daher zu vermeiden ist.

Neben Stahlräumleisten wurden auch die gewählten Kombinationsräumleisten dem Verschleißversuch unterzogen. Die ermittelte Abnutzung bei der gleichen Laufleistung war jedoch insgesamt deutlich geringer und mit mehr Streuung behaftet, sodass Prognosen auf dieser Basis nur eine begrenzte Belastbarkeit aufweisen. In künftigen Versuchen ist daher auf diesen Umstand abzustellen und zudem der deutlich höhere Preis sowie die niedrigere Ausfallsgrenze in der Auswertung zu berücksichtigen.

4 Rieselfähigkeit von Streumitteln

4.1 Einleitung

Unabhängig davon, wie schnell und wie gut auf ein Niederschlagsereignis reagiert wird, kann auch das beste Räumgerät die Straßen nicht frei von Schnee und Matsch halten. Um dem entgegenzuwirken, werden Taumittel verschiedenster Zusammensetzungen auf unterschiedliche Weise ausgebracht. In diesem Zusammenhang unterscheidet man präventives Streuen vor einem Niederschlagsereignis und kuratives Streuen nach einem Ereignis. Aufbauend auf theoretischen Überlegungen und praktischen Erfahrungen erfolgt in Österreich soweit als möglich eine präventive Ausbringung von befeuchtetem Taumittel vor Niederschlagsereignissen. In Österreich wird NaCl in Form von Feuchtsalz FS ausgebracht, wobei sich die Ausbringungsweisen regional stark unterscheiden. Je nach Anforderungsprofil und Geräteausstattung erfolgt die Ausbringung von NaCl mit einem Soleanteil von 30 % (FS30), 50 % (FS50) und 70 % (FS70). Insbesondere für den präventiven Einsatz bzw. vor Reifereignissen bei Temperaturen um den Gefrierpunkt kann auch eine reine Solestreuung (FS100) erfolgen.

Ziel dieser präventiven Feuchtsalzstreuung ist die Bildung einer flüssigen Salzlösung zwischen der Fahrbahnoberfläche und dem fallenden Schnee. Dieser Solefilm soll einem Festfrieren des Niederschlags und damit einer Herabsetzung der Griffigkeit entgegenwirken und in weiterer Folge eine leichtere Schneeräumung ermöglichen. Die Befeuchtung des Tausalzes am Streuteller bewirkt gemäß vorhergehenden Untersuchungen von TU Wien und Hoffmann Consulting eine Verminderung der Aus-

Folge ausgeschieden und die Auswertung wiederholt. Das Zustandsmodell für die verbleibenden Stahlräumleisten ist nun wesentlich robuster (Bild 5 mit Anstieg adj. R² von 0,5022 auf 0,8862). Dementsprechend ist die Ausfallsverteilung schmäler und die mittlere Laufleistung steigt auf 192,6 km (Bild 6). Im Vergleich zu den Befragungsergebnissen zum Tauschintervall bzw. den typischen Räums-

trecken eines Winters mit 15 bis 25 Schneefallereignissen ist die Laufleistung im Versuch vergleichsweise kurz. Dies mag zum Teil auf die Versuchsanordnung oder die Vorspannung zurückzuführen sein, liegt aber vor allem an dem geringen Schneefahrbahnanteil von ca. 30 % der Versuchsstrecke. Praktisch bedeutet dies, dass eine Räumung bei geringem Anteil bzw. ohne Restschnee am Asphalt

Auftausalz	Korngröße [mm]	Antibackmittel	Antibackmittel-gehalt [mg/kg]	Proben-bezeichnung	Feuchtigkeitsgehalt [%]				Bestimmung [Stk]	Anzahl [Stk]
Steinsalz/ Rock Salt	0/3	keines	0	RS1-0[0/3]	0	0,25	0,5	0,75	3	12
	0/2	keines	0	RS2-0[0/2]	0	0,25	0,5	0,75	3	12
	0/3	Natriumferrocyanid	70-100	RS3-70[0/3]	0	0,25	0,5	0,75	3	12
	0/2	Natriumferrocyanid	70-100	RS4-70[0/2]	0	0,25	0,5	0,75	3	12
Siedesalz/ Vacuum Salt	fein	keines	0	VS1-0	0	0,25	0,5	0,75	3	12
	fein	keines	0	VS2-0	0	0,25	0,5	0,75	3	12
	fein	keines	0	VS3-0	0	0,25	0,5	0,75	3	12
	fein	Natriumferrocyanid	8	VS4-8	0	0,25	0,5	0,75	3	12
	fein	Natriumferrocyanid	8	VS5-8	0	0,25	0,5	0,75	3	12
	fein	biologisch	12	VS6-12-Bio	0	0,25	0,5	0,75	3	12
	fein	Natriumferrocyanid	22	VS7-22	0	0,25	0,5	0,75	3	12
	fein	Natriumferrocyanid	80-100	VS8-80	0	0,25	0,5	0,75	3	12

Tabelle 3: Prüfprogramm Rieselfähigkeit

Auftausalz	Korngröße [mm]	Antibackmittel	Antibackmittel-gehalt [mg/kg]	Proben-bezeichnung	Einwirkzeit [min]				Bestimmung [Stk]	Anzahl [Stk]
					FS0	FS0	FS100	FS100		
Steinsalz	0/3	keines	0	RS1-0[0/3]	60	240	60	240	4	16
	0/3	Natriumferrocyanid	70-100	RS3-70[0/3]	60	240	60	240	4	16
Siedesalz	fein	keines	0	VS3-0	60	240	60	240	4	16
	fein	Natriumferrocyanid	80-100	VS8-80	60	240	60	240	4	16

Tabelle 4: Prüfprogramm Tauleistung mit und ohne Antibackmittel

bringungsverluste und eine bessere Haftung auf der Straßenoberfläche [4, 5].

Doch diese Befeuchtung darf erst unmittelbar vor dem Streuen auf die Fahrbahn erfolgen, da das Tausalz sonst zu klumpen beginnt und festbackt. Daher wurde im vorgestellten Forschungsprojekt auch die Rieselfähigkeit von Natriumchlorid in Abhängigkeit von seiner Feuchtigkeit und dem Vorhandensein spezieller Zusätze untersucht. Ein zu hoher Feuchtegehalt oder eine ungewollte Anfeuchtung ist daher vor der Ausbringung ungünstig, insbesondere für die Lagerung von NaCl in Hallen und Salzsilos. So kann ein Feuchtegehalt unter 1 % bereits zu Klumpenbildung und stark beeinträchtigter Rieselfähigkeit führen und in weiterer Folge Verstopfungen in Salzsilos hervorrufen und damit eine erschwerte Beladung der Streufahrzeuge zur Folge haben. Anhand erster Versuche zur Rieselfähigkeit auf Basis der Auslaufbox nach Sonntag (Bild 7) konnten ein wiederholbares Prüfverfahren etabliert und die Auswirkungen von Trocknungsvorgängen auf feste Taumittel quantifiziert werden [6].
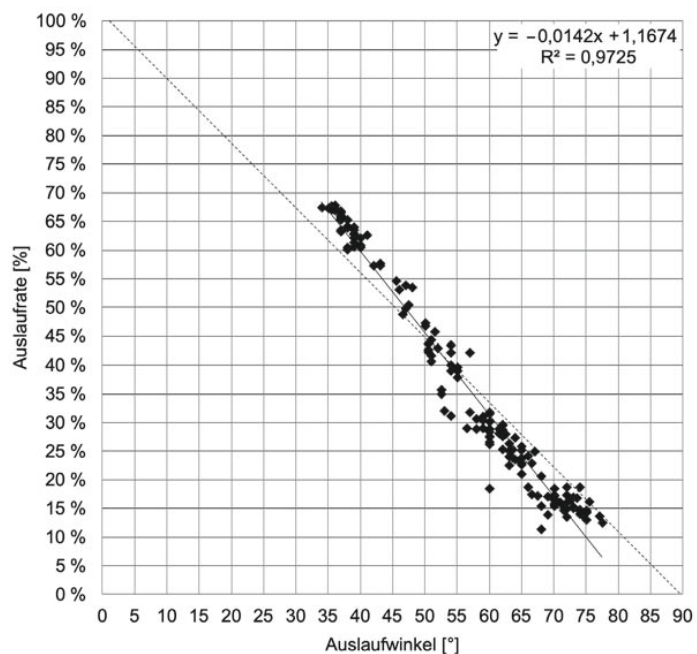

$y = -0,0142x + 1,1674$
$R^2 = 0,9725$

Bild 8: Korrelation der Auslaufrate und des Auslaufwinkels

Bild 9: Zusammenhang der Auslaufrate und von Auslaufwinkel in Abhängigkeit des Antibackmittels und Feuchtigkeit
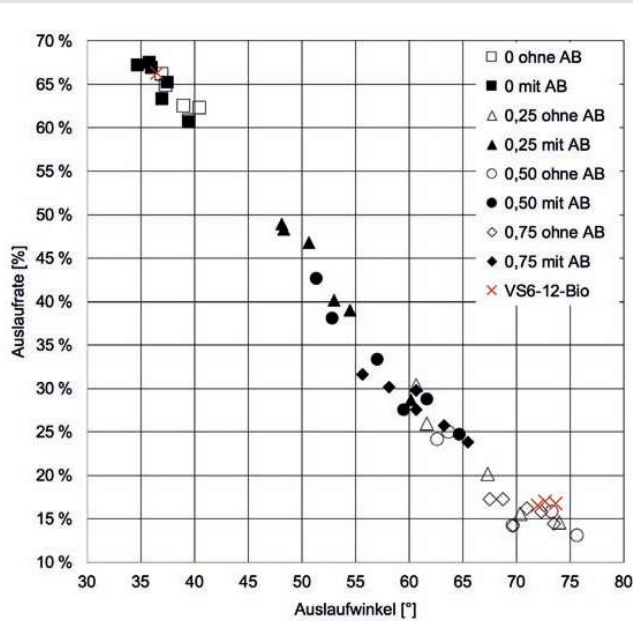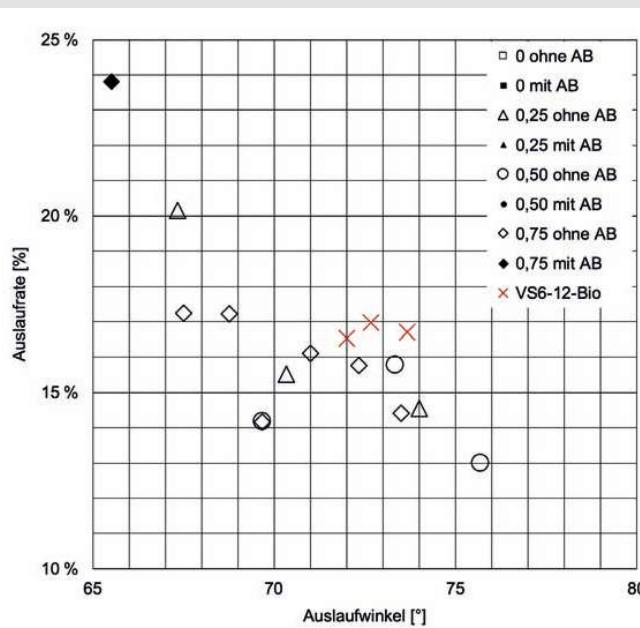

Bild 10: Verhalten des Streusalzes VS6-12-Bio

kontaktiert. Die ausgewählten Salze sind in Tabelle 2 aufgelistet und unterscheiden sich im Wesentlichen durch ihre Abbau- bzw. Produktionsmethoden, Korngrößen und Antibackmittelgehalte. Als Antibackmittel wurde von annähernd allen Lieferanten die Zugabe von Natriumferrocyanid $Na_4[Fe(CN)_6]$ (Natriumhexacyanoferrat) rückgemeldet. Nur ein Lieferant vertreibt cyanidfreies und biologisch abbaubares Antibackmittel (biologisch). Für die systematische Untersuchung der Rieselfähigkeit wurden insgesamt 12 Produkte von 4 Lieferanten in das Prüfprogramm aufgenommen (in Tabelle 2 fett markiert).

4.3 Prüfprogramm Rieselfähigkeit und Tauleistung

Auf Basis der 12 verschiedenen Produkte und 4 untersuchten Feuchtegehalte (0; 0,25; 0,5; 0,75 M.-%) ergaben sich insgesamt 48 Prüfkombinationen. Alle Prüfungen wurden mit Dreifachbestimmung ausgeführt, wodurch sich über 140 Einzelversuche ergaben (siehe Tabelle 3). Die in weiterer Folge verwendete Nomenklatur ist der Tabelle 3 in der Spalte Probenbezeichnung zu entnehmen und setzt sich wie folgt zusammen:

RS3-70[0/3] = Rock Salt (Steinsalz) – Nr. **3 – 70** mg/kg Antibackmittelgehalt [**0/3** mm Korngröße]

VS7-22 = Vacuum Salt (Siedesalz) – Nr. **7 – 22** mg/kg Antibackmittelgehalt

Die Tauleistung wurde für Tausalze mit und ohne Antibackmittel sowohl für Trockensalz (FS0) als auch für reine Sole (FS100) ermittelt. Als Einwirkungsdauer wurden 60 und 240 Minuten, als Prüftemperatur –5 °C gewählt. Die Prüfungen wurden in Vierfachbestimmung durchgeführt und ergaben somit über 60 Einzelprüfungen (siehe Tabelle 4).

4.4 Ergebnisse – Rieselfähigkeit

Die Versuchsmethode mit der Auslaufbox nach Sonntag hat sich für die Beurteilung der Rieselfähigkeit von Tausalzen gut bewährt, denn zwischen den Parametern Auslaufrate und Auslaufwinkel besteht eine sehr gute Korrelation. Weiters sind die Unterschiede zwischen dem Vorhandensein von Antibackmittel sowie den verschiedenen Feuchtigkeitsgehalten deutlich erkennbar (Bilder 8 bis 10). Aus der Gegenüberstellung aller Messergebnisse in Form von Auslaufrate und Auslaufwinkel ergibt sich die folgende Regressi-

4.2 Methodik

Um den Einfluss bestimmter Feuchtigkeitsgehalte auf die Rieselfähigkeit zu untersuchen, wurden Tausalze unterschiedlicher Herkunft (Steinsalz, Siedesalz) mit verschiedenen Antibackmitteln und variierenden Antibackmittelgehalten geprüft. Damit sollten insbesondere die auf Grundlage der ÖNORM EN 16811-1:2016-11 [7] basierenden Vorgaben der RVS 12.04.16 [8] hinsichtlich Anforderungen für den Antibackmittel-

gehalt von Natriumchlorid überprüft werden. Zusätzlich wurde der mögliche Einfluss der zugesetzten Antibackmittel auf die Tauleistung ausgewählter Tausalze sowohl in Form von Trockensalz (FS0) als auch in Form von reiner Sole (FS100) untersucht.

Zur Identifizierung der in Österreich verfügbaren NaCl-Salze und Antibackmittel sowie der zugesetzten Mengen wurden die bekannten Lieferanten der Autobahn- und Straßenmeistereien am Markt in Österreich

onsgerade y = –0,0142x + 1,1674 in Bild 8 (Bestimmtheitsmaß R^2 = 0,97).

In Bild 9 sind die Salze mit und ohne Antibackmittel in Abhängigkeit von ihrem Feuchtegehalt ausgewertet und hervorgehoben. Dabei sind die mit ausgefülltem Symbol dargestellten Salze mit Antibackmittel versehen, jene ohne Füllung ohne Zusätze. Ferner sind die verschiedenen Feuchtigkeitsgehalte (0; 0,25; 0,50 und 0,75 M.-%) mit unterschiedlichen Symbolen dargestellt. Davon ausgenommen ist das Siedesalz VS6-12-Bio, welches unabhängig von seinem Feuchtegehalt einer eigenen Kategorie zugeordnet wurde.

In Bild 10 ist der Bereich aus Bild 9 hervorgehoben, in dem sich ein Großteil der Ergebnisse des Salzes mit biologischem Antibackmittel (VS6-12-Bio) befindet. Dies soll den Umstand verdeutlichen, dass sich Salz mit biologischem Antibackmittel bezüglich der Rieselfähigkeit jedenfalls wie Salz ohne Antibackmittel oder schlechter verhält.

Die Rieselfähigkeit von trockenen Tausalzen ist für alle geprüften Varianten annähernd gleich und somit unabhängig vom Antibackmittelgehalt, wobei Siedesalze, vermutlich wegen der geringeren Korngröße, gegenüber Steinsalzen rieselfähiger sind. Insgesamt zeigen die Ergebnisse, dass der Feuchtegehalt des Tausalzes einen sehr wesentlichen Einfluss auf die Rieselfähigkeit hat. Der Grenzwert der Feuchte von 0,5 M.-% sollte daher nicht überschritten werden, da die Rieselfähigkeit bei höherem Feuchtegehalt stark abnimmt.

Auslaufrate [%]	Feuchtigkeit [M%]			
	0 M%	0,25 M%	0,50 M%	0,75 M%
RS1-0-[0/3]	100 %	48,8 %	38,7 %	23,2 %
RS2-0-[0/2]	100 %	25,5 %	23,3 %	23,3 %
RS3-70-[0/3]	100 %	79,6 %	70,3 %	52,0 %
RS4-70-[0/2]	100 %	63,3 %	52,7 %	43,5 %
VS1-0	100 %	41,4 %	39,9 %	27,6 %
VS2-0	100 %	22,4 %	24,3 %	24,9 %
VS3-0	100 %	30,5 %	19,6 %	23,8 %
VS4-8	100 %	59,7 %	42,2 %	39,4 %
VS5-8	100 %	42,4 %	36,6 %	35,3 %
VS6-12-Bio	100 %	25,6 %	24,9 %	25,2 %
VS7-22	100 %	80,2 %	56,9 %	45,0 %
VS8-80	100 %	69,5 %	42,7 %	44,2 %

Tabelle 5: Auslaufrate bezogen auf den prozentualen Auslauf vollkommener Trockenheit

Vergleicht man diesen Wert mit dem in der ÖNORM EN 16811-1:2016-11 [7] festgesetzten Grenzwert für trockenes Salz, nämlich weniger als 0,6 M.-% Feuchtigkeit, so lässt dies auf eine zu wenig restriktive Auslegung der Norm schließen. Außerdem wird darin eine Mindestfeuchtigkeit von 0,2 M.-% für Steinsalz empfohlen, um bei Manipulation Staubentwicklung zu verringern. Betrachtet man ausschließlich die Rieselversuche von Steinsalz, so ist zu erkennen, dass eine Feuchtigkeit von 0,25 bis 0,50 M.-% eine Verschlechterung der Auslaufrate auf 50 % des Ursprungswertes ohne Antibackmittel (–50 Prozentpunkte) und auf 80 % des Ursprungs-

wertes mit Antibackmittel (–20 Prozentpunkte) hervorruft. Die genauen Werte sind in Tabelle 5 aufgelistet, wobei darin die Auslaufrate relativ zur Auslaufrate bei 0 M.-% Feuchtigkeit dargestellt wird. Dementsprechend wird für Ausschreibungen im Gegensatz zur ÖNORM ein möglichst niedriger Feuchtegehalt in der Anlieferung empfohlen.

Die Untersuchungen bestätigen weiters die Wirkungslosigkeit des biologischen Antibackmittels (VS6-12-Bio) im Hinblick auf die Auslaufrate. Unabhängig vom Feuchtegehalt des Salzes bleibt die Auslaufrate bei knapp einem Viertel des ursprünglichen Wertes (–75 Prozentpunkte). Unter Berücksichtigung der
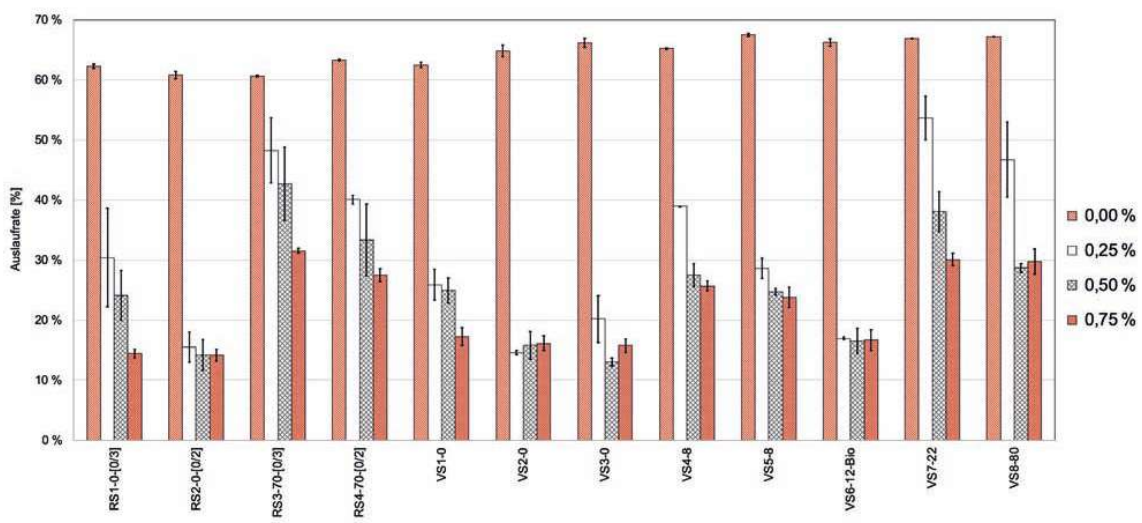

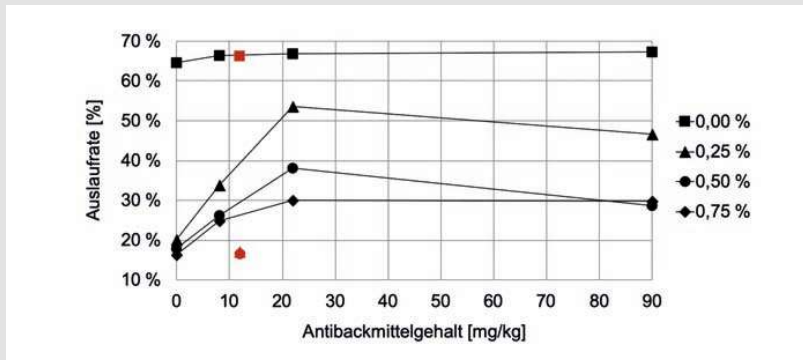Bild 11: Auslaufraten in Abhängigkeit von Taumittel und Feuchtigkeit

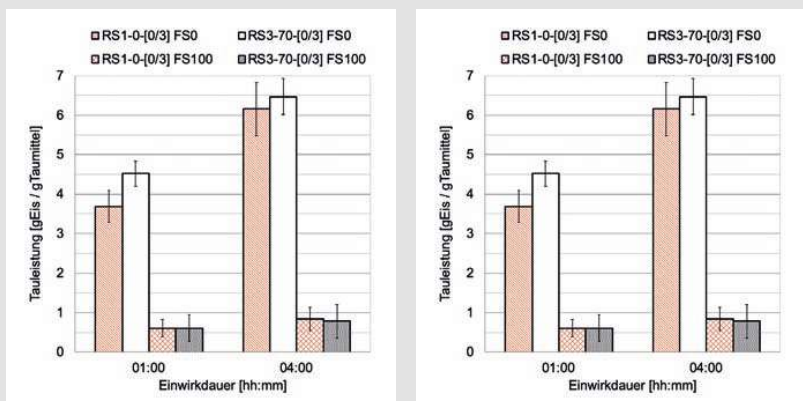**Bild 12:** Optimierung des Antibackmittelgehaltes für Siedesalze

Bild 13: Tauleistung Steinsalz RS und Siedesalz VS als Trockensalz FS0 und reine Sole FS100 mit und ohne Antibackmittel

Unsicherheiten sind die Werte mit VS6-12-Bio gleich gut oder schlechter als Salz ohne Antibackmittelzusatz.

Weiters zeigen Steinsalze mit einem Größtkorn von 2 mm eine geringere Rieselfähigkeit und sind anfälliger auf Verklumpungen als Steinsalze mit einem Größtkorn von 3 mm. Im feuchten Zustand weisen Siedesalze allerdings eine geringere Rieselfähigkeit auf als Steinsalze, außer der Antibackmittelgehalt beträgt mehr als 22 mg je kg Salz. Die Ergebnisse bezüglich der Auslaufrate (inklusive Standardabweichungen) aller geprüften Tausalze sind nachstehend in Abhängigkeit von ihrer Feuchtigkeit dargestellt (Bild 11).

Auf Basis der durchgeführten Prüfungen können die optimalen Antibackmittelgehalte vorerst nur abgeschätzt werden, da keine Tausalze mit anderen Antibackmittelgehalten zur Verfügung standen. Anhand der vorliegenden Daten lässt sich für eine ausreichende Rieselfähigkeit der notwendige Antibackmittelgehalt für Steinsalz nicht abschätzen, für Siedesalz kann derzeit ein Anteil von ca. 20 bis 25 mg/kg als ausreichend angesehen werden (Bild 12), da eine

deutliche Erhöhung des Antibackmittelgehaltes auf mehr als 80 mg/kg keine Verbesserung der Rieselfähigkeit im Vergleich zu 22 mg/kg bringt. Zusätzlich ist das Siedesalz mit der biologischen Antibackmittelalternative in Bild 12 rot hervorgehoben.

4.5 Ergebnisse – Tauleistung

Zur Beurteilung des Einflusses von Antibackmittel auf die Tauleistung wurde auf ein bewährtes Verfahren zur Bestimmung der Tauleistung [6] zurückgegriffen. Dieses erlaubt sowohl Aussagen über feste als auch über flüssige Taumittel. Hierbei wurde in den Versuchen Trockensalz im Ausmaß von ca. 10 g bzw. reine Sole (20-%-NaCl-Lösung) mit ca. 12 g auf eine definierte Eisplatte aufgebracht und das dadurch getaute Eis nach 60 oder 240 Minuten Einwirkzeit abgegossen. Der Quotient aus der Menge des aufgebrachten Salzes bzw. der aufgebrachten Sole und der Menge des getauten Eises entspricht der Tauleistung (in Abhängigkeit von der Einwirkdauer).

Da das gelieferte Steinsalz grobe Verunreinigungen enthielt, waren Abweichungen in

den Ergebnissen zu erwarten. Dennoch lässt sich feststellen, dass die Tauleistung von Steinsalz RS als 20 %-NaCl-Sole (FS100) von seinem Antibackmittelgehalt unabhängig ist. Als reines Trockensalz (FS0) deuten die Ergebnisse auf eine bessere Leistung des Salzes mit Antibackmittel hin, vermutlich bedingt durch die bereits genannte Verunreinigung. (Bild 13a) Auch die Tauleistung von Siedesalz VS (Bild 13b) weist bezüglich des Vorhandenseins von Antibackmittel keinen signifikanten Unterschied auf. Dies gilt sowohl für Trockensalz FS0 als auch für eine reine 20-%-NaCl-Sole (FS100).

Zusammengefasst ergeben sich für Stein- und Siedesalz keine negativen Auswirkungen durch Antibackmittel in Bezug auf Rieselfähigkeit und Tauleistung, weder für Trockenmaterial (FS0), noch für reine Sole (FS100). Zusätzlich lassen sich zwei zentrale Erkenntnisse ableiten: Für Trockensalz FS0 steigt die Taurate bei gröberem Steinsalz mit der Zeit viel stärker an als bei feinem Siedesalz. Weiters ist die Tauleistung der 20-%-NaCl-Sole (FS100) in gelöster Form für beide Salze annähernd konstant.

Literaturverzeichnis

[1] FSV (2010): Richtlinien und Vorschriften für den Straßenbau – RVS 12.04.12 Qualitätssicherung Betrieb – Winterdienst – Schneeräumung und Streuung; Wien; Ausgabe 10/2010

[2] Schulz, R. R. (2006): Rautiefenmessung an Betonoberflächen; Vortragsskriptum; Frankfurt

[3] Hoffmann, M. (2019): Lebenszykluskosten der Straßeninfrastruktur; ISBN: 978-3-901912-36-8 Monografie zur Habilitation an der Technischen Universität Wien; Wien (560 S.)

[4] Hoffmann, M.; Steininger, M.; Böhmer, A.; Neuhold, J. (2015): Technische und wirtschaftliche Aspekte von Streuungen mit erhöhtem Soleanteil; Straße und Autobahn, Nr. 9/2015; S. 618–626, Kirschbaum Verlag, Bonn

[5] Hoffmann, M.; Kluger-Eigl, W.; Hofko, B.; Blab, R.; Steyrer, G.; Berghold, H.; Maier-Farkas, H.; Neuhold, J.; Gattringer, J.; Nutz, P. (2018): Thawing capacity, freezing time and high shares of brine as main factors in the success of preventive winter maintenance; Peer-reviewed paper XVth PIARC International Winter Road Congress, Danzig; 16 S.

[6] Hofko, B.; Steiner, D.; Hoffmann, M. (2015): Eignungskriterien für auftauende Streumittel; Berichts-Nr. 045, für Bundesländer, ASFINAG, BMVIT; Wien

[7] Austrian Standards (2016): ÖNORM EN 16811-1:2016-11: Winterdienstausrüstung – Enteisungsmittel – Teil 1: Natriumchlorid – Anforderungen und Prüfmethoden; Wien

[8] FSV (2011): Richtlinien und Vorschriften für den Straßenbau – RVS 12.04.16 Qualitätssicherung Betrieb – Winterdienst – Streumittel; Wien; Ausgabe 11/2017